DESY 09-158
January 2010

ISSN 0418-9833

arXiv:0911.0884v2 [hep-ex] 15 Jan 2010

Combined Measurement and QCD Analysis of the Inclusive $e^{\pm}p$ Scattering Cross Sections at HERA

H1 and ZEUS Collaborations

Abstract

A combination is presented of the inclusive deep inelastic cross sections measured by the H1 and ZEUS Collaborations in neutral and charged current unpolarised $e^{\pm}p$ scattering at HERA during the period 1994-2000. The data span six orders of magnitude in negative four-momentum-transfer squared, Q^2, and in Bjorken x. The combination method used takes the correlations of systematic uncertainties into account, resulting in an improved accuracy. The combined data are the sole input in a NLO QCD analysis which determines a new set of parton distributions, HERAPDF1.0, with small experimental uncertainties. This set includes an estimate of the model and parametrisation uncertainties of the fit result.

The H1 and ZEUS Collaborations

F.D. Aaron[13,a8], H. Abramowicz[72,a36], I. Abt[57], L. Adamczyk[19], M. Adamus[84], M. Aldaya Martin[31], C. Alexa[13], V. Andreev[54], S. Antonelli[9], P. Antonioli[8], A. Antonov[55], B. Antunovic[31], M. Arneodo[77], V. Aushev[36,a31], O. Bachynska[31], S. Backovic[64], A. Baghdasaryan[86], A. Bamberger[27], A.N. Barakbaev[2], G. Barbagli[25], G. Bari[8], F. Barreiro[50], E. Barrelet[63], W. Bartel[31], D. Bartsch[10], M. Basile[9], K. Begzsuren[80], O. Behnke[31], J. Behr[31], U. Behrens[31], L. Bellagamba[8], A. Belousov[54], A. Bertolin[60], S. Bhadra[88], M. Bindi[9], J.C. Bizot[58], C. Blohm[31], T. Bołd[19], E.G. Boos[2], M. Borodin[36], K. Borras[31], D. Boscherini[8], D. Bot[31], V. Boudry[62], S.K. Boutle[42,a27], I. Bozovic-Jelisavcic[5], J. Bracinik[7], G. Brandt[31], M. Brinkmann[30], V. Brisson[58], I. Brock[10], E. Brownson[49], R. Brugnera[61], N. Brümmer[16], D. Bruncko[37], A. Bruni[8], G. Bruni[8], B. Brzozowska[83], A. Bunyatyan[32,86], G. Buschhorn[57], P.J. Bussey[29], J.M. Butterworth[42], B. Bylsma[16], L. Bystritskaya[53], A. Caldwell[57], A.J. Campbell[31], K.B. Cantun Avila[47], M. Capua[17], R. Carlin[61], C.D. Catterall[88], K. Cerny[66], V. Cerny[37,a6], S. Chekanov[4], V. Chekelian[57], A. Cholewa[31], J. Chwastowski[18], J. Ciborowski[83,a42], R. Ciesielski[31], L. Cifarelli[9], F. Cindolo[8], A. Contin[9], J.G. Contreras[47], A.M. Cooper-Sarkar[59], N. Coppola[31], M. Corradi[8], F. Corriveau[52], M. Costa[76], J.A. Coughlan[22], G. Cozzika[28], J. Cvach[65], G. D'Agostini[69], J.B. Dainton[41], F. Dal Corso[60], K. Daum[85,a2], M. Deák[31], J. de Favereau[45], B. Delcourt[58], J. del Peso[50], J. Delvax[12], R.K. Dementiev[56], S. De Pasquale[9,a11], M. Derrick[4], R.C.E. Devenish[59], E.A. De Wolf[12], C. Diaconu[51], D. Dobur[27], V. Dodonov[32], B.A. Dolgoshein[55], A. Dossanov[57], A.T. Doyle[29], V. Drugakov[89], A. Dubak[64,a5], L.S. Durkin[16], S. Dusini[60], G. Eckerlin[31], V. Efremenko[53], S. Egli[82], Y. Eisenberg[67], A. Eliseev[54], E. Elsen[31], P.F. Ermolov [56,†], A. Eskreys[18], A. Falkiewicz[18], S. Fang[31], L. Favart[12], S. Fazio[17], A. Fedotov[53], R. Felst[31], J. Feltesse[28,a7], J. Ferencei[37], J. Ferrando[59], M.I. Ferrero[76], J. Figiel[18], D.-J. Fischer[31], M. Fleischer[31], A. Fomenko[54], M. Forrest[29], B. Foster[59], S. Fourletov[78,a40], E. Gabathuler[41], A. Galas[18], E. Gallo[25], A. Garfagnini[61], J. Gayler[31], A. Geiser[31], S. Ghazaryan[31], I. Gialas[15,a27], L.K. Gladilin[56], D. Gladkov[55], C. Glasman[50], A. Glazov[31], I. Glushkov[89], L. Goerlich[18], N. Gogitidze[54], Yu.A. Golubkov[56], P. Göttlicher[31,a17], M. Gouzevitch[31], C. Grab[90], I. Grabowska-Bołd[19], J. Grebenyuk[31], T. Greenshaw[41], I. Gregor[31], B.R. Grell[31], G. Grigorescu[3], G. Grindhammer[57], G. Grzelak[83], C. Gwenlan[59,a33], T. Haas[31], S. Habib[30], D. Haidt[31], W. Hain[31], R. Hamatsu[75], J.C. Hart[22], H. Hartmann[10], G. Hartner[88], C. Helebrant[31], R.C.W. Henderson[40], E. Hennekemper[34], H. Henschel[89], M. Herbst[34], G. Herrera[48], M. Hildebrandt[82], E. Hilger[10], K.H. Hiller[89], D. Hochman[67], D. Hoffmann[51], U. Holm[30], R. Hori[74], R. Horisberger[82], K. Horton[59,a34], T. Hreus[12,a3], A. Hüttmann[31], G. Iacobucci[8], Z.A. Ibrahim[38], Y. Iga[70], R. Ingbir[72], M. Ishitsuka[73], M. Jacquet[58], H.-P. Jakob[10], X. Janssen[12], F. Januschek[31], M. Jimenez[50], T.W. Jones[42], L. Jönsson[46], A.W. Jung[34], H. Jung[31], M. Jüngst[10], I. Kadenko[36], B. Kahle[31], B. Kamaluddin[38], S. Kananov[72], T. Kanno[73], M. Kapichine[24], U. Karshon[67], F. Karstens[27], I.I. Katkov[31,a18], J. Katzy[31], M. Kaur[14], P. Kaur[14,a13], I.R. Kenyon[7], A. Keramidas[3], L.A. Khein[56], C. Kiesling[57], J.Y. Kim[39,a45], D. Kisielewska[19], S. Kitamura[75,a37], R. Klanner[30], M. Klein[41], U. Klein[31,a19], C. Kleinwort[31], T. Kluge[41], A. Knutsson[31], E. Koffeman[3], R. Kogler[57], D. Kollar[57], P. Kooijman[3], Ie. Korol[36], I.A. Korzhavina[56], P. Kostka[89], A. Kotański[20,a15], U. Kötz[31], H. Kowalski[31], M. Kraemer[31], K. Krastev[31], J. Kretzschmar[41], A. Kropivnitskaya[53], K. Krüger[34], P. Kulinski[83], O. Kuprash[36], K. Kutak[31], M. Kuze[73], V.A. Kuzmin[56], M.P.J. Landon[43], W. Lange[89], G. Laštovička-Medin[64], P. Laycock[41], A. Lebedev[54], A. Lee[16], V. Lendermann[34], B.B. Levchenko[56,a32], S. Levonian[31], A. Levy[72], G. Li[58], V. Libov[31], S. Limentani[61], T.Y. Ling[16], K. Lipka[31], A. Liptaj[57], M. Lisovyi[31], B. List[30], J. List[31], E. Lobodzinska[31], W. Lohmann[89], B. Löhr[31], E. Lohrmann[30],

J.H. Loizides[42], N. Loktionova[54], K.R. Long[44], A. Longhin[60], D. Lontkovskyi[36], R. Lopez-Fernandez[48], V. Lubimov[53], J. Łukasik[19,a14], O.Yu. Lukina[56], P. Łużniak[83,a43], J. Maeda[73], S. Magill[4], A. Makankine[24], I. Makarenko[36], E. Malinovski[54], J. Malka[83,a43], R. Mankel[31,a20], P. Marage[12], A. Margotti[8], G. Marini[69], Ll. Marti[31], J.F. Martin[78], H.-U. Martyn[1], A. Mastroberardino[17], T. Matsumoto[79,a28], M.C.K. Mattingly[6], S.J. Maxfield[41], A. Mehta[41], I.-A. Melzer-Pellmann[31], A.B. Meyer[31], H. Meyer[31], H. Meyer[85], J. Meyer[31], S. Miglioranzi[31,a21], S. Mikocki[18], I. Milcewicz-Mika[18], F. Mohamad Idris[38], V. Monaco[76], A. Montanari[31], F. Moreau[62], A. Morozov[24], J.D. Morris[11,a12], J.V. Morris[22], M.U. Mozer[12], M. Mudrinic[5], K. Müller[91], P. Murín[37,a3], B. Musgrave[4], K. Nagano[79], T. Namsoo[31], R. Nania[8], Th. Naumann[89], P.R. Newman[7], D. Nicholass[4,a10], C. Niebuhr[31], A. Nigro[69], A. Nikiforov[31], D. Nikitin[24], Y. Ning[35], U. Noor[88], D. Notz[31], G. Nowak[18], K. Nowak[91], R.J. Nowak[83], A.E. Nuncio-Quiroz[10], B.Y. Oh[81], N. Okazaki[74], K. Oliver[59], K. Olkiewicz[18], J.E. Olsson[31], Yu. Onishchuk[36], S. Osman[46], O. Ota[75,a38], D. Ozerov[53], V. Palichik[24], I. Panagoulias[31,a1,b13], M. Pandurovic[5], Th. Papadopoulou[31,a1,b13], K. Papageorgiu[15], A. Parenti[31], C. Pascaud[58], G.D. Patel[41], E. Paul[10], J.M. Pawlak[83], B. Pawlik[18], O. Pejchal[66], P.G. Pelfer[26], A. Pellegrino[3], E. Perez[28,a4], W. Perlanski[83,a43], H. Perrey[30], A. Petrukhin[53], I. Picuric[64], S. Piec[89], K. Piotrzkowski[45], D. Pitzl[31], R. Plačakytė[31], P. Plucinski[84,a44], B. Pokorny[30], N.S. Pokrovskiy[2], R. Polifka[66], A. Polini[8], B. Povh[32], A.S. Proskuryakov[56], M. Przybycień[19], V. Radescu[31], A.J. Rahmat[41], N. Raicevic[64], A. Raspiareza[57], A. Raval[31], T. Ravdandorj[80], D.D. Reeder[49], P. Reimer[65], B. Reisert[57], Z. Ren[35], J. Repond[4], Y.D. Ri[75,a39], E. Rizvi[43], A. Robertson[59], P. Robmann[91], B. Roland[12], P. Roloff[31], E. Ron[50], R. Roosen[12], A. Rostovtsev[53], M. Rotaru[13], I. Rubinsky[31], J.E. Ruiz Tabasco[47], S. Rusakov[54], M. Ruspa[77], R. Sacchi[76], D. Sálek[66], A. Salii[36], U. Samson[10], D.P.C. Sankey[22], G. Sartorelli[9], M. Sauter[33], E. Sauvan[51], A.A. Savin[49], D.H. Saxon[29], M. Schioppa[17], S. Schlenstedt[89], P. Schleper[30], W.B. Schmidke[57], S. Schmitt[31], U. Schneekloth[31], L. Schoeffel[28], V. Schönberg[10], A. Schöning[33], T. Schörner-Sadenius[30], H.-C. Schultz-Coulon[34], J. Schwartz[52], F. Sciulli[35], F. Sefkow[31], R.N. Shaw-West[7], L.M. Shcheglova[56], R. Shehzadi[10], S. Shimizu[74,a21], L.N. Shtarkov[54], S. Shushkevich[57], I. Singh[14,a13], I.O. Skillicorn[29], T. Sloan[40], W. Słomiński[20,a16], I. Smiljanic[5], W.H. Smith[49], V. Sola[76], A. Solano[76], Y. Soloviev[54], D. Son[21], P. Sopicki[18], Iu. Sorokin[36], V. Sosnovtsev[55], D. South[23], V. Spaskov[24], A. Specka[62], A. Spiridonov[31,a22], H. Stadie[30], L. Stanco[60], Z. Staykova[31], M. Steder[31], B. Stella[68], A. Stern[72], T.P. Stewart[78], A. Stifutkin[55], G. Stoicea[13], P. Stopa[18], U. Straumann[91], S. Suchkov[55], D. Sunar[12], G. Susinno[17], L. Suszycki[19], T. Sykora[12], J. Sztuk[30], D. Szuba[31,a23], J. Szuba[31,a24], A.D. Tapper[44], E. Tassi[17,a41], V. Tchoulakov[24], J. Terrón[50], T. Theedt[31], G. Thompson[43], P.D. Thompson[7], H. Tiecke[3], K. Tokushuku[79,a29], T. Toll[30], F. Tomasz[37], J. Tomaszewska[31,a25], T.H. Tran[58], D. Traynor[43], T.N. Trinh[51], P. Truöl[91], I. Tsakov[71], B. Tseepeldorj[80,a9], T. Tsurugai[87], M. Turcato[30], J. Turnau[18], T. Tymieniecka[84,a46], K. Urban[34], C. Uribe-Estrada[50], A. Valkárová[66], C. Vallée[51], P. Van Mechelen[12], A. Vargas Trevino[31], Y. Vazdik[54], M. Vázquez[3,a21], A. Verbytskyi[31], V. Viazlo[36], S. Vinokurova[31], N.N. Vlasov[27,a26], V. Volchinski[86], O. Volynets[36], M. von den Driesch[31], R. Walczak[59], W.A.T. Wan Abdullah[38], D. Wegener[23], J.J. Whitmore[81,a35], J. Whyte[88], L. Wiggers[3], M. Wing[42], Ch. Wissing[31], M. Wlasenko[10], G. Wolf[31], H. Wolfe[49], K. Wrona[31], E. Wünsch[31], A.G. Yagües-Molina[31], S. Yamada[79], Y. Yamazaki[79,a30], R. Yoshida[4], C. Youngman[31], J. Žáček[66], J. Zálešák[65], A.F. Żarnecki[83], L. Zawiejski[18], O. Zeniaev[36], W. Zeuner[31,a20], Z. Zhang[58], B.O. Zhautykov[2], A. Zhokin[53], C. Zhou[52], A. Zichichi[9], T. Zimmermann[90], H. Zohrabyan[86], M. Zolko[36], F. Zomer[58], D.S. Zotkin[56]

[1] *I. Physikalisches Institut der RWTH, Aachen, Germany*
[2] *Institute of Physics and Technology of Ministry of Education and Science of Kazakhstan, Almaty, Kazakhstan*
[3] *NIKHEF and University of Amsterdam, Amsterdam, Netherlands* [b20]
[4] *Argonne National Laboratory, Argonne, Illinois 60439-4815, USA* [b25]
[5] *Vinca Institute of Nuclear Sciences, Belgrade, Serbia*
[6] *Andrews University, Berrien Springs, Michigan 49104-0380, USA*
[7] *School of Physics and Astronomy, University of Birmingham, Birmingham, United Kingdom* [b24]
[8] *INFN Bologna, Bologna, Italy* [b17]
[9] *University and INFN Bologna, Bologna, Italy* [b17]
[10] *Physikalisches Institut der Universität Bonn, Bonn, Germany* [b2]
[11] *H.H. Wills Physics Laboratory, University of Bristol, Bristol, United Kingdom* [b24]
[12] *Inter-University Institute for High Energies ULB-VUB, Brussels; Universiteit Antwerpen, Antwerpen; Belgium* [b3]
[13] *National Institute for Physics and Nuclear Engineering (NIPNE), Bucharest, Romania*
[14] *Panjab University, Department of Physics, Chandigarh, India*
[15] *Department of Engineering in Management and Finance, Univ. of the Aegean, Chios, Greece*
[16] *Physics Department, Ohio State University, Columbus, Ohio 43210, USA* [b25]
[17] *Calabria University, Physics Department and INFN, Cosenza, Italy* [b17]
[18] *The Henryk Niewodniczanski Institute of Nuclear Physics, Polish Academy of Sciences, Cracow, Poland* [b4,b5]
[19] *Faculty of Physics and Applied Computer Science, AGH-University of Science and Technology, Cracow, Poland* [b27]
[20] *Department of Physics, Jagellonian University, Cracow, Poland*
[21] *Kyungpook National University, Center for High Energy Physics, Daegu, South Korea* [b19]
[22] *Rutherford Appleton Laboratory, Chilton, Didcot, United Kingdom* [b24]
[23] *Institut für Physik, TU Dortmund, Dortmund, Germany* [b1]
[24] *Joint Institute for Nuclear Research, Dubna, Russia*
[25] *INFN Florence, Florence, Italy* [b17]
[26] *University and INFN Florence, Florence, Italy* [b17]
[27] *Fakultät für Physik der Universität Freiburg i.Br., Freiburg i.Br., Germany* [b2]
[28] *CEA, DSM/Irfu, CE-Saclay, Gif-sur-Yvette, France*
[29] *Department of Physics and Astronomy, University of Glasgow, Glasgow, United Kingdom* [b24]
[30] *Institut für Experimentalphysik, Universität Hamburg, Hamburg, Germany* [b1,b2]
[31] *Deutsches Elektronen-Synchrotron DESY, Hamburg, Germany*
[32] *Max-Planck-Institut für Kernphysik, Heidelberg, Germany*
[33] *Physikalisches Institut, Universität Heidelberg, Heidelberg, Germany* [b1]
[34] *Kirchhoff-Institut für Physik, Universität Heidelberg, Heidelberg, Germany* [b1]
[35] *Nevis Laboratories, Columbia University, Irvington on Hudson, New York 10027, USA* [b26]
[36] *Institute for Nuclear Research, National Academy of Sciences, and Kiev National University, Kiev, Ukraine*
[37] *Institute of Experimental Physics, Slovak Academy of Sciences, Košice, Slovak Republic* [b7]
[38] *Jabatan Fizik, Universiti Malaya, 50603 Kuala Lumpur, Malaysia* [b29]
[39] *Chonnam National University, Kwangju, South Korea*
[40] *Department of Physics, University of Lancaster, Lancaster, United Kingdom* [b24]

[41] *Department of Physics, University of Liverpool, Liverpool, United Kingdom* [b24]
[42] *Physics and Astronomy Department, University College London, London, United Kingdom* [b24]
[43] *Queen Mary and Westfield College, London, United Kingdom* [b24]
[44] *Imperial College London, High Energy Nuclear Physics Group, London, United Kingdom* [b24]
[45] *Institut de Physique Nucléaire, Université Catholique de Louvain, Louvain-la-Neuve, Belgium* [b28]
[46] *Physics Department, University of Lund, Lund, Sweden* [b8]
[47] *Departamento de Fisica Aplicada, CINVESTAV, Mérida, Yucatán, Mexico* [b11]
[48] *Departamento de Fisica, CINVESTAV, México City, Mexico* [b11]
[49] *Department of Physics, University of Wisconsin, Madison, Wisconsin 53706, USA* [b25]
[50] *Departamento de Física Teórica, Universidad Autónoma de Madrid, Madrid, Spain* [b23]
[51] *CPPM, CNRS/IN2P3 - Univ. Mediterranee, Marseille, France*
[52] *Department of Physics, McGill University, Montréal, Québec, Canada H3A 2T8* [b14]
[53] *Institute for Theoretical and Experimental Physics, Moscow, Russia* [b12]
[54] *Lebedev Physical Institute, Moscow, Russia* [b6]
[55] *Moscow Engineering Physics Institute, Moscow, Russia* [b21]
[56] *Moscow State University, Institute of Nuclear Physics, Moscow, Russia* [b22]
[57] *Max-Planck-Institut für Physik, München, Germany*
[58] *LAL, Univ. Paris-Sud, CNRS/IN2P3, Orsay, France*
[59] *Department of Physics, University of Oxford, Oxford, United Kingdom* [b24]
[60] *INFN Padova, Padova, Italy* [b17]
[61] *Dipartimento di Fisica dell'Università and INFN, Padova, Italy* [b17]
[62] *LLR, Ecole Polytechnique, CNRS/IN2P3, Palaiseau, France*
[63] *LPNHE, Universités Paris VI and VII, CNRS/IN2P3, Paris, France*
[64] *Faculty of Science, University of Montenegro, Podgorica, Montenegro* [b6]
[65] *Institute of Physics, Academy of Sciences of the Czech Republic, Praha, Czech Republic* [b9]
[66] *Faculty of Mathematics and Physics, Charles University, Praha, Czech Republic* [b9]
[67] *Department of Particle Physics, Weizmann Institute, Rehovot, Israel* [b15]
[68] *Dipartimento di Fisica Università di Roma Tre and INFN Roma 3, Roma, Italy*
[69] *Dipartimento di Fisica, Università 'La Sapienza' and INFN, Rome, Italy* [b17]
[70] *Polytechnic University, Sagamihara, Japan* [b18]
[71] *Institute for Nuclear Research and Nuclear Energy, Sofia, Bulgaria* [b6]
[72] *Raymond and Beverly Sackler Faculty of Exact Sciences, School of Physics, Tel Aviv University, Tel Aviv, Israel* [b16]
[73] *Department of Physics, Tokyo Institute of Technology, Tokyo, Japan* [b18]
[74] *Department of Physics, University of Tokyo, Tokyo, Japan* [b18]
[75] *Tokyo Metropolitan University, Department of Physics, Tokyo, Japan* [b18]
[76] *Università di Torino and INFN, Torino, Italy* [b17]
[77] *Università del Piemonte Orientale, Novara, and INFN, Torino, Italy* [b17]
[78] *Department of Physics, University of Toronto, Toronto, Ontario, Canada M5S 1A7* [b14]
[79] *Institute of Particle and Nuclear Studies, KEK, Tsukuba, Japan* [b18]
[80] *Institute of Physics and Technology of the Mongolian Academy of Sciences, Ulaanbaatar, Mongolia*
[81] *Department of Physics, Pennsylvania State University, University Park, Pennsylvania 16802, USA* [b26]

[82] *Paul Scherrer Institut, Villigen, Switzerland*
[83] *Warsaw University, Institute of Experimental Physics, Warsaw, Poland*
[84] *Institute for Nuclear Studies, Warsaw, Poland*
[85] *Fachbereich C, Universität Wuppertal, Wuppertal, Germany*
[86] *Yerevan Physics Institute, Yerevan, Armenia*
[87] *Meiji Gakuin University, Faculty of General Education, Yokohama, Japan* [b18]
[88] *Department of Physics, York University, Ontario, Canada M3J1P3* [b14]
[89] *Deutsches Elektronen-Synchrotron DESY, Zeuthen, Germany*
[90] *Institut für Teilchenphysik, ETH, Zürich, Switzerland* [b10]
[91] *Physik-Institut der Universität Zürich, Zürich, Switzerland* [b10]

[a1] *Also at Physics Department, National Technical University, Zografou Campus, GR-15773 Athens, Greece*
[a2] *Also at Rechenzentrum, Universität Wuppertal, Wuppertal, Germany*
[a3] *Also at University of P.J. Šafárik, Košice, Slovak Republic*
[a4] *Also at CERN, Geneva, Switzerland*
[a5] *Also at Max-Planck-Institut für Physik, München, Germany*
[a6] *Also at Comenius University, Bratislava, Slovak Republic*
[a7] *Also at DESY and University Hamburg, Helmholtz Humboldt Research Award*
[a8] *Also at Faculty of Physics, University of Bucharest, Bucharest, Romania*
[a9] *Also at Ulaanbaatar University, Ulaanbaatar, Mongolia*
[a10] *Also affiliated with University College London, United Kingdom*
[a11] *Now at University of Salerno, Italy*
[a12] *Now at Queen Mary University of London, United Kingdom*
[a13] *Also working at Max Planck Institute, Munich, Germany*
[a14] *Now at Institute of Aviation, Warsaw, Poland*
[a15] *Supported by the research grant No. 1 P03B 04529 (2005-2008)*
[a16] *This work was supported in part by the Marie Curie Actions Transfer of Knowledge project COCOS (contract MTKD-CT-2004-517186)*
[a17] *Now at DESY group FEB, Hamburg, Germany*
[a18] *Also at Moscow State University, Russia*
[a19] *Now at University of Liverpool, United Kingdom*
[a20] *On leave of absence at CERN, Geneva, Switzerland*
[a21] *Now at CERN, Geneva, Switzerland*
[a22] *Also at Institut of Theoretical and Experimental Physics, Moscow, Russia*
[a23] *Also at INP, Cracow, Poland*
[a24] *Also at FPACS, AGH-UST, Cracow, Poland*
[a25] *Partially supported by Warsaw University, Poland*
[a26] *Partially supported by Moscow State University, Russia*
[a27] *Also affiliated with DESY, Germany*
[a28] *Now at Japan Synchrotron Radiation Research Institute (JASRI), Hyogo, Japan*
[a29] *Also at University of Tokyo, Japan*
[a30] *Now at Kobe University, Japan*
[a31] *Supported by DESY, Germany*
[a32] *Partially supported by Russian Foundation for Basic Research grant No. 05-02-39028-NSFC-a*
[a33] *STFC Advanced Fellow*
[a34] *Nee Korcsak-Gorzo*
[a35] *This material was based on work supported by the National Science Foundation, while working at the Foundation.*

[a36] *Also at Max Planck Institute, Munich, Germany, Alexander von Humboldt Research Award*
[a37] *Now at Nihon Institute of Medical Science, Japan*
[a38] *Now at SunMelx Co. Ltd., Tokyo, Japan*
[a39] *Now at Osaka University, Osaka, Japan*
[a40] *Now at University of Bonn, Germany*
[a41] *also Senior Alexander von Humboldt Research Fellow at Hamburg University*
[a42] *Also at Łódź University, Poland*
[a43] *Member of Łódź University, Poland*
[a44] *Now at Lund University, Lund, Sweden*
[a45] *Supported by Chonnam National University, South Korea, in 2009*
[a46] *Also at University of Podlasie, Siedlce, Poland*

[b1] *Supported by the German Federal Ministry for Education and Research (BMBF), under contract numbers 05H09GUF, 05H09VHC, 05H09VHF and 05H16PEA*
[b2] *Supported by the German Federal Ministry for Education and Research (BMBF), under contract numbers 05 HZ6PDA, 05 HZ6GUA, 05 HZ6VFA and 05 HZ4KHA*
[b3] *Supported by FNRS-FWO-Vlaanderen, IISN-IIKW and IWT and by Interuniversity Attraction Poles Programme, Belgian Science Policy*
[b4] *Supported by the Polish State Committee for Scientific Research, project No. DESY/256/2006 - 154/DES/2006/03*
[b5] *Partially Supported by Polish Ministry of Science and Higher Education, grant PBS/DESY/70/2006*
[b6] *Supported by the Deutsche Forschungsgemeinschaft*
[b7] *Supported by VEGA SR grant no. 2/7062/ 27*
[b8] *Supported by the Swedish Natural Science Research Council*
[b9] *Supported by the Ministry of Education of the Czech Republic under the projects LC527, INGO-1P05LA259 and MSM0021620859*
[b10] *Supported by the Swiss National Science Foundation*
[b11] *Supported by CONACYT, México, grant 48778-F*
[b12] *Russian Foundation for Basic Research (RFBR), grant no 1329.2008.2*
[b13] *This project is co-funded by the European Social Fund (75% and National Resources (25%) - (EPEAEK II) - PYTHAGORAS II*
[b14] *Supported by the Natural Sciences and Engineering Research Council of Canada (NSERC)*
[b15] *Supported in part by the MINERVA Gesellschaft für Forschung GmbH, the Israel Science Foundation (grant No. 293/02-11.2) and the US-Israel Binational Science Foundation*
[b16] *Supported by the Israel Science Foundation*
[b17] *Supported by the Italian National Institute for Nuclear Physics (INFN)*
[b18] *Supported by the Japanese Ministry of Education, Culture, Sports, Science and Technology (MEXT) and its grants for Scientific Research*
[b19] *Supported by the Korean Ministry of Education and Korea Science and Engineering Foundation*
[b20] *Supported by the Netherlands Foundation for Research on Matter (FOM)*
[b21] *Partially supported by the German Federal Ministry for Education and Research (BMBF)*
[b22] *Supported by RF Presidential grant N 1456.2008.2 for the leading scientific schools and by the Russian Ministry of Education and Science through its grant for Scientific Research on High Energy Physics*
[b23] *Supported by the Spanish Ministry of Education and Science through funds provided by CICYT*
[b24] *Supported by the UK Science and Technology Facilities Council*
[b25] *Supported by the US Department of Energy*
[b26] *Supported by the US National Science Foundation. Any opinion, findings and conclusions or recommendations expressed in this material are those of the authors and do not necessarily reflect the views of the National Science Foundation.*

[b27] *Supported by the Polish Ministry of Science and Higher Education as a scientific project (2009-2010)*
[b28] *Supported by FNRS and its associated funds (IISN and FRIA) and by an Inter-University Attraction Poles Programme subsidised by the Belgian Federal Science Policy Office*
[b29] *Supported by an FRGS grant from the Malaysian government*

[†] *deceased*

1 Introduction

Deep inelastic scattering (DIS) at HERA has been central to the exploration of proton structure and quark-gluon interaction dynamics as prescribed in perturbative Quantum Chromodynamics (QCD). HERA allowed inelastic ep interactions to be studied at high centre-of-mass energy, $\sqrt{s} \simeq 320\,\text{GeV}$, where $s = 4E_eE_p$, the lepton beam energy $E_e \simeq 27.5\,\text{GeV}$ and the proton beam energy $E_p = 920\,\text{GeV}$ for most of the running period. Operation of HERA proceeded in two phases, HERA I, from 1992-2000, and HERA II, from 2002-2007. The luminosity collected by each of the collider experiments, H1 and ZEUS, in unpolarised e^+p and e^-p scattering during the first phase was approximately $100\,\text{pb}^{-1}$and $15\,\text{pb}^{-1}$, respectively.

The paper presents the combination of the published H1 [1–5] and ZEUS [6–14] measurements from HERA I on inclusive DIS in neutral (NC) and charged current (CC) reactions which cover a wide range of negative four-momentum-transfer squared, Q^2, and Bjorken x. The combination is performed using a method introduced in [15] and extended in [1]. This also provides a model-independent check of the data consistency. The correlated systematic uncertainties and global normalisations are fitted such that one coherent data set is obtained. Since H1 and ZEUS have employed different experimental techniques, using different detectors and methods of kinematic reconstruction, the combination leads to a significantly reduced uncertainty.

The combined data set contains complete information on inclusive DIS cross sections published by the H1 and ZEUS collaborations based on data collected in the years 1994-2000. The kinematic range of the NC data is $6 \cdot 10^{-7} \leq x \leq 0.65$ and $0.045 \leq Q^2 \leq 30000\,\text{GeV}^2$, for values of inelasticity y between 0.005 and 0.95, where $y = Q^2/sx$. The kinematic range of the CC data is $1.3 \cdot 10^{-2} \leq x \leq 0.40$ and $300 \leq Q^2 \leq 30000\,\text{GeV}^2$, for values of y between 0.037 and 0.76. An extensive overview of the results on HERA I data from both H1 and ZEUS is given in [16].

Analyses of the x and Q^2 dependences of the NC and CC DIS cross sections measured at HERA have determined sets of quark and gluon momentum distributions in the proton, both from H1 [2] and ZEUS [17]. In such analyses, the lower Q^2 NC data determine the low-x sea quark and gluon distributions. The high-Q^2 CC data, together with the difference between NC e^+p and e^-p cross sections at high Q^2, constrain the valence quark distributions. The use of the HERA CC data allows the down quark distribution in the proton to be determined without assuming isospin symmetry. In addition, the use of HERA data alone for the determination of parton distribution functions (PDFs) eliminates the need for heavy target corrections, which must be applied to DIS data from nuclear targets. In this paper the combined HERA data are used to determine a new set of parton distributions termed HERAPDF1.0. Consistency of the input data ensures that the experimental uncertainty of the HERAPDF1.0 set can be determined using rigorous statistical methods. Uncertainties resulting from model assumptions and from the choice of PDF parametrisation are also considered, similarly to [2].

The paper is organised as follows. In section 2 the measurements by H1 and ZEUS and the input data are described. In section 3 the combination of the NC and CC data sets from H1 and ZEUS is discussed. The QCD analysis is described in section 4. A summary is given in section 5.

2 Measurements of Inclusive DIS Cross Sections

2.1 Cross Sections and Parton Distributions

The neutral current deep inelastic $e^{\pm}p$ scattering cross section, at tree level, is given by a linear combination of generalised structure functions. For unpolarised beams it can be expressed as

$$\sigma^{\pm}_{r,\mathrm{NC}} = \frac{\mathrm{d}^2\sigma^{e^{\pm}p}_{\mathrm{NC}}}{\mathrm{d}x\mathrm{d}Q^2} \cdot \frac{Q^4 x}{2\pi\alpha^2 Y_+} = \tilde{F}_2 \mp \frac{Y_-}{Y_+} x\tilde{F}_3 - \frac{y^2}{Y_+}\tilde{F}_L \,, \tag{1}$$

where the electromagnetic coupling constant α, the photon propagator and a helicity factor are absorbed in the definition of the reduced cross section $\sigma^{\pm}_{r,\mathrm{NC}}$, and $Y_{\pm} = 1 \pm (1-y)^2$. The functions $\tilde{F}_2$, $\tilde{F}_L$ and $x\tilde{F}_3$ depend on the electroweak parameters as [18]

$$\begin{aligned} \tilde{F}_2 &= F_2 - \kappa_Z v_e \cdot F_2^{\gamma Z} + \kappa_Z^2 (v_e^2 + a_e^2) \cdot F_2^Z \,, \\ \tilde{F}_L &= F_L - \kappa_Z v_e \cdot F_L^{\gamma Z} + \kappa_Z^2 (v_e^2 + a_e^2) \cdot F_L^Z \,, \\ x\tilde{F}_3 &= \kappa_Z a_e \cdot xF_3^{\gamma Z} - \kappa_Z^2 \cdot 2 v_e a_e \cdot xF_3^Z \,. \end{aligned} \tag{2}$$

Here v_e and a_e are the vector and axial-vector weak couplings of the electron to the Z boson and $\kappa_Z(Q^2) = Q^2/[(Q^2 + M_Z^2)(4\sin^2\theta_W \cos^2\theta_W)]$. The effective values for the electroweak mixing angle, $\sin^2\theta_W = 0.2315$, and the Z boson mass, $M_Z = 91.187$ GeV, are used [19]. At low Q^2, the contribution of Z exchange is negligible and $\sigma_{r,\mathrm{NC}} = F_2 - y^2 F_L / Y_+$. The contribution of the term containing the structure function F_L is only significant for large values of y.

In the Quark Parton Model (QPM), $\tilde{F}_L = 0$ [20] and the other functions in equation 2 are given as

$$\begin{aligned} (F_2, F_2^{\gamma Z}, F_2^Z) &= [(e_u^2, 2e_u v_u, v_u^2 + a_u^2)(xU + x\bar{U}) + (e_d^2, 2e_d v_d, v_d^2 + a_d^2)(xD + x\bar{D})] \,, \\ (xF_3^{\gamma Z}, xF_3^Z) &= 2[(e_u a_u, v_u a_u)(xU - x\bar{U}) + (e_d a_d, v_d a_d)(xD - x\bar{D})] \,, \end{aligned} \tag{3}$$

where e_u, e_d denote the electric charge of up- or down-type quarks while $v_{u,d}$ and $a_{u,d}$ are the vector and axial-vector weak couplings of the up- or down-type quarks to the Z boson. Here xU, xD, $x\bar{U}$ and $x\bar{D}$ denote the sums of up-type, of down-type and of their anti-quark distributions, respectively. Below the b quark mass threshold, these sums are related to the quark distributions as follows

$$xU = xu + xc \,, \qquad x\bar{U} = x\bar{u} + x\bar{c} \,, \qquad xD = xd + xs \,, \qquad x\bar{D} = x\bar{d} + x\bar{s} \,, \tag{4}$$

where xs and xc are the strange and charm quark distributions. Assuming symmetry between sea quarks and anti-quarks, the valence quark distributions result from

$$xu_v = xU - x\bar{U} \,, \qquad xd_v = xD - x\bar{D} \,. \tag{5}$$

Defining a reduced cross section for the inclusive unpolarised charged current $e^{\pm}p$ scattering as

$$\sigma^{\pm}_{r,\mathrm{CC}} = \frac{2\pi x}{G_F^2}\left[\frac{M_W^2+Q^2}{M_W^2}\right]^2 \frac{\mathrm{d}^2\sigma^{e^{\pm}p}_{\mathrm{CC}}}{\mathrm{d}x\mathrm{d}Q^2} \tag{6}$$

gives a sum of charged current structure functions, analogous to equation 1, as

$$\sigma^{\pm}_{r,CC} = \frac{Y_+}{2}W_2^{\pm} \mp \frac{Y_-}{2}xW_3^{\pm} - \frac{y^2}{2}W_L^{\pm}\,. \tag{7}$$

For the Fermi constant, an effective value $G_F = 1.16639\times10^{-5}$ GeV^{-2} is used, the W boson mass is $M_W = 80.41$ GeV [19]. In the QPM $W_L^{\pm} = 0$ and the CC structure functions represent sums and differences of quark and anti-quark-type distributions depending on the charge of the lepton beam as

$$W_2^+ = x\overline{U} + xD\,, \qquad xW_3^+ = xD - x\overline{U}\,, \qquad W_2^- = xU + x\overline{D}\,, \qquad xW_3^- = xU - x\overline{D}\,. \tag{8}$$

From these equations it follows that

$$\sigma^+_{r,\mathrm{CC}} = x\overline{U} + (1-y)^2 xD\,, \qquad \sigma^-_{r,\mathrm{CC}} = xU + (1-y)^2 x\overline{D}\,. \tag{9}$$

Therefore the NC and CC measurements may be used to determine the combined sea quark distribution functions, $x\overline{U}$ and $x\overline{D}$, and the valence quark distributions, xu_v and xd_v. A QCD analysis in the DGLAP formalism [21–25] also allows the gluon momentum distribution, xg, in the proton to be determined from scaling violations.

2.2 Reconstruction of Kinematics

The deep inelastic ep scattering cross section of the inclusive neutral and charged current reactions depends on the centre-of-mass energy s and on two kinematic variables, Q^2 and x. Usually x is obtained from the measurement of the inelasticity y and from Q^2 and s through the relationship $x = Q^2/(sy)$. The salient feature of the HERA collider experiments is the possibility to determine the NC event kinematics from the scattered electron[1] e, or from the hadronic final state h, or using a combination of the two. The choice of the most appropriate kinematic reconstruction method for a given phase space region is based on resolution, measurement accuracy and radiative correction effects and has been optimised differently for the two experiments. The use of different reconstruction techniques by the two experiments contributes to the improved accuracy of the combined data set.

For NC scattering, in the "electron method", the inelasticity and the negative four-momentum-transfer squared can be calculated using the electron kinematics as

$$y_e = 1 - \frac{\Sigma_e}{2E_e}\,, \qquad Q^2_e = \frac{P^2_{T,e}}{1-y_e}\,, \qquad x_e = \frac{Q^2_e}{sy_e}\,. \tag{10}$$

Here $\Sigma_e = E'_e(1-\cos\theta_e)$, where θ_e is the angle between the scattered electron direction and the proton beam direction[2], E'_e is the scattered electron energy, and $P_{T,e}$ is its transverse momentum.

[1] In this paper, the term electron is used for both electrons and positrons, unless otherwise stated.

[2] In the right-handed H1 and ZEUS coordinate systems, the z axis points along the proton beam direction, termed the forward direction. The x (y) axis is directed horizontally (vertically).

Similar relations are obtained from the hadronic final state reconstruction [26], and are used for CC scattering,

$$y_h = \frac{\Sigma_h}{2E_e}, \qquad Q^2_h = \frac{P^2_{T,h}}{1-y_h}, \qquad x_h = \frac{Q^2_h}{sy_h}, \tag{11}$$

where $\Sigma_h = \sum_i (E_i - p_{z,i})$ is the hadronic $E - P_z$ variable with the sum extending over the reconstructed hadronic final state particles i, and $P_{T,h} = \left|\sum_i \boldsymbol{p}_{\perp,i}\right|$ is the total transverse momentum of the hadronic final state with $\boldsymbol{p}_{\perp,i}$ being the transverse momentum vector of the particle i. The combination of $P_{T,h}$ and Σ_h defines the hadronic scattering angle

$$\tan\frac{\theta_h}{2} = \frac{\Sigma_h}{P_{T,h}} \tag{12}$$

which, within the QPM, corresponds to the direction of the struck quark. In the "sigma method" [27] the total $E - P_z$ variable

$$E - P_z = E'_e(1-\cos\theta_e) + \sum_i (E_i - p_{z,i}) = \Sigma_e + \Sigma_h \tag{13}$$

is introduced. For non-radiative events this variable equals $2E_e$ such that equations 10 and 11 can be modified as

$$y_\Sigma = \frac{\Sigma_h}{E-P_z}, \qquad Q^2_\Sigma = \frac{P^2_{T,e}}{1-y_\Sigma}, \qquad x_\Sigma = \frac{Q^2_\Sigma}{sy_\Sigma}. \tag{14}$$

A hybrid "e-sigma method" [3,7,27] uses Q^2_e and x_Σ to reconstruct the event kinematics

$$y_{e\Sigma} = \frac{Q^2_e}{sx_\Sigma} = \frac{2E_e}{E-P_z}y_\Sigma, \qquad Q^2_{e\Sigma} = Q^2_e, \qquad x_{e\Sigma} = x_\Sigma. \tag{15}$$

An extension of the sigma method [1,2] is

$$y_{\Sigma'} = y_\Sigma, \qquad Q^2_{\Sigma'} = Q^2_\Sigma, \qquad x_{\Sigma'} = \frac{Q^2_\Sigma}{2E_p(E-P_z)y_\Sigma} = \frac{Q^2_\Sigma}{2E_p\Sigma_h}. \tag{16}$$

This modification takes radiative effects at the lepton vertex into account by replacing the electron beam energy in the calculation of x, in a similar manner to y_Σ.

The "double angle method" [28,29] is used to reconstruct Q^2 and x from the electron and hadronic scattering angles as

$$y_{DA} = \frac{\tan(\theta_h/2)}{\tan(\theta_e/2)+\tan(\theta_h/2)}, \qquad Q^2_{DA} = 4E^2_e \cdot \frac{\cot(\theta_e/2)}{\tan(\theta_e/2)+\tan(\theta_h/2)}, \qquad x_{DA} = \frac{Q^2_{DA}}{sy_{DA}}. \tag{17}$$

The method is largely insensitive to hadronization and, to first order, is independent of the detector energy scales. However, the hadronic angle is less well-determined than the electron angle due to particle loss in the beampipe. In the "PT method" of reconstruction [30] the well-measured electron kinematics is used to obtain a good event-by-event estimate of the hadronic energy loss, by employing $\delta_{PT} = P_{T,h}/P_{T,e}$. This improves both the resolution and uncertainties of the reconstructed y and Q^2. The PT method uses all measured variables to optimise the resolution over the entire kinematic range measured, namely,

$$\tan\frac{\theta_{PT}}{2} = \frac{\Sigma_{PT}}{P_{T,e}}, \quad \text{where} \quad \Sigma_{PT} = 2E_e\frac{C(\theta_h, P_{T,h}, \delta_{PT})\cdot\Sigma_h}{\Sigma_e + C(\theta_h, P_{T,h}, \delta_{PT})\cdot\Sigma_h}. \tag{18}$$

The variable θ_{PT} is then substituted for θ_h in the formulae for the double angle method to determine x, y and Q^2. The detector-specific function C is calculated using Monte Carlo simulations as $\Sigma_{true,h}/\Sigma_h$, depending on θ_h, $P_{T,h}$ and δ_{PT}.

The methods of kinematic reconstruction used by H1 and ZEUS are given in table 1 as part of the specification of the input data sets.

2.3 Detectors

The H1 [31–33] and ZEUS [34] detectors had nearly 4π hermetic coverage. They were built following similar physics considerations but opted for different technical solutions, both for the calorimetric and the tracking measurements.

The main component of the H1 detector was the finely segmented Liquid Argon calorimeter (LAr). It had an inner electromagnetic part and an outer hadronic part. The resolutions, σ_E, as measured with test beams, are about $0.11\sqrt{E/\mathrm{GeV}}$ and $0.50\sqrt{E/\mathrm{GeV}}$ for electromagnetic and hadronic particles, respectively. The LAr was surrounded by a superconducting coil providing a solenoidal magnetic field of 1.16 T and an instrumented iron structure acting as a shower tail catcher and a muon detector. In 1996 a major upgrade was performed during which the backward detectors were replaced by a Backward Drift Chamber (BDC) attached to a new lead fibre calorimeter (SpaCal) with a high resolution ($0.07\sqrt{E/\mathrm{GeV}}$) electromagnetic section, which comprised 27.5 radiation lengths, followed by a hadronic section. The SpaCal calorimeter had a total depth of two hadronic interaction lengths. In the upgraded configuration, the innermost central tracking detector of H1 contained two silicon detectors, the central and backward trackers, CST and BST. These were surrounded by the Central Inner Proportional chamber, CIP, and the Central Jet Chamber, CJC, which was the main tracking device of H1, with wires strung parallel to the beam axis. The CJC had two concentric parts. The CJC was complemented by drift chambers to measure the z coordinate, and a further proportional chamber between the CJC chambers was used for triggering. Tracks in the forward direction were measured in the Forward Tracking Detector, FTD, a set of drift chamber modules of different orientation.

The main component of the ZEUS detector was the uranium-scintillator calorimeter (CAL) consisting of three parts: forward (FCAL), barrel (BCAL) and rear (RCAL). Each part was segmented into one electromagnetic section (EMC) and either one (in RCAL) or two (in BCAL and FCAL) hadronic sections (HAC). Under test-beam conditions, the energy resolutions were $0.18\sqrt{E/\mathrm{GeV}}$ and $0.35\sqrt{E/\mathrm{GeV}}$ for the EMC and HAC sections, respectively. The timing resolution of the CAL was ~ 1 ns for energy deposits greater than 4.5 GeV. Scintillator-tile presampler detectors were mounted in front of the CAL. The RCAL was instrumented at a depth of 3.3 radiation lengths with a silicon-pad hadron-electron separator (HES). Charged particles were tracked in the central tracking detector (CTD) which operated in a magnetic field of 1.4 T provided by a thin superconducting solenoid, positioned inside the BCAL and presampler. The CTD was organised in nine superlayers with five axial layers and four stereo layers. Planar drift chambers provided additional tracking in the forward and rear directions. The small angle rear tracking detector (SRTD), consisting of two orthogonal planes of scintillator strips, was used to measure electrons at large θ_e. The angular coverage in the electron beam direction was extended with the addition of a small Tungsten-scintillator calorimeter (BPC), located behind the RCAL

Data Set		x Range		Q^2 Range GeV^2		$\mathcal{L}$ pb^{-1}	e^+/e^-	$\sqrt{s}$ GeV	x,Q^2 Reconstruction Method Equation	Reference
H1 svx-mb	95-00	5×10^{-6}	0.02	0.2	12	2.1	e^+p	301-319	10,14,16	[1]
H1 low Q^2	96-00	2×10^{-4}	0.1	12	150	22	e^+p	301-319	10,14,16	[2]
H1 NC	94-97	0.0032	0.65	150	30000	35.6	e^+p	301	15	[3]
H1 CC	94-97	0.013	0.40	300	15000	35.6	e^+p	301	11	[3]
H1 NC	98-99	0.0032	0.65	150	30000	16.4	e^-p	319	15	[4]
H1 CC	98-99	0.013	0.40	300	15000	16.4	e^-p	319	11	[4]
H1 NC HY	98-99	0.0013	0.01	100	800	16.4	e^-p	319	10	[5]
H1 NC	99-00	0.0013	0.65	100	30000	65.2	e^+p	319	15	[5]
H1 CC	99-00	0.013	0.40	300	15000	65.2	e^+p	319	11	[5]
ZEUS BPC	95	2×10^{-6}	6×10^{-5}	0.11	0.65	1.65	e^+p	301	10	[6]
ZEUS BPT	97	6×10^{-7}	0.001	0.045	0.65	3.9	e^+p	301	10, 15	[7]
ZEUS SVX	95	1.2×10^{-5}	0.0019	0.6	17	0.2	e^+p	301	10	[8]
ZEUS NC	96-97	6×10^{-5}	0.65	2.7	30000	30.0	e^+p	301	18	[9]
ZEUS CC	94-97	0.015	0.42	280	17000	47.7	e^+p	301	11	[10]
ZEUS NC	98-99	0.005	0.65	200	30000	15.9	e^-p	319	17	[11]
ZEUS CC	98-99	0.015	0.42	280	30000	16.4	e^-p	319	11	[12]
ZEUS NC	99-00	0.005	0.65	200	30000	63.2	e^+p	319	17	[13]
ZEUS CC	99-00	0.008	0.42	280	17000	60.9	e^+p	319	11	[14]

Table 1: H1 and ZEUS data sets used for the combination. The H1 svx-mb [1] and H1 low Q^2 [2] data sets comprise averages including data collected at E_p = 820 GeV [35,36] and E_p = 920 GeV. The formulae for x, Q^2 reconstruction are given in section 2.2.

at $z = -294$ cm close to the beam axis, and a silicon microstrip tracking device (BPT) installed in front of the BPC.

Both H1 and ZEUS were also equipped with photon taggers, positioned at $\simeq 100$ m down the e beam line, for a determination of the luminosity from Bethe-Heitler scattering, $ep \to ep\gamma$. The measurement accuracy of the luminosity was about 1 – 2% for each of the experiments.

2.4 Data Samples

A summary of the data used in this analysis is given in Table 1. In the first years until 1997, the proton beam energy E_p was set to 820 GeV. In 1998 it was increased to 920 GeV. The NC data cover a wide range in x and Q^2. The lowest $Q^2 \geq 0.045$ GeV^2 data come from the measurements of ZEUS using the BPC and BPT [6,7]. The Q^2 range from 0.2 GeV^2 to 1.5 GeV^2 is covered using special HERA runs, in which the interaction vertex position was shifted forward allowing for larger angles of the backward scattered electron to be accepted [1,8,35]. The lowest Q^2 for the shifted vertex data was reached using events, in which the effective electron beam energy was reduced by initial state radiation [1]. Values of $Q^2 \geq 1.5$ GeV^2 were measured using the nominal vertex settings. For $Q^2 \leq 10$ GeV^2, the cross section is very high and the data were collected using dedicated trigger setups [1,9,36]. The highest accuracy of the cross-section measurement is achieved for $10 \leq Q^2 \leq 100$ GeV^2 [2,9,36]. For $Q^2 \geq 100$ GeV^2, the statistical uncertainty of the data becomes relatively large. The high Q^2 data included here were collected with positron [3,5,9,13] and with electron [4,11] beams. The CC data for e^+p and e^-p scattering cover the range $300 \leq Q^2 \leq 30000$ GeV^2 [3,5,10,12,14].

3 Combination of the Measurements

3.1 Combination Method

The combination of the data sets uses the χ^2 minimisation method described in [1]. The χ^2 function takes into account the correlated systematic uncertainties for the H1 and ZEUS cross-section measurements. For a single data set the χ^2 is defined as

$$\chi^2_{\text{exp}}(\boldsymbol{m},\boldsymbol{b}) = \sum_i \frac{\left[m^i - \sum_j \gamma^i_j m^i b_j - \mu^i\right]^2}{\delta^2_{i,\text{stat}}\,\mu^i\left(m^i - \sum_j \gamma^i_j m^i b_j\right) + \left(\delta_{i,\text{uncor}}\, m^i\right)^2} + \sum_j b_j^2\,. \tag{19}$$

Here μ^i is the measured value at a point i and γ^i_j, $\delta_{i,\text{stat}}$ and $\delta_{i,\text{uncor}}$ are relative correlated systematic, relative statistical and relative uncorrelated systematic uncertainties, respectively. The function χ^2_{exp} depends on the predictions m^i for the measurements (denoted as the vector $\boldsymbol{m}$) and the shifts b_j (denoted as the vector $\boldsymbol{b}$) of the correlated systematic error sources. For the reduced cross-section measurements $\mu^i = \sigma^i_r$ and i denotes a (x, Q^2) point. The summation over j extends over all correlated systematic sources. The predictions m^i are given by the assumption that there is a single true value of the cross section corresponding to each data point i and each process, neutral or charged current e^+p or e^-p scattering.

Equation 19 takes into account that the quoted uncertainties are based on measured cross sections, which are subject to statistical fluctuations. Under the assumption that the statistical uncertainties are proportional to the square root of the number of events and that the systematic uncertainties are proportional to $\boldsymbol{m}$, the minimum of equation 19 provides an unbiased estimator of $\boldsymbol{m}$. For the present cross section measurements, the leading systematic uncertainties stem from the acceptance correction and luminosity determination. Therefore, the correlated and uncorrelated systematic uncertainties are of multiplicative nature, i.e. they increase proportionally to the central values. In equation 19 the multiplicative nature of these uncertainties is taken into account by multiplying the relative errors γ^i_j and $\delta_{i,\text{uncor}}$ by the expectation m^i. For the inclusive DIS cross-section measurements the background contribution is small and the statistical uncertainties are defined by the square root of the number of events used to determine σ^i_r. The expected number of events is determined by the expected cross section and it can be also corrected for the biases due to the correlated systematic uncertainties. This is taken into account by the $\delta^2_{i,\text{stat}}\,\mu^i\left(m^i - \sum_j \gamma^i_j m^i b_j\right)$ term.

Several data sets providing a number of measurements are represented by a total χ^2 function, which is built from the sum of the χ^2_{exp} functions for each data set e

$$\chi^2_{\text{tot}} = \sum_e \chi^2_{\text{exp},e}\,. \tag{20}$$

The data averaging procedure allows the rearrangement of equation 20 such that it takes a form similar to equation 19

$$\chi^2_{\text{tot}}(\boldsymbol{m},\boldsymbol{b'}) = \chi^2_{\text{min}} + \sum_{i=1}^{N_M} \frac{\left[m^i - \sum_j \gamma^{i,\text{ave}}_j m^i b'_j - \mu^{i,\text{ave}}\right]^2}{\delta^2_{i,\text{ave,stat}}\,\mu^{i,\text{ave}}\left(m^i - \sum_j \gamma^{i,\text{ave}}_j m^i b'_j\right) + \left(\delta_{i,\text{ave,uncor}}\, m^i\right)^2} + \sum_j (b'_j)^2. \tag{21}$$

Here $\mu^{i,\mathrm{ave}}$ is the average value at a point i and $\gamma_j^{i,\mathrm{ave}}$, $\delta_{i,\mathrm{ave,stat}}$ and $\delta_{i,\mathrm{ave,uncor}}$ are its relative correlated systematic, relative statistical and relative uncorrelated systematic uncertainties, respectively. The value of χ^2_{min} corresponds to the minimum of equation 20. The ratio $\chi^2_{\mathrm{min}}/n_{\mathrm{dof}}$ is a measure of the consistency of the data sets. The number of degrees of freedom, n_{dof}, is calculated as the difference between the total number of measurements and the number of averaged points N_M. The systematic uncertainties b'_j are obtained from the original ones, b_j, by an orthogonal transformation [1]. The summation of j extends over all independent systematic error sources.

The original double differential cross-section measurements are published with their statistical and systematic uncertainties. The statistical uncertainties correspond to $\delta_{i,\mathrm{stat}}$ in equation 19. The systematic uncertainties are classified as either point-to-point correlated or point-to-point uncorrelated, corresponding to γ_i^j and $\delta_{i,\mathrm{uncor}}$, respectively. Several measurements [7,8,10–14] are reported with asymmetric systematic uncertainties and they are symmetrised before performing the averaging. The resulting average is found to be insensitive to the details of the symmetrisation procedure. Global normalisations of the data sets are split into an overall normalisation uncertainty of 0.5%, common to all data sets, due to uncertainties of higher order corrections to the Bethe-Heitler process used for the luminosity calculation, and experimental uncertainties which are treated as correlated systematic sources γ_i^j. Sources of point-to-point correlated uncertainties may be in common for CC and NC data as well as for several data sets of the same experiment. The correlations of the systematic uncertainties across the data sets are given in table 5. The systematic uncertainties are treated as independent between H1 and ZEUS apart from the 0.5% overall normalisation uncertainty.

All the NC and CC cross-section data from H1 and ZEUS are combined in one simultaneous minimisation. Therefore resulting shifts of the correlated systematic uncertainties propagate coherently to both CC and NC data.

3.2 Corrections and Uncertainties

3.2.1 Extrapolation to Common (x, Q^2) Grid

Prior to the combination, the H1 and ZEUS data are transformed to a common grid of (x, Q^2) points. The grid points are chosen such that the interpolation corrections are minimal taking advantage of the fact that the original (x, Q^2) grids of the H1 and ZEUS experiments are similar. Furthermore, the chosen grid ensures that no two separate measurements of the same data set interpolate to a common grid point[3]. For $Q^2 \geq 0.2$ GeV^2, for the majority of the grid points both H1 and ZEUS measurements enter the combination. For some of the grid points there is no nearby counterpart from the other experiment, giving points in the combined cross section which originate from either H1 or ZEUS only. Note that through the systematic error correlation, such data points may be nevertheless shifted with respect to the original measurement in the averaging procedure.

The transformation of a measurement from the given (x, Q^2) to the nearest $(x_{\mathrm{grid}}, Q^2_{\mathrm{grid}})$ point on the grid is performed by multiplying the measured cross section by a ratio of theoretically

[3] An exception is made for the ZEUS SVX [8] data for which five pairs of points are first averaged using statistical uncertainties and then added to the combination.

calculated double differential cross sections at $(x_{\rm grid}, Q^2_{\rm grid})$ and (x, Q^2). This interpolation is repeated iteratively. For the first iteration, the H1 PDF 2000 parametrisation [5] is used for $Q^2 \geq 3$ GeV^2, where it is applicable, and the fractal model fit [1] for $Q^2 < 3$ GeV^2. For the second iteration, a QCD fit to the first iteration of the averaged data (see section 4) is used for $Q^2 \geq 3$ GeV^2 and the fractal model fit for $Q^2 < 3$ GeV^2. The difference between cross-section measurements obtained after the first and second iterations is smaller than a few per mille for the NC and 2% for the CC data. The QCD fit obtained using the data from the first iteration is to per mille precision identical to the fit obtained using the data from the second iteration. Therefore, no further iterations are performed. This procedure is checked using the ZEUS-JETS parametrisation [17] for the first iteration. The resulting cross-section difference is negligible compared to the experimental precision.

3.2.2 Centre-of-Mass Energy Correction

The data sets considered for the combination contain sub-samples taken with a proton beam energy of $E_p = 820$ GeV and $E_p = 920$ GeV. Both the CC and NC scattering reduced cross sections depend weakly on the energy via terms containing the inelasticity y. For the CC data for all values of y and for the NC data for $y < 0.35$, the uncertainty on the theoretically estimated difference between cross sections for $E_p = 820$ GeV and $E_p = 920$ GeV is negligible compared to the experimental precision. Therefore the data are corrected to a common centre-of-mass energy corresponding to $E_p = 920$ GeV and then averaged. The NC data for $y \geq 0.35$ are kept separate for the two proton beam energies.

The correction is calculated multiplicatively for the CC data which is given in full double differential form

$$\frac{\mathrm{d}^2\sigma^{e^\pm p}_{\mathrm{CC\ 920}}}{\mathrm{d}x\mathrm{d}Q^2} = \frac{\mathrm{d}^2\sigma^{e^\pm p}_{\mathrm{CC\ 820}}}{\mathrm{d}x\mathrm{d}Q^2}\left[\frac{\mathrm{d}^2\sigma^{\mathrm{th},\ e^\pm p}_{\mathrm{CC\ 920}}}{\mathrm{d}x\mathrm{d}Q^2}\Big/\frac{\mathrm{d}^2\sigma^{\mathrm{th},\ e^\pm p}_{\mathrm{CC\ 820}}}{\mathrm{d}x\mathrm{d}Q^2}\right] \tag{22}$$

and additively for the NC data which is quoted in reduced double differential form

$$\sigma^{\pm}_{r,\mathrm{NC\ 920}} = \sigma^{\pm}_{r,\mathrm{NC\ 820}} + \Delta\sigma^{\mathrm{th},\pm}_{r,\mathrm{NC}}(x, Q^2, y_{820}, y_{920})\,. \tag{23}$$

Here y_{820} and y_{920} are the inelasticities for the two proton beam energies calculated as $y = Q^2/4E_eE_px$. The theoretical cross sections follow the same prescription used for the extrapolation correction in section 3.2.1. For the neutral current case,

$$\Delta\sigma^{\mathrm{th},\pm}_{r,\mathrm{NC}}(x, Q^2, y_{820}, y_{920}) = \tilde{F}^{\mathrm{th}}_L(x, Q^2)\left[\frac{y^2_{820}}{Y_{+\,820}} - \frac{y^2_{920}}{Y_{+\,920}}\right] + x\tilde{F}^{\mathrm{th}}_3(x, Q^2)\left[\pm\frac{Y_{-\,820}}{Y_{+\,820}} \mp \frac{Y_{-\,920}}{Y_{+\,920}}\right], \tag{24}$$

where $Y_{\pm\,820,920} = 1 \pm (1 - y_{820,920})^2$. The largest uncertainty in equation 24 stems from the calculation of the structure function $\tilde{F}^{\mathrm{th}}_L$. To estimate the uncertainty on the combined data arising from the centre-of-mass energy correction another average is performed assuming $\tilde{F}^{\mathrm{th}}_L = 0$. The difference between this and the nominal average is at most 0.1% and thus the uncertainty on the averaged cross section resulting from the centre-of-mass energy correction is negligible.

3.2.3 Procedural Uncertainties

The χ^2 function given by equation 19 treats all systematic uncertainties as multiplicative, i.e. proportional to the expected central values. While this generally holds for the normalisation uncertainties, this may not be the case for the other uncertainties. To study the sensitivity of the average result to this issue, an alternative averaging is performed, for which only normalisation uncertainties are taken as multiplicative while all other uncertainties are treated as additive. The difference between this average and the nominal average result is used as a correlated procedural error $\delta_{\text{ave,rel}}$. The typical size of $\delta_{\text{ave,rel}}$ is below 0.5% for the low Q^2 data reaching a few percent for high Q^2.

The H1 and ZEUS collaborations use similar methods for detector calibration and employ similar Monte Carlo simulation models for radiative corrections, for the hadronic final state simulation and for photoproduction background subtraction. Such similarities may lead to correlations between the H1 and ZEUS measurements. To investigate the effect of possible correlations, 12 sources of similar systematic uncertainties of the two experiments are identified. These are related to the photoproduction background, the electromagnetic and hadronic energy scales and the electron scattering angle. Then 2^{12} different averages are calculated assuming each of the 12 pairs to be correlated or uncorrelated, and these alternative averages are compared to the nominal average for which all sources are assumed to be uncorrelated. By studying these averages it is found that the only two systematic sources which result in significantly different average cross sections are the photoproduction background and the hadronic energy scale. The differences between the nominal average and the averages in which systematic sources for the photoproduction background and hadronic energy scale are considered to be correlated are taken as additional procedural uncertainties $\delta_{\text{ave},\gamma p}$ and $\delta_{\text{ave,had}}$. Typical values of $\delta_{\text{ave},\gamma p}$ and $\delta_{\text{ave,had}}$ are below 0.5%. As expected, $\delta_{\text{ave},\gamma p}$ is larger at high $y > 0.5$ while $\delta_{\text{ave,had}}$ is significant for low y only.

3.3 Results

The average NC and CC cross sections and the structure function F_2 together with statistical, uncorrelated systematic and procedural uncertainties are given in tables 6-17. The full information about correlation between cross-section measurements can be found elsewhere [37]. The total integrated luminosity of the combined data set corresponds to about 200 pb^{-1} for e^+p and 30 pb^{-1} for e^-p. In total 1402 data points are combined to 741 cross-section measurements. The data show good consistency, with $\chi^2/n_{\text{dof}} = 636.5/656$. For the measurement at the point i of the data set e which has measurements of other data sets averaging to the same (x, Q^2) point, the pull $p^{i,e}$ can be defined

$$p^{i,e} = \frac{\mu^{i,e} - \mu^{i,\text{ave}} \left(1 - \sum_j \gamma_j^{i,e} b_{j,\text{ave}}\right)}{\sqrt{\Delta_{i,e}^2 - \Delta_{i,\text{ave}}^2}}, \tag{25}$$

where $\Delta_{i,e}$ ($\Delta_{i,\text{ave}}$) is the statistical and uncorrelated systematic uncertainty added in quadrature for the measurement e (average). The distribution of pulls shows no tensions for all processes across the kinematic plane, see figure 1.

Data set	Shift	
	b	$(b\gamma_{\text{norm}})$
H1 svx-mb [1]	−0.24	(−0.2%)
H1 low Q^2 [2]	−0.45	(−0.4%)
H1 94 – 97 [3]	−0.65	(−0.9%)
H1 98 – 99 [4,5]	−0.05	(−0.1%)
H1 99 – 00 [5]	−0.19	(−0.3%)
ZEUS BPC [6]	0.23	(0.3%)
ZEUS BPT [7]	−0.03	(−0.1%)
ZEUS SVX [8]	0.78	(1.2%)
ZEUS 94 – 97 [9,10]	0.44	(0.8%)
ZEUS 96 – 97 low Q^2 [9]	−1.10	(−1.1%)
ZEUS 98 – 99 [11,12]	0.05	(0.1%)
ZEUS 99 – 00 [13,14]	−0.18	(−0.4%)

Table 2: Shifts of global normalisation of the data sets in units of the normalisation uncertainty (and in percent of the original cross sections).

There are in total 110 sources of correlated systematic uncertainty, including global normalisations, characterising the separate data sets. None of these systematic sources shifts by more than $2\,\sigma$ of the nominal value in the averaging procedure. The distribution of pulls for the correlated systematic sources, defined as $p_s = b_{j,\text{ave}}/(1-\Delta^2_{b_j,\text{ave}})^{1/2}$, where $\Delta_{b_j,\text{ave}}$ is the uncertainty of the source j after the averaging, is given in figure 2. The shifts of the global normalisation for each input data set are given in table 2. The absolute normalisation of the combined data set is to a large extent defined by the most precise measurements of NC e^+p cross section in the $10 \le Q^2 \le 100$ GeV^2 kinematic range. Here the H1 [2] and ZEUS [9] results move towards each other and the other data sets follow this adjustment.

The influence of several correlated systematic uncertainties is reduced significantly for the averaged result. For example, the uncertainty due to the H1 LAr calorimeter energy scale is reduced by 55% while the uncertainty due to the ZEUS photoproduction background is reduced by 65%. There are two main reasons for this significant reduction. Since H1 and ZEUS use different reconstruction methods, described in section 2.2, similar systematic sources influence the measured cross section differently as a function of x and Q^2. Therefore, requiring the cross sections to agree at all x and Q^2 constrains the systematics efficiently. In addition, for certain regions of the phase space, one of the two experiments has superior precision compared to the other. For these regions, the less precise measurement is fitted to the more precise one, with a simultaneous reduction of the correlated systematic uncertainty. This reduction propagates to the other average points, including those which are based solely on the measurement from one experiment.

For $Q^2 \ge 100$ GeV^2 the precision of the H1 and ZEUS measurements is about equal and thus the systematic uncertainties are reduced uniformly. For $2.5 \le Q^2 < 100$ GeV^2 and for $Q^2 < 1$ GeV^2 the precision is dominated by the H1 [1,2] and by the ZEUS [7] measurements, respectively. Therefore the overall reduction of the uncertainties is smaller, and it is essentially obtained from the reduction of the correlated systematic uncertainty. For example, for $Q^2 \sim 30$ GeV^2 the obtained precision of 1.1% is dominated by the data of [2], where 1.3% uncertainties are reported. The correlated error part of the full uncertainty is reduced from about

75% in [2] to 55% in the combined measurement. The total uncertainty is typically smaller than 2% for $3 < Q^2 < 500$ GeV^2 and reaches 1% for $20 < Q^2 < 100$ GeV^2. The uncertainties are larger for high inelasticity $y > 0.6$ due to the photoproduction background.

In figures 3 and 4, averaged data are compared to the input H1 and ZEUS data. In figures 5 and 6, the combined NC e^+p data at very low Q^2 and at low Q^2 are shown. In figures 7 and 8, the combined NC e^+p and e^-p data at high Q^2 are shown. In figure 9 the e^+p NC reduced cross section, for $Q^2 > 1\,\text{GeV}^2$, is shown as a function of Q^2 for the HERA combined e^+p data and for fixed-target data [38,39] across the whole of the measured kinematic plane. The combined NC $e^\pm p$ reduced cross sections are compared in the high-Q^2 region in figure 10. In figures 11 and 12 the combined data set is shown for CC scattering at high Q^2. The HERAPDF1.0 fit, described in the next section, is compared to the data in the kinematic region suitable for the application of perturbative QCD.

4 QCD Analysis of the Combined Data

4.1 Definition of χ^2 and Treatment of Systematic Uncertainties

The combined data set on NC and CC e^+p and e^-p inclusive cross sections is used as the sole input for a next-to-leading order (NLO) QCD PDF fit, called HERAPDF1.0. The form of the χ^2 used for this fit follows equation 19. The consistency of the present input data justifies the use of the conventional χ^2 tolerance, $\Delta\chi^2 = 1$, when determining the experimental uncertainties on the HERAPDF1.0 fit.

The role of correlated systematic uncertainties should be considered carefully when defining the χ^2 for PDF fits. Global fits have used the Hessian method [40,41], the Offset method [42,43] and quadratic combination [44,45]. In fits to HERA data alone, H1 have used the Hessian method [2,5] and ZEUS have used the Offset method [17]. These different methods can lead to quite different estimates of the PDF central values and uncertainties [46,47], with the Offset method giving the largest uncertainties if the correlated systematic uncertainties are larger than the statistical uncertainties of the data sets.

In the present analysis, the combination of the H1 and ZEUS data sets is done by a Hessian procedure under the assumption that there is only one true cross-section value for each process (NC or CC, e^+p or e^-p scattering) at each (x, Q^2) point. This results in a data set with correlated systematic uncertainties which are smaller or comparable to the statistical and uncorrelated uncertainties. Thus the central values and experimental uncertainties on the PDFs which are extracted from the combined data are not much dependent on the method of treatment of correlated systematic uncertainties in the fitting procedure. The most conservative estimate of uncertainties still results from the use of the Offset method for all 113 systematic errors. However, this procedure is very cumbersome and in practice a very similar uncertainty estimate is obtained from using the Offset method only for the largest correlated systematic errors, namely the three procedural errors (see section 3.2.3). Thus for the central fit, the 110 systematic uncertainties which result from the ZEUS and H1 data sets are combined in quadrature, and the three sources of uncertainty which result from the combination procedure are treated by the offset method. The χ^2 per degree of freedom for this fit is 574/582; for a fit combining all 113

uncertainties in quadrature the χ^2 is 532 and for a fit treating all 113 by the Hessian method the χ^2 is 579. The resulting experimental uncertainties on the PDFs are small. Therefore, a thorough consideration of further uncertainties due to model assumptions and parametrisation dependence is necessary.

4.2 Theoretical Formalism and Assumptions

The QCD predictions for the structure functions are obtained by solving the DGLAP evolution equations [21–25] at NLO in the $\overline{\text{MS}}$ scheme with the renormalisation and factorisation scales chosen to be Q^2. The programme QCDNUM [48] is used and checked against the programme QCDfit [49]. The DGLAP equations yield the PDFs at all values of Q^2 if they are provided as functions of x at some input scale Q_0^2. This scale is chosen to be $Q_0^2 = 1.9$ GeV^2 such that the starting scale is below the charm mass threshold, $Q_0^2 < m_c^2$. The light quark coefficient functions are calculated in QCDNUM. The heavy quark coefficient functions are calculated in the general-mass variable-flavour-number scheme of [50], with recent modifications [51,52]. The heavy quark masses $m_c = 1.4$ GeV and $m_b = 4.75$ GeV are chosen following [45]. The strong coupling constant is fixed to $\alpha_s(M_Z^2) = 0.1176$ [19].

The HERA data have a minimum invariant mass of the hadronic system, W, of 15 GeV and a maximum x of 0.65, such that they are in a kinematic region where there is no sensitivity to target mass and large-x higher-twist contributions. A minimum Q^2 cut of $Q^2_{min} = 3.5$ GeV^2 is imposed to remain in the kinematic region where perturbative QCD should be applicable.

PDFs are parametrised at the input scale by the generic form

$$xf(x) = Ax^B(1-x)^C(1+\epsilon\sqrt{x}+Dx+Ex^2). \tag{26}$$

The parametrised PDFs are the gluon distribution xg, the valence quark distributions xu_v, xd_v, and the u-type and d-type anti-quark distributions $x\bar{U}$, $x\bar{D}$. Here $x\bar{U} = x\bar{u}$, $x\bar{D} = x\bar{d} + x\bar{s}$ at the chosen starting scale. The central fit is found by first setting the ϵ, D and E parameters to zero (this leaves 9 parameters free) and then introducing them in the fit procedure, one at a time, to determine the best fit. The best 10 parameter fit has $E_{u_v} \neq 0$. The other ϵ, D and E parameters are then added, one at a time, to determine the best 11 parameter fit. The 11 parameter fits do not represent a significant improvement in fit quality compared to the best 10 parameter fit[4]. The 10 parameter fit, selected as the central fit, has a good χ^2 per degree of freedom, 574/582, and satisfies the criteria that all the PDFs are positive and they obey the valence quark approximation that $xd_v > x\bar{d}$ at large x. The resulting parametrisations are

$$xg(x) = A_g x^{B_g}(1-x)^{C_g}, \tag{27}$$
$$xu_v(x) = A_{u_v} x^{B_{u_v}}(1-x)^{C_{u_v}}\left(1+E_{u_v}x^2\right), \tag{28}$$
$$xd_v(x) = A_{d_v} x^{B_{d_v}}(1-x)^{C_{d_v}}, \tag{29}$$
$$x\bar{U}(x) = A_{\bar{U}} x^{B_{\bar{U}}}(1-x)^{C_{\bar{U}}}, \tag{30}$$
$$x\bar{D}(x) = A_{\bar{D}} x^{B_{\bar{D}}}(1-x)^{C_{\bar{D}}}. \tag{31}$$

The normalisation parameters, A_g, A_{u_v}, A_{d_v}, are constrained by the quark number sum rules and momentum sum rule. The B parameters $B_{\bar{U}}$ and $B_{\bar{D}}$ are set equal, $B_{\bar{U}} = B_{\bar{D}}$, such that there is

[4]The largest decrease in χ^2 is $\Delta\chi^2 = -5$, for a fit which has $xd_v < x\bar{d}$ at large x.

	A	B	C	E
xg	6.8	0.22	9.0	
xu_v	3.7	0.67	4.7	9.7
xd_v	2.2	0.67	4.3	
$x\bar{U}$	0.113	−0.165	2.6	
$x\bar{D}$	0.163	−0.165	2.4	

Table 3: Central values of the HERAPDF1.0 parameters.

Variation	Standard Value	Lower Limit	Upper Limit
f_s	0.31	0.23	0.38
m_c [GeV]	1.4	1.35[(a)]	1.65
m_b [GeV]	4.75	4.3	5.0
Q^2_{min} [GeV^2]	3.5	2.5	5.0
Q^2_0 [GeV^2]	1.9	1.5[(b)]	2.5[(c,d)]
		[(a)] $Q^2_0 = 1.8$	[(c)] $m_c = 1.6$
		[(b)] $f_s = 0.29$	[(d)] $f_s = 0.34$

Table 4: Standard values of input parameters and the variations considered.

a single B parameter for the sea distributions. The strange quark distribution is expressed as x-independent fraction, f_s, of the d-type sea, $x\bar{s} = f_s x\bar{D}$ at Q^2_0. The central value $f_s = 0.31$ is chosen to be consistent with determinations of this fraction using neutrino-induced di-muon production [45,53]. The further constraint $A_{\bar{U}} = A_{\bar{D}}(1 - f_s)$, together with the requirement $B_{\bar{U}} = B_{\bar{D}}$, ensures that $x\bar{u} \to x\bar{d}$ as $x \to 0$. For the central fit, the valence B parameters, B_{u_v} and B_{d_v} are also set equal, but this assumption is dropped when parametrisation variations are considered. The central values of the parameters are given in Table 3.

Model uncertainties and parametrisation uncertainties of the central fit solution are evaluated by varying the input assumptions. The variation of numerical values chosen for the central fit is specified in Table 4. The variation of f_s is chosen to span the ranges determined in [45,53]. The variations of Q^2_0 and f_s are not independent, since QCD evolution will ensure that the strangeness fraction increases as Q^2_0 increases. The value $f_s = 0.29$ is used for $Q^2_0 = 1.5$ GeV^2 and the value $f_s = 0.34$ is used for $Q^2_0 = 2.5$ GeV^2 in order to be consistent with the choice $f_s = 0.31$ at $Q^2_0 = 1.9$ GeV^2. The variations of Q^2_0 and m_c are also not independent, since $Q_0 < m_c$ is required in the fit programme. Thus when $m_c = 1.35$ GeV, the starting scale used is $Q^2_0 = 1.8\,\text{GeV}^2$. Similarly, when $Q^2_0 = 2.5$ GeV^2 the charm mass used is $m_c = 1.6$ GeV. In practice, the variations of f_s, m_c, m_b, mostly affect the model uncertainty of the $x\bar{s}$, $x\bar{c}$, $x\bar{b}$, quark distributions, respectively, and have little effect on other parton flavours. The difference between the central fit and the fits corresponding to model variations of m_c, m_b, f_s, Q^2_{min} are added in quadrature, separately for positive and negative deviations, and represent the model uncertainty of the HERAPDF1.0 set.

The variation in Q^2_0 is regarded as a parametrisation uncertainty, rather than a model uncertainty. At the starting scale the gluon parametrisation is valence like. For the downward variation of the starting scale, $Q^2_0 = 1.5$ GeV^2, a parametrisation which explicitly allows for a negative gluon contribution at low x is considered: a term of the form $A'_g x^{B'_g}(1-x)^{C'_g}$ is subtracted from the gluon of the standard parametrisation, where $C'_g = 25$ is fixed[5] and A'_g and B'_g

[5]The fit is not sensitive to this value provided it is high enough ($C'_g > 15$) that the term does not contribute at

are fitted. The variations of Q_0^2 mostly increase the PDF uncertainties of the sea and gluon at small x. A further variation of parametrisation, allowing $B_{u_v} \neq B_{d_v}$, increases the uncertainties on the valence quarks at low x. Finally, variation of the number of terms in the polynomial $(1 + \epsilon\sqrt{x} + Dx + Ex^2)$ is considered for each fitted parton distribution. All the 11 parameter fits which have $E_{u_v} \neq 0$ and one more ϵ, D or E parameter non-zero are considered as possible variants[6]. In practice only a small number of them have significantly different PDF shapes from the central fit, notably: $D_{u_v} \neq 0$, $D_{\bar{U}} \neq 0$ and $D_{\bar{D}} \neq 0$. These variations mostly increase the PDF uncertainty at high x, but the valence PDFs at low x are also affected because of the constraint of the quark number sum rules. The difference between all these parametrisation variations and the central fit is stored and an envelope representing the maximal deviation at each x value is constructed to represent the parametrisation uncertainty. This parametrisation uncertainty should be regarded as indicative rather than exhaustive, for example the reduction on the high-x gluon uncertainty at $x \approx 0.5$ is due to restrictions of the parameterisations rather than a strong data constraint. The total PDF uncertainty is obtained by adding in quadrature experimental, model and parametrisation uncertainties.

In summary, the HERAPDF1.0 analysis has two notable features. Firstly, it uses a consistent data set with small correlated systematic uncertainties and applies the conventional χ^2 tolerance, $\Delta\chi^2 = 1$, when determining the experimental uncertainties on the PDFs. This data set includes four different processes, NC and CC, e^+p and e^-p scattering, such that there is sufficient information to extract $x\bar{U}$, $x\bar{D}$, xd_v, xu_v PDFs and the gluon PDF from the scaling violations. Secondly, this analysis makes an assessment of uncertainties introduced both by model assumptions and by assumptions about the form of the parametrisation.

4.3 Fit Results

Figures 13-15 show the HERAPDF1.0 distributions, xu_v, xd_v, xS, xg, as a function of x at the starting scale $Q^2 = 1.9\,\text{GeV}^2$ and at $Q^2 = 10$ and 10000 GeV^2, where $xS = 2x(\bar{U} + \bar{D})$ is the sea PDF. Note that for $Q^2 > m_c^2$, $x\bar{U} = x\bar{u} + x\bar{c}$, and for $Q^2 > m_b^2$, $x\bar{D} = x\bar{d} + x\bar{s} + x\bar{b}$, so that the heavy quarks are included in the sea distributions. The break-up of xS into the flavours $xu_{sea} = 2x\bar{u}$, $xd_{sea} = 2x\bar{d}$, $xs_{sea} = 2x\bar{s}$, $xc_{sea} = 2x\bar{c}$, $xb_{sea} = 2x\bar{b}$ is illustrated so that the relative importance of each flavour at different Q^2 may be assessed. Fractional uncertainty bands are shown below each PDF. The experimental, model and parametrisation uncertainties are shown separately. The model and parametrisation uncertainties are asymmetric. For the sea and gluon distributions, the variations in parametrisation which have non-zero ϵ, D and E affect the large-x region, and the uncertainties arising from the variation of Q_0^2 and Q_{min}^2 affect the small-x region. In particular the parametrisation variation which includes a negative gluon term increases the uncertainty on the gluon at low x and low Q^2. However the gluon distribution itself is not negative in the fitted kinematic region. For the valence distributions the non-zero ϵ, D and E parametrisation uncertainty is important for all x, and is their dominant uncertainty. The total uncertainties at low x decrease with increasing Q^2 due to QCD evolution and reach, for instance, 2% uncertainty on xg at $Q^2 = 10000$ GeV^2 and $x < 0.01$.

The break-up of the PDFs into different flavours is further illustrated in figures 16 and 17, where the quark distributions $xU, xD, x\bar{U}, x\bar{D}$ and $x\bar{u}, x\bar{d}, x\bar{c}, x\bar{s}$ are shown at $Q^2 = 10$ GeV^2.

large x.

[6]The criteria that all PDFs should be positive or that $xd_v > x\bar{d}$ at high x are not imposed on these variants.

The PDFs $xU, xD, x\bar{U}, x\bar{D}$ are closely related to the measurements, see equations 3, 9, and are very well constrained at low x. The U flavour is better constrained than the D flavour because of the dominance of this flavour in all interactions except e^+p CC scattering. The quark distributions $x\bar{d}, x\bar{s}$ are derived from $x\bar{D}$ through the assumption on the value of f_s, and the uncertainty on $x\bar{s}$ directly reflects the uncertainty on this fraction. The uncertainty on $x\bar{d}$ follows closely that on $x\bar{D}$ and the uncertainty on $x\bar{u}$ follows closely that on $x\bar{U}$. The charm PDF, $x\bar{c}$, is shown at $Q^2 = 10$ GeV^2, so that the condition $Q^2 \gg m_c^2$ is fulfilled and it may be regarded as a fully active parton. However, it is strongly related to the gluon density such that it is affected by the same variations which affect the gluon PDF (variation of Q_0^2 and Q_{min}^2) as well as by the variation of m_c. The dominant uncertainty on the charm PDF comes from the variation $Q_0^2 = 2.5$ GeV^2. The uncertainty on the bottom PDF, $x\bar{b}$ (not shown), is dominated by the variation of m_b.

Figure 18 shows summary plots of the HERAPDF1.0 distributions at the starting scale $Q^2 = 1.9$ GeV^2 and at $Q^2 = 10$ GeV^2. Figure 19 shows such plots on a logarithmic scale such that the behaviour and the uncertainties of the PDFs at high x are emphasised.

A cross check of the sensitivity to the heavy-flavour treatment is made by performing a fit using an alternative general-mass variable-flavour-number scheme, the ACOT scheme [54]. The result of this fit is shown for $Q^2 = 10$ GeV^2 in figure 20. The PDFs determined using the ACOT scheme are within the total uncertainty of the standard fit.

The sensitivity of the HERAPDF1.0 fit to the value of α_S is estimated by varying α_S by ± 0.002 [19]. Only the gluon PDF is significantly affected. The change of the gluon PDF is outside the total uncertainty bands of the standard fit, as illustrated in figure 21.

5 Conclusions

Inclusive cross sections of neutral and charged current $e^\pm p$ scattering measured by the H1 and ZEUS Collaborations are combined. The kinematic range of the NC data extends from $6 \cdot 10^{-7}$ to 0.65 in Bjorken x for $0.045 \leq Q^2 \leq 30000\,\text{GeV}^2$ and inelasticity values y between 0.005 and 0.95. The CC data cover a range $0.013 \leq x \leq 0.4$ and $300 \leq Q^2 \leq 30000\,\text{GeV}^2$ for y between 0.037 and 0.76. The combination comprises all inclusive data from the first period of the operation of HERA. The input data from H1 and ZEUS are consistent with each other at $\chi^2/n_{\text{dof}} = 636.5/656$. The total uncertainty of the combined data set reaches 1% for NC scattering in the best measured region, $20 < Q^2 < 100$ GeV^2.

A NLO QCD analysis is performed based exclusively on these combined $e^\pm p$ scattering cross-section data. A new set of parton distribution functions, HERAPDF1.0, is obtained using a variable-flavour-number scheme. The analysis yields small experimental uncertainties and includes estimates for model and parametrisation uncertainties. Due to the precision of the combined data set, the parametrisation HERAPDF1.0 has total uncertainties at the level of a few percent at low x.

Acknowledgements

We are grateful to the HERA machine group whose outstanding efforts have made these experiments possible. We appreciate the contributions to the construction and maintenance of the H1 and ZEUS detectors of many people who are not listed as authors. We thank our funding agencies for financial support, the DESY technical staff for continuous assistance and the DESY directorate for their support and for the hospitality they extended to the non-DESY members of the collaborations.

References

[1] F. Aaron *et al.* [H1 Collaboration] (2009), [arXiv:0904.0929].

[2] F. Aaron *et al.* [H1 Collaboration] (2009), [arXiv:0904.3513].

[3] C. Adloff *et al.* [H1 Collaboration], Eur. Phys. J. **C13**, 609 (2000), [hep-ex/9908059].

[4] C. Adloff *et al.* [H1 Collaboration], Eur. Phys. J. **C19**, 269 (2001), [hep-ex/0012052].

[5] C. Adloff *et al.* [H1 Collaboration], Eur. Phys. J. C **30**, 1 (2003), [hep-ex/0304003].

[6] J. Breitweg *et al.* [ZEUS Collaboration], Phys. Lett. **B407**, 432 (1997), [hep-ex/9707025].

[7] J. Breitweg *et al.* [ZEUS Collaboration], Phys. Lett. B **487**, 53 (2000), [hep-ex/0005018].

[8] J. Breitweg *et al.* [ZEUS Collaboration], Eur. Phys. J. **C7**, 609 (1999), [hep-ex/9809005].

[9] S. Chekanov *et al.* [ZEUS Collaboration], Eur. Phys. J. C **21**, 443 (2001), [hep-ex/0105090].

[10] J. Breitweg *et al.* [ZEUS Collaboration], Eur. Phys. J. C **12**, 411 (2000), [Erratum-ibid. C**27** (2003) 305, [hep-ex/9907010].

[11] S. Chekanov *et al.* [ZEUS Collaboration], Eur. Phys. J. **C28**, 175 (2003), [hep-ex/0208040].

[12] S. Chekanov *et al.* [ZEUS Collaboration], Phys. Lett. **B539**, 197 (2002), [Erratum-ibid. B**552** (2003) 308], [hep-ex/0205091].

[13] S. Chekanov *et al.* [ZEUS Collaboration], Phys. Rev. D **70**, 052001 (2004), [hep-ex/0401003].

[14] S. Chekanov *et al.* [ZEUS Collaboration], Eur. Phys. J. **C32**, 1 (2003), [hep-ex/0307043].

[15] A. Glazov, AIP Conf. Proc. **792**, 237 (2005).

[16] M. Klein and R. Yoshida, Prog. Part. Nucl. Phys. **61**, 343 (2008), [arXiv:0805.3334].

[17] S. Chekanov *et al.* [ZEUS Collaboration], Eur. Phys. J. **C42**, 1 (2005), [hep-ph/0503274].

[18] M. Klein and T. Riemann, Z. Phys. C **24**, 151 (1984).

[19] C. Amsler *et al.* (Particle Data Group), Phys. Lett. **B667**, 1 (2008).

[20] C. G. Callan and D. J. Gross, Phys. Rev. Lett. **22**, 156 (1969).

[21] V. N. Gribov and L. N. Lipatov, Sov. J. Nucl. Phys. **15**, 438 (1972).

[22] V. N. Gribov and L. N. Lipatov, Sov. J. Nucl. Phys. **15**, 675 (1972).

[23] L. N. Lipatov, Sov. J. Nucl. Phys. **20**, 94 (1975).

[24] Y. L. Dokshitzer, Sov. Phys. JETP **46**, 641 (1977).

[25] G. Altarelli and G. Parisi, Nucl. Phys. B **126**, 298 (1977).

[26] F. Jacquet and A. Blondel, in *ep Facility for Europe, Hamburg 1979* (DESY 79/48, 1979).

[27] U. Bassler and G. Bernardi, Nucl. Instr. and Meth. A **361**, 197 (1995), [hep-ex/9412004].

[28] S. Bentvelsen *et al.*, in *Proc. of the Workshop on HERA Physics*, edited by W. Buchmuller and G. Ingelman (DESY, Hamburg, 1992), vol. 1, p. 23.

[29] K. Hoeger, in *Proc. of the Workshop on HERA Physics*, edited by W. Buchmuller and G. Ingelman (DESY, Hamburg, 1992), vol. 1, p. 43.

[30] M. Derrick *et al.* [ZEUS Collaboration], Z. Phys. **C72**, 399 (1996), [hep-ex/9607002].

[31] I. Abt *et al.* [H1 Collaboration], Nucl. Instr. and Meth. A **386**, 310 (1997).

[32] I. Abt *et al.* [H1 Collaboration], Nucl. Instr. and Meth. A **386**, 348 (1997).

[33] R. D. Appuhn *et al.* [H1 Collaboration], Nucl. Instr. and Meth. A **386**, 397 (1997).

[34] ZEUS Collaboration, U. Holm (editor)., the ZEUS Detector. Status Report (unpublished), DESY (1993), URL http://www-zeus.desy.de/bluebook/bluebook.html.

[35] C. Adloff *et al.* [H1 Collaboration], Nucl. Phys. B **497**, 3 (1997), [hep-ex/9703012].

[36] C. Adloff *et al.* [H1 Collaboration], Eur. Phys. J. C **21**, 33 (2001), [hep-ex/0012053].

[37] The combined data together with the full correlation information is provided at URL https://www.desy.de/h1zeus/ .

[38] A. Benvenuti *et al.* [BCDMS Collaboration], Phys. Lett. **B223**, 485 (1989).

[39] M. Arneodo *et al.* [NMC Collaboration], Nucl. Phys. **B483**, 3 (1997).

[40] J. Pumplin *et al.*, JHEP **0207**, 012 (2002), [hep-ph/0201195].

[41] S. Alekhin, Phys. Rev. D **68**, 014002 (2003), [hep-ph/0211096].

[42] M. Botje, Eur. Phys. J. **C14**, 285 (2000), [hep-ph/9912439].

[43] S. Chekanov *et al.* [ZEUS Collaboration], Phys. Rev. D **67**, 012007 (2003), [hep-ex/0208023].

[44] A. D. Martin, R. G. Roberts, W. J. Stirling, and R. S. Thorne, Eur. Phys. J. **C23**, 73 (2002), [hep-ph/0110215].

[45] A. D. Martin, W. J. Stirling, R. S. Thorne, and G. Watt (2009), [arXiv:0901.0002].

[46] A. Cooper-Sarkar and C. Gwenlan (2005), [hep-ph/0508304].

[47] S. I. Alekhin, Nucl. Instrum. Meth. **A502**, 761 (2003).

[48] M. Botje, QCDNUM version 17β, URL http://www.nikhef.nl/h24/qcdnum/index.html.

[49] C. Pascaud and F. Zomer, preprint LAL-95-05.

[50] R. S. Thorne and R. G. Roberts, Phys. Rev. D **57**, 6871 (1998), [hep-ph/9709442].

[51] R. S. Thorne, Phys. Rev. **D73**, 054019 (2006), [hep-ph/0601245].

[52] R. S. Thorne, private communication, 2008.

[53] P. M. Nadolsky *et al.*, Phys. Rev. **D78**, 013004 (2008), [arXiv:0802.0007].

[54] M. Kramer, F. I. Olness, and D. E. Soper, Phys. Rev. **D62**, 096007 (2000), [hep-ph/0003035].

Source	Data Samples
H1 E'_e	δ_1 H1 NC[4] — δ_1 H1 NC HY[5] — δ_1 H1 NC[3] — δ_1 H1 NC[5]
H1 E_h	δ_2 H1 CC[3] — δ_2 H1 CC[5] — δ_2 H1 CC[4] — δ_3 H1 NC[4] — δ_3 H1 NC HY[5] — δ_3 H1 NC[3] — δ_3 H1 NC[5]
H1 γp asymmetry	δ_6 H1 NC HY[5] — δ_6 H1 NC[5]
H1 γp background	δ_4 H1 CC[3] — δ_4 H1 CC[5] — δ_4 H1 CC[4] — δ_5 H1 NC[4] — δ_5 H1 NC HY[5] — δ_5 H1 NC[3] — δ_5 H1 NC[5]
H1 θ_e	δ_2 H1 NC[4] — δ_2 H1 NC HY[5] — δ_2 H1 NC[5]
H1 CC cuts	δ_1 H1 CC[5] — δ_1 H1 CC[4]
H1 LAr Noise	δ_3 H1 CC[3] — δ_3 H1 CC[5] — δ_3 H1 CC[4] — δ_4 H1 NC[4] — δ_4 H1 NC HY[5] — δ_4 H1 NC[3] — δ_4 H1 NC[5]
H1 Lumi 94 – 97	δ_5 H1 CC[3] — δ_6 H1 NC[3]
H1 Lumi 98 – 99	δ_5 H1 CC[4] — δ_6 H1 NC[4] — δ_7 H1 NC HY[5]
H1 Lumi 99 – 00	δ_5 H1 CC[5] — δ_7 H1 NC[5]
ZEUS E'_e	δ_1 ZEUS NC[11] — δ_1 ZEUS NC[13]
ZEUS E_h a	δ_1 ZEUS CC[12] — δ_1 ZEUS CC[14]
ZEUS E_h b	δ_2 ZEUS CC[12] — δ_2 ZEUS CC[14]
ZEUS E_h in BCAL	δ_2 ZEUS CC[10] — δ_6 ZEUS NC[9]
ZEUS E_h in FCAL	δ_1 ZEUS CC[10] — δ_5 ZEUS NC[9]
ZEUS δ cut	δ_8 ZEUS BPC[6] — δ_1 ZEUS BPT[7]
ZEUS γp background	δ_2 ZEUS NC[11] — δ_2 ZEUS NC[13]
ZEUS γp background	δ_9 ZEUS BPC[6] — δ_{14} ZEUS BPT[7] — δ_8 ZEUS SVX[8]
ZEUS y_h cut	δ_3 ZEUS BPC[6] — δ_2 ZEUS BPT[7]
ZEUS BPC linearity	δ_5 ZEUS BPC[6] — δ_9 ZEUS BPT[7]
ZEUS BPC shower	δ_4 ZEUS BPC[6] — δ_3 ZEUS BPT[7]
ZEUS CAL energy	δ_2 ZEUS BPC[6] — δ_{12} ZEUS BPT[7] — δ_9 ZEUS SVX[8]
ZEUS Cuts_1	δ_3 ZEUS NC[11] — δ_3 ZEUS NC[13]
ZEUS Cuts_2	δ_4 ZEUS NC[11] — δ_4 ZEUS NC[13]
ZEUS HFS model	δ_3 ZEUS CC[10] — δ_3 ZEUS CC[12] — δ_6 ZEUS NC[11] — δ_6 ZEUS NC[13] — δ_3 ZEUS CC[14]
ZEUS Lumi 94 – 97	δ_4 ZEUS CC[10] — δ_{11} ZEUS NC[9]
ZEUS Lumi 98 – 99	δ_4 ZEUS CC[12] — δ_7 ZEUS NC[11]
ZEUS Lumi 99 – 00	δ_9 ZEUS NC[13] — δ_4 ZEUS CC[14]

Table 5: List of systematic sources that are correlated across the data samples. The type of the systematic uncertainty is given in the "source" column. The labels δ_i denote the sources according to the sequential ordering in the list of the correlated systematic uncertainties of the corresponding publication. An overall 0.5% normalisation uncertainty, common to all data sets, is not included in this list.

Bin #	Q^2 GeV^2	x	y	$\sigma_r^{+\ \mathrm{ave}}$	F_2^{ave}	$\delta_{\mathrm{ave,stat}}$ %	$\delta_{\mathrm{ave,uncor}}$ %	$\delta_{\mathrm{ave,cor}}$ %	$\delta_{\mathrm{ave,exp\ tot}}$ %	$\delta_{\mathrm{ave,rel}}$ %	$\delta_{\mathrm{ave,gp}}$ %	$\delta_{\mathrm{ave,had}}$ %	$\delta_{\mathrm{ave,tot}}$ %	$\sqrt{s}$ GeV
1	0.045	0.621×10^{-6}	0.803	0.080	—	5.05	1.50	7.29	8.99	2.83	2.28	1.14	9.77	301
2	0.065	0.897×10^{-6}	0.803	0.111	—	2.97	1.50	6.27	7.10	2.78	2.11	1.21	8.00	301
3	0.065	0.102×10^{-5}	0.706	0.111	—	4.69	1.50	5.98	7.75	3.56	1.16	1.47	8.73	301
4	0.085	0.117×10^{-5}	0.805	0.136	—	2.95	1.50	5.54	6.45	2.57	2.12	1.37	7.39	301
5	0.085	0.134×10^{-5}	0.703	0.130	—	2.27	1.50	4.01	4.85	1.80	1.57	1.00	5.49	301
6	0.085	0.156×10^{-5}	0.604	0.126	—	4.78	1.50	4.52	6.75	1.03	0.76	0.24	6.87	301
7	0.1	0.151×10^{-5}	0.808	0.165	—	3.48	1.50	5.49	6.67	3.16	1.97	1.73	7.83	301
8	0.1	0.173×10^{-5}	0.705	0.166	—	1.81	0.99	3.25	3.85	2.28	1.33	0.99	4.77	301
9	0.1	0.202×10^{-5}	0.604	0.157	—	1.79	0.89	2.43	3.15	1.62	0.67	0.49	3.64	301
10	0.1	0.243×10^{-5}	0.502	0.149	0.154	3.75	1.50	3.49	5.34	1.11	0.46	0.20	5.48	301
11	0.15	0.207×10^{-5}	0.803	0.228	—	4.35	1.50	4.58	6.49	2.37	1.94	1.75	7.39	301
12	0.15	0.236×10^{-5}	0.705	0.199	—	2.01	1.02	3.05	3.79	1.71	1.60	0.74	4.52	301
13	0.15	0.276×10^{-5}	0.603	0.201	—	1.62	0.92	2.24	2.91	1.40	0.87	0.38	3.37	301
14	0.15	0.331×10^{-5}	0.502	0.201	0.207	1.53	0.78	2.10	2.71	1.31	0.19	0.34	3.04	301
15	0.15	0.414×10^{-5}	0.402	0.187	0.190	1.97	0.83	2.32	3.15	0.82	0.11	0.17	3.27	301
16	0.15	0.502×10^{-5}	0.295	0.185	0.187	3.79	1.50	3.59	5.43	1.33	−0.24	0.32	5.60	319
17	0.2	0.315×10^{-5}	0.704	0.250	—	2.48	0.94	2.96	3.98	1.89	1.50	0.99	4.76	301
18	0.2	0.368×10^{-5}	0.603	0.246	—	1.98	0.94	2.10	3.04	1.39	0.72	0.37	3.44	301
19	0.2	0.441×10^{-5}	0.503	0.240	0.247	1.62	0.74	1.97	2.66	1.15	0.36	0.17	2.92	301
20	0.2	0.552×10^{-5}	0.402	0.235	0.240	1.48	0.65	1.84	2.45	1.18	0.04	0.30	2.74	301
21	0.2	0.669×10^{-5}	0.295	0.227	0.229	1.65	0.78	1.63	2.45	0.86	−0.24	0.10	2.61	319
22	0.2	0.849×10^{-5}	0.233	0.224	0.225	1.61	0.61	2.13	2.74	1.06	−0.19	0.27	2.96	319
23	0.2	0.110×10^{-4}	0.180	0.208	0.209	2.78	1.50	2.79	4.21	0.95	−0.21	0.26	4.33	319
24	0.2	0.398×10^{-4}	0.050	0.211	0.211	14.92	11.94	5.17	19.8	−0.54	−3.10	−4.60	20.57	319
25	0.2	0.251×10^{-3}	0.008	0.181	0.181	13.45	6.17	2.96	15.1	−0.03	−1.23	2.59	15.36	319
26	0.25	0.394×10^{-5}	0.703	0.280	—	4.09	1.50	2.83	5.19	1.78	1.28	0.89	5.71	301
27	0.25	0.460×10^{-5}	0.603	0.280	—	2.09	0.92	2.58	3.44	1.67	1.27	0.36	4.05	301
28	0.25	0.552×10^{-5}	0.502	0.282	0.291	1.79	0.92	1.87	2.74	1.27	0.27	0.28	3.05	301
29	0.25	0.690×10^{-5}	0.402	0.276	0.281	1.56	0.79	1.84	2.54	1.18	0.02	0.21	2.81	301
30	0.25	0.836×10^{-5}	0.295	0.266	0.269	1.45	0.73	1.85	2.46	1.17	−0.23	0.27	2.75	319
31	0.25	0.106×10^{-4}	0.233	0.261	0.262	1.29	0.66	1.77	2.29	1.16	−0.32	0.21	2.59	319
32	0.25	0.138×10^{-4}	0.179	0.250	0.251	1.26	0.71	1.78	2.30	1.22	−0.28	0.41	2.65	319
33	0.25	0.230×10^{-4}	0.107	0.245	0.245	1.40	1.50	2.33	3.11	1.92	−0.18	1.96	4.15	319
34	0.25	0.398×10^{-4}	0.062	0.237	0.237	3.32	1.54	2.74	4.57	0.79	−0.67	−0.96	4.79	319
35	0.25	0.110×10^{-3}	0.022	0.200	0.200	3.95	1.50	2.45	4.88	0.81	−0.17	−0.04	4.95	319
36	0.25	0.251×10^{-3}	0.010	0.196	0.196	3.74	1.44	3.23	5.15	−0.17	−0.25	−0.58	5.19	319
37	0.25	0.394×10^{-3}	0.006	0.195	0.195	4.15	1.50	3.58	5.68	1.49	−0.22	0.79	5.93	319
38	0.25	0.158×10^{-2}	0.002	0.199	0.199	10.97	5.29	2.36	12.4	0.14	−0.17	2.67	12.69	301
39	0.35	0.512×10^{-5}	0.758	0.350	—	3.42	1.50	3.33	5.00	1.95	0.85	0.37	5.45	301
40	0.35	0.512×10^{-5}	0.675	0.437	—	22.06	12.78	1.80	25.6	−0.15	−1.02	0.68	25.59	319
41	0.35	0.610×10^{-5}	0.636	0.358	—	5.74	11.03	4.78	13.3	0.64	3.76	1.03	13.89	301
42	0.35	0.662×10^{-5}	0.586	0.336	0.351	2.07	0.91	1.88	2.94	1.20	0.41	0.33	3.22	301
43	0.35	0.828×10^{-5}	0.469	0.335	0.344	1.82	0.93	1.90	2.80	1.25	−0.07	0.21	3.07	301
44	0.35	0.100×10^{-4}	0.346	0.348	0.353	1.62	0.79	1.73	2.50	1.20	−0.28	0.29	2.80	319
45	0.35	0.127×10^{-4}	0.272	0.326	0.329	1.43	0.79	1.80	2.43	1.16	−0.29	0.20	2.72	319
46	0.35	0.165×10^{-4}	0.210	0.316	0.317	1.21	0.63	1.82	2.27	1.20	−0.28	0.26	2.59	319
47	0.35	0.320×10^{-4}	0.108	0.299	0.299	1.14	0.72	2.51	2.85	2.25	−0.39	2.05	4.19	319
48	0.35	0.662×10^{-4}	0.052	0.283	0.284	2.62	1.50	1.65	3.44	0.45	−0.24	−0.18	3.48	319
49	0.35	0.130×10^{-3}	0.027	0.259	0.259	2.52	1.43	1.46	3.24	0.75	−0.33	0.06	3.35	319
50	0.35	0.220×10^{-3}	0.016	0.242	0.242	2.67	1.50	1.95	3.63	1.11	−0.34	0.16	3.81	319
51	0.35	0.500×10^{-3}	0.007	0.242	0.242	2.51	1.42	1.75	3.37	1.31	−0.25	1.12	3.79	319
52	0.35	0.251×10^{-2}	0.001	0.202	0.202	9.97	4.55	1.47	11.1	0.35	0.16	0.77	11.09	319
53	0.4	0.883×10^{-5}	0.502	0.354	0.365	3.86	1.50	2.56	4.87	1.29	0.52	0.16	5.07	301
54	0.4	0.110×10^{-4}	0.403	0.372	0.378	2.18	0.88	2.20	3.22	1.48	0.04	0.22	3.55	301
55	0.4	0.133×10^{-4}	0.297	0.357	0.360	1.97	0.88	1.98	2.93	1.34	−0.27	0.29	3.25	319
56	0.4	0.170×10^{-4}	0.233	0.355	0.357	1.66	0.83	1.81	2.59	1.18	−0.31	0.09	2.86	319
57	0.4	0.220×10^{-4}	0.180	0.336	0.337	1.45	0.78	1.80	2.44	1.25	−0.32	0.42	2.79	319
58	0.4	0.368×10^{-4}	0.107	0.332	0.333	1.26	0.77	2.49	2.89	2.27	−0.33	2.14	4.27	319
59	0.4	0.883×10^{-4}	0.045	0.321	0.321	2.71	1.50	1.49	3.44	0.98	−0.26	0.41	3.61	319
60	0.4	0.176×10^{-3}	0.022	0.288	0.288	2.78	1.50	1.70	3.59	0.72	−0.32	−0.22	3.68	319
61	0.4	0.294×10^{-3}	0.013	0.277	0.277	2.74	1.50	1.59	3.51	0.99	−0.28	0.33	3.67	319
62	0.4	0.631×10^{-3}	0.006	0.261	0.261	2.74	1.50	2.00	3.71	1.28	−0.28	0.38	3.95	319

Table 6: HERA combined reduced cross section $\sigma_r^{+\ \mathrm{ave}}$ for NC e^+p scattering. F_2^{ave} represents the structure function F_2 calculated from σ_r^{ave} by using the HERAPDF1.0 parametrisation of $\tilde{F}_L, x\tilde{F}_3, F_2^{\gamma Z}$ for $Q^2 \geq 2$ GeV^2 and assuming $R \equiv F_L/(F_2 - F_L) = 0.25$ for $Q^2 < 2$ GeV^2. F_2 is given for $y < 0.6$. $\delta_{\mathrm{ave,stat}}$, $\delta_{\mathrm{ave,uncor}}$, $\delta_{\mathrm{ave,cor}}$ and $\delta_{\mathrm{ave,exp\ tot}}$ represent the statistical, uncorrelated systematic, correlated systematic and total experimental uncertainty, respectively. $\delta_{\mathrm{ave,rel}}$, $\delta_{\mathrm{ave,gp}}$ and $\delta_{\mathrm{ave,had}}$ are the three correlated sources of uncertainties arising from the combination procedure, see section 3.2.3. $\delta_{\mathrm{ave,tot}}$ is the total uncertainty calculated by adding $\delta_{\mathrm{ave,exp\ tot}}$ and the procedural errors in quadrature. The uncertainties are quoted in percent relative to $\sigma_r^{+\ \mathrm{ave}}$. The overall normalisation uncertainty of 0.5% is not included.

Bin #	Q^2 GeV^2	x	y	$\sigma_r^{+\,\mathrm{ave}}$	F_2^{ave}	$\delta_{\mathrm{ave,stat}}$ %	$\delta_{\mathrm{ave,uncor}}$ %	$\delta_{\mathrm{ave,cor}}$ %	$\delta_{\mathrm{ave,exp\ tot}}$ %	$\delta_{\mathrm{ave,rel}}$ %	$\delta_{\mathrm{ave,gp}}$ %	$\delta_{\mathrm{ave,had}}$ %	$\delta_{\mathrm{ave,tot}}$ %	$\sqrt{s}$ GeV
63	0.5	0.732×10^{-5}	0.675	0.428	—	5.55	5.73	4.17	9.01	−0.49	−2.46	−0.38	9.36	319
64	0.5	0.860×10^{-5}	0.645	0.443	—	3.74	9.17	3.57	10.5	0.58	2.86	0.70	10.95	301
65	0.5	0.158×10^{-4}	0.313	0.429	0.433	3.53	1.48	2.33	4.48	1.22	−0.17	0.14	4.65	319
66	0.5	0.212×10^{-4}	0.233	0.392	0.394	2.06	0.80	1.95	2.94	1.12	−0.25	−0.05	3.16	319
67	0.5	0.276×10^{-4}	0.179	0.379	0.380	1.71	0.76	1.94	2.69	1.35	−0.30	0.39	3.05	319
68	0.5	0.398×10^{-4}	0.124	0.367	0.368	1.48	0.81	2.57	3.07	2.32	−0.52	2.05	4.39	319
69	0.5	0.100×10^{-3}	0.049	0.349	0.349	1.74	1.45	1.50	2.71	0.69	−0.32	−0.10	2.82	319
70	0.5	0.251×10^{-3}	0.020	0.308	0.308	1.87	1.43	1.55	2.82	0.41	−0.24	−0.36	2.88	319
71	0.5	0.368×10^{-3}	0.013	0.301	0.301	2.02	1.50	1.61	2.99	0.80	−0.23	0.16	3.10	319
72	0.5	0.800×10^{-3}	0.006	0.288	0.288	2.04	1.38	1.46	2.87	0.91	−0.18	0.49	3.05	319
73	0.5	0.320×10^{-2}	0.002	0.183	0.183	11.35	6.39	1.23	13.1	0.25	0.32	0.55	13.10	301
74	0.65	0.952×10^{-5}	0.675	0.465	—	4.02	2.90	2.56	5.58	−0.17	−1.33	0.23	5.74	319
75	0.65	0.112×10^{-4}	0.643	0.514	—	4.25	2.62	2.90	5.77	0.86	2.58	0.69	6.42	301
76	0.65	0.158×10^{-4}	0.407	0.464	0.472	3.09	5.44	1.51	6.44	0.13	−0.01	0.55	6.46	319
77	0.65	0.164×10^{-4}	0.439	0.509	0.520	3.02	7.28	2.37	8.23	0.42	1.05	0.38	8.32	301
78	0.65	0.398×10^{-4}	0.161	0.475	0.476	2.73	0.68	2.31	3.64	1.43	−0.14	0.14	3.92	319
79	0.65	0.598×10^{-4}	0.107	0.420	0.420	1.99	0.74	3.14	3.79	2.69	−0.23	2.11	5.11	319
80	0.65	0.100×10^{-3}	0.064	0.410	0.411	2.08	1.47	1.98	3.23	1.00	−0.50	0.16	3.42	319
81	0.65	0.251×10^{-3}	0.026	0.362	0.362	2.14	1.39	1.62	3.02	0.77	−0.17	0.51	3.17	319
82	0.65	0.478×10^{-3}	0.013	0.333	0.333	2.29	1.50	1.87	3.31	0.83	−0.30	0.31	3.44	319
83	0.65	0.800×10^{-3}	0.008	0.319	0.319	2.14	1.35	1.57	2.97	0.64	−0.18	0.34	3.06	319
84	0.65	0.320×10^{-2}	0.002	0.225	0.225	5.80	3.18	1.19	6.72	0.27	0.00	0.74	6.77	319
85	0.85	0.124×10^{-4}	0.677	0.553	—	2.57	2.52	2.20	4.22	−0.10	−1.01	0.01	4.34	319
86	0.85	0.138×10^{-4}	0.683	0.616	—	5.20	9.45	5.07	11.9	0.72	4.08	1.06	12.66	301
87	0.85	0.200×10^{-4}	0.471	0.602	0.617	2.96	2.12	2.03	4.17	0.62	1.39	0.49	4.46	301
88	0.85	0.200×10^{-4}	0.420	0.613	0.625	1.95	5.36	1.58	5.92	0.25	0.31	0.54	5.96	319
89	0.85	0.398×10^{-4}	0.211	0.561	0.564	2.02	1.85	1.75	3.26	0.29	0.49	0.42	3.33	319
90	0.85	0.500×10^{-4}	0.168	0.544	0.546	2.92	4.52	2.32	5.86	0.41	0.24	0.24	5.89	319
91	0.85	0.100×10^{-3}	0.084	0.502	0.503	2.65	3.78	3.74	5.94	0.17	1.73	0.08	6.19	319
92	0.85	0.251×10^{-3}	0.033	0.398	0.399	5.99	2.98	2.29	7.08	−0.01	0.73	0.83	7.16	319
93	0.85	0.800×10^{-3}	0.010	0.351	0.351	4.60	2.67	1.40	5.50	0.33	0.46	0.26	5.53	319
94	0.85	0.320×10^{-2}	0.003	0.309	0.309	4.53	2.83	0.94	5.42	0.24	0.14	−0.07	5.43	301
95	1.2	0.176×10^{-4}	0.674	0.591	—	2.56	2.16	2.60	4.24	−0.19	−0.35	0.06	4.26	319
96	1.2	0.200×10^{-4}	0.665	0.742	—	3.60	8.36	3.64	9.80	0.57	2.88	0.92	10.27	301
97	1.2	0.200×10^{-4}	0.593	0.669	0.699	2.62	2.51	1.31	3.86	0.14	−0.13	0.60	3.91	319
98	1.2	0.320×10^{-4}	0.416	0.667	0.680	2.75	1.79	2.02	3.85	0.59	1.53	0.50	4.22	301
99	1.2	0.320×10^{-4}	0.371	0.688	0.698	1.67	2.73	1.27	3.44	0.20	0.16	0.50	3.49	319
100	1.2	0.631×10^{-4}	0.188	0.651	0.653	1.39	1.46	1.37	2.44	0.38	0.47	0.44	2.55	319
101	1.2	0.800×10^{-4}	0.148	0.598	0.600	2.04	1.36	1.85	3.07	0.39	0.36	0.21	3.12	319
102	1.2	0.130×10^{-3}	0.091	0.545	0.545	2.42	4.97	1.55	5.74	0.21	0.35	0.09	5.75	319
103	1.2	0.158×10^{-3}	0.075	0.534	0.534	1.54	1.35	1.38	2.48	0.69	0.54	0.37	2.65	319
104	1.2	0.398×10^{-3}	0.030	0.495	0.495	2.11	3.36	1.30	4.18	0.17	0.43	0.67	4.26	319
105	1.2	0.130×10^{-2}	0.009	0.374	0.374	3.54	2.67	1.33	4.63	0.37	0.26	−0.09	4.65	319
106	1.2	0.500×10^{-2}	0.002	0.299	0.299	4.50	2.61	1.49	5.41	0.14	0.51	−0.58	5.46	319
107	1.5	0.185×10^{-4}	0.800	0.602	—	3.19	3.48	6.12	7.72	−0.26	8.31	0.08	11.35	319
108	1.5	0.220×10^{-4}	0.675	0.695	—	1.94	1.78	1.69	3.14	0.03	0.97	0.16	3.29	319
109	1.5	0.320×10^{-4}	0.520	0.821	0.847	1.17	3.20	2.12	4.02	0.60	5.18	0.43	6.60	301
110	1.5	0.320×10^{-4}	0.463	0.755	0.774	1.73	2.15	1.13	2.98	0.17	0.20	0.41	3.02	319
111	1.5	0.500×10^{-4}	0.296	0.763	0.770	1.04	1.98	1.07	2.48	0.32	0.74	0.52	2.66	319
112	1.5	0.800×10^{-4}	0.185	0.702	0.705	1.26	2.15	1.31	2.81	0.36	0.32	0.52	2.90	319
113	1.5	0.130×10^{-3}	0.114	0.649	0.649	1.46	2.43	1.49	3.20	0.35	0.46	0.54	3.30	319
114	1.5	0.200×10^{-3}	0.074	0.616	0.616	2.07	2.86	1.59	3.87	0.36	0.37	−0.01	3.91	319
115	1.5	0.320×10^{-3}	0.046	0.580	0.580	1.48	2.26	1.55	3.12	0.20	0.58	1.02	3.34	319
116	1.5	0.500×10^{-3}	0.030	0.550	0.550	2.51	7.05	1.83	7.70	0.23	0.11	0.29	7.71	319
117	1.5	0.800×10^{-3}	0.019	0.493	0.493	2.36	2.47	1.29	3.65	0.34	0.38	0.11	3.69	319
118	1.5	0.100×10^{-2}	0.015	0.465	0.465	5.21	3.74	1.31	6.55	0.38	0.02	0.56	6.58	319
119	1.5	0.320×10^{-2}	0.005	0.412	0.412	2.30	2.04	1.34	3.36	0.43	0.18	−0.61	3.45	301
120	1.5	0.130×10^{-1}	0.001	0.324	0.324	4.01	2.49	4.81	6.74	−0.29	1.08	−1.42	6.98	319
121	2.	0.247×10^{-4}	0.800	0.766	—	2.33	2.70	4.62	5.84	−0.03	6.20	−0.06	8.52	319
122	2.	0.293×10^{-4}	0.675	0.787	—	1.49	1.65	1.53	2.70	0.06	0.93	0.02	2.86	319
123	2.	0.327×10^{-4}	0.678	0.855	—	2.66	2.13	2.86	4.45	0.81	3.72	0.56	5.88	301
124	2.	0.500×10^{-4}	0.443	0.859	0.863	1.31	1.64	1.20	2.42	0.44	1.55	0.39	2.93	301
125	2.	0.500×10^{-4}	0.395	0.825	0.830	1.52	1.93	0.91	2.62	0.23	0.29	0.33	2.67	319
126	2.	0.800×10^{-4}	0.247	0.764	0.765	0.97	1.34	0.89	1.88	0.34	0.21	0.42	1.97	319
127	2.	0.130×10^{-3}	0.152	0.727	0.727	1.10	1.30	0.98	1.97	0.32	0.17	0.31	2.03	319
128	2.	0.200×10^{-3}	0.099	0.684	0.684	1.12	1.32	1.12	2.06	0.42	0.31	−0.05	2.12	319
129	2.	0.320×10^{-3}	0.062	0.631	0.631	1.01	1.65	1.23	2.29	0.27	0.13	0.38	2.34	319
130	2.	0.500×10^{-3}	0.040	0.578	0.578	1.17	2.04	1.30	2.69	0.25	−0.13	0.40	2.73	319
131	2.	0.100×10^{-2}	0.020	0.512	0.512	0.98	1.79	1.00	2.28	0.28	0.08	−0.11	2.30	319
132	2.	0.320×10^{-2}	0.006	0.428	0.428	1.07	1.89	1.40	2.59	0.40	0.17	−0.84	2.76	319
133	2.	0.130×10^{-1}	0.002	0.358	0.358	2.39	2.13	3.97	5.10	−0.14	0.89	−1.21	5.32	301

Table 7: Continuation of table 6.

Bin #	Q^2 GeV^2	x	y	$\sigma_r^{+\,\mathrm{ave}}$	F_2^{ave}	$\delta_{\mathrm{ave,stat}}$ %	$\delta_{\mathrm{ave,uncor}}$ %	$\delta_{\mathrm{ave,cor}}$ %	$\delta_{\mathrm{ave,exp\ tot}}$ %	$\delta_{\mathrm{ave,rel}}$ %	$\delta_{\mathrm{ave,gp}}$ %	$\delta_{\mathrm{ave,had}}$ %	$\delta_{\mathrm{ave,tot}}$ %	$\sqrt{s}$ GeV
134	2.7	0.309×10^{-4}	0.864	0.855	—	2.47	2.67	3.33	4.93	0.06	4.62	0.25	6.76	319
135	2.7	0.366×10^{-4}	0.729	0.881	—	2.29	2.29	1.72	3.67	0.09	2.19	0.05	4.27	319
136	2.7	0.409×10^{-4}	0.732	0.975	—	1.54	6.21	1.93	6.68	0.57	4.64	0.61	8.18	301
137	2.7	0.500×10^{-4}	0.599	0.894	0.913	1.06	1.27	1.30	2.11	0.77	2.43	0.54	3.35	301
138	2.7	0.500×10^{-4}	0.534	0.882	0.901	1.51	1.65	0.93	2.42	0.17	0.41	0.10	2.46	319
139	2.7	0.800×10^{-4}	0.374	0.892	0.899	3.28	1.00	1.81	3.87	0.39	0.65	0.75	4.02	301
140	2.7	0.800×10^{-4}	0.333	0.886	0.892	0.72	1.03	0.73	1.45	0.29	0.40	0.30	1.56	319
141	2.7	0.130×10^{-3}	0.205	0.804	0.806	0.62	0.87	0.69	1.28	0.40	−0.02	0.24	1.36	319
142	2.7	0.200×10^{-3}	0.133	0.780	0.780	0.76	1.61	0.83	1.96	0.30	0.28	0.10	2.01	319
143	2.7	0.320×10^{-3}	0.083	0.702	0.702	0.84	1.27	0.86	1.75	0.44	0.20	0.09	1.82	319
144	2.7	0.500×10^{-3}	0.053	0.647	0.647	0.69	1.35	0.96	1.79	0.33	0.06	0.30	1.84	319
145	2.7	0.800×10^{-3}	0.033	0.596	0.596	0.87	1.84	0.80	2.19	0.28	0.10	0.20	2.22	319
146	2.7	0.130×10^{-2}	0.021	0.570	0.570	0.68	1.63	0.90	1.98	0.33	0.04	−0.16	2.02	319
147	2.7	0.200×10^{-2}	0.013	0.484	0.484	0.90	2.74	0.90	3.02	0.22	0.16	0.33	3.05	319
148	2.7	0.500×10^{-2}	0.005	0.460	0.460	0.74	1.82	1.37	2.40	0.38	0.24	−0.90	2.60	319
149	2.7	0.200×10^{-1}	0.001	0.358	0.358	2.54	2.45	7.39	8.19	−0.52	1.25	−1.80	8.49	319
150	3.5	0.432×10^{-4}	0.800	0.868	—	3.10	2.83	3.74	5.63	−0.07	4.91	−0.32	7.48	319
151	3.5	0.512×10^{-4}	0.675	0.937	—	2.17	2.25	1.66	3.54	0.10	2.04	−0.01	4.09	319
152	3.5	0.573×10^{-4}	0.677	1.017	—	1.94	3.35	2.64	4.69	1.16	4.70	0.56	6.76	301
153	3.5	0.800×10^{-4}	0.485	0.979	0.997	0.98	1.22	1.02	1.87	0.37	1.71	0.43	2.59	301
154	3.5	0.800×10^{-4}	0.432	0.954	0.972	1.26	1.67	0.80	2.24	0.21	0.37	0.14	2.28	319
155	3.5	0.130×10^{-3}	0.266	0.922	0.928	0.66	0.86	0.67	1.27	0.27	0.14	0.26	1.33	319
156	3.5	0.200×10^{-3}	0.173	0.858	0.860	0.68	0.83	0.69	1.28	0.27	−0.09	0.21	1.32	319
157	3.5	0.320×10^{-3}	0.108	0.795	0.796	0.72	0.88	0.75	1.36	0.44	0.17	0.04	1.44	319
158	3.5	0.500×10^{-3}	0.069	0.754	0.754	0.75	1.17	0.77	1.59	0.24	0.14	0.33	1.65	319
159	3.5	0.800×10^{-3}	0.043	0.663	0.663	0.67	1.16	0.80	1.56	0.23	−0.22	0.24	1.61	319
160	3.5	0.130×10^{-2}	0.027	0.627	0.627	0.87	1.38	0.86	1.84	0.29	0.20	0.17	1.88	319
161	3.5	0.200×10^{-2}	0.017	0.571	0.571	0.51	0.87	0.73	1.24	0.33	0.03	0.15	1.30	319
162	3.5	0.800×10^{-2}	0.004	0.463	0.463	0.59	1.12	1.03	1.64	0.38	0.13	0.00	1.68	319
163	4.5	0.618×10^{-4}	0.720	0.957	—	3.13	2.78	3.52	5.47	0.16	4.80	0.70	7.32	319
164	4.5	0.732×10^{-4}	0.607	1.018	—	1.60	2.21	1.11	2.94	0.13	1.06	−0.01	3.13	319
165	4.5	0.818×10^{-4}	0.610	1.118	—	1.60	1.06	1.45	2.40	0.84	2.58	0.61	3.67	301
166	4.5	0.130×10^{-3}	0.384	1.015	1.029	1.02	1.68	0.81	2.12	0.31	0.61	0.35	2.26	301
167	4.5	0.130×10^{-3}	0.342	1.031	1.045	1.30	1.00	0.70	1.78	0.30	0.33	0.21	1.85	319
168	4.5	0.200×10^{-3}	0.222	0.967	0.972	0.74	0.91	0.71	1.37	0.32	−0.02	0.25	1.42	319
169	4.5	0.320×10^{-3}	0.139	0.898	0.899	0.80	0.96	0.66	1.41	0.22	0.00	0.14	1.44	319
170	4.5	0.500×10^{-3}	0.089	0.800	0.801	0.83	0.88	0.74	1.42	0.46	−0.02	0.25	1.52	319
171	4.5	0.800×10^{-3}	0.056	0.724	0.724	0.82	1.29	0.76	1.70	0.22	−0.11	0.16	1.73	319
172	4.5	0.130×10^{-2}	0.034	0.669	0.669	0.85	1.31	0.87	1.78	0.26	0.00	0.09	1.80	319
173	4.5	0.200×10^{-2}	0.022	0.618	0.618	0.88	1.31	0.79	1.77	0.20	−0.34	0.24	1.83	319
174	4.5	0.320×10^{-2}	0.014	0.575	0.575	0.67	1.23	0.86	1.64	0.28	0.10	0.29	1.70	319
175	4.5	0.130×10^{-1}	0.003	0.432	0.432	0.71	1.86	1.46	2.46	0.25	0.34	0.74	2.61	319
176	6.5	0.803×10^{-4}	0.800	1.078	—	3.11	2.64	2.44	4.76	0.08	3.33	0.12	5.81	319
177	6.5	0.951×10^{-4}	0.757	1.165	—	2.41	0.99	2.80	3.82	0.70	4.23	0.47	5.76	301
178	6.5	0.951×10^{-4}	0.675	1.050	—	2.96	2.31	1.64	4.10	0.09	2.09	0.03	4.60	319
179	6.5	0.130×10^{-3}	0.554	1.180	1.227	1.11	0.60	1.04	1.63	0.43	1.84	0.39	2.53	301
180	6.5	0.130×10^{-3}	0.494	1.122	1.167	1.67	2.22	0.83	2.90	0.17	0.20	0.01	2.91	319
181	6.5	0.200×10^{-3}	0.360	1.118	1.134	1.15	1.41	0.78	1.98	0.32	0.29	0.41	2.07	301
182	6.5	0.200×10^{-3}	0.321	1.131	1.147	1.08	0.63	0.69	1.43	0.20	0.29	0.24	1.49	319
183	6.5	0.320×10^{-3}	0.201	1.006	1.010	0.78	0.73	0.67	1.26	0.25	−0.18	0.10	1.31	319
184	6.5	0.500×10^{-3}	0.128	0.938	0.939	0.74	1.16	0.73	1.56	0.22	0.17	0.13	1.59	319
185	6.5	0.800×10^{-3}	0.080	0.857	0.857	0.79	0.89	0.73	1.40	0.36	0.01	0.30	1.47	319
186	6.5	0.130×10^{-2}	0.049	0.761	0.761	0.80	1.08	0.72	1.52	0.21	−0.02	0.11	1.54	319
187	6.5	0.200×10^{-2}	0.032	0.699	0.699	0.75	0.87	0.69	1.34	0.11	−0.05	0.30	1.38	319
188	6.5	0.320×10^{-2}	0.020	0.644	0.644	0.67	1.20	0.83	1.61	0.25	0.07	0.11	1.63	319
189	6.5	0.500×10^{-2}	0.013	0.581	0.581	0.94	0.85	0.89	1.54	0.16	0.05	0.28	1.58	319
190	6.5	0.130×10^{-1}	0.005	0.485	0.485	0.68	1.82	1.25	2.31	0.24	0.24	0.81	2.47	319
191	6.5	0.200×10^{-1}	0.003	0.497	0.497	1.14	1.89	1.59	2.72	0.26	−0.03	0.39	2.76	319
192	8.5	0.105×10^{-3}	0.800	1.178	—	3.72	2.80	2.14	5.13	0.10	2.88	0.45	5.90	319
193	8.5	0.124×10^{-3}	0.675	1.209	—	2.26	2.28	1.05	3.38	0.12	0.92	−0.04	3.50	319
194	8.5	0.139×10^{-3}	0.678	1.181	—	1.59	1.25	2.32	3.08	0.84	5.61	0.51	6.47	301
195	8.5	0.200×10^{-3}	0.471	1.221	1.258	1.07	0.81	0.83	1.58	0.31	1.07	0.27	1.95	301
196	8.5	0.200×10^{-3}	0.420	1.178	1.213	1.52	2.22	0.79	2.80	0.18	0.03	−0.01	2.81	319
197	8.5	0.320×10^{-3}	0.262	1.115	1.126	0.85	0.84	0.66	1.36	0.32	−0.05	0.16	1.41	319
198	8.5	0.500×10^{-3}	0.168	1.022	1.026	0.81	0.93	0.67	1.40	0.22	−0.19	0.15	1.44	319
199	8.5	0.800×10^{-3}	0.105	0.936	0.937	0.88	0.80	0.69	1.38	0.23	−0.03	0.09	1.40	319
200	8.5	0.130×10^{-2}	0.065	0.844	0.845	0.91	0.83	0.68	1.41	0.23	0.02	0.25	1.45	319
201	8.5	0.200×10^{-2}	0.042	0.773	0.773	0.98	1.32	0.76	1.81	0.19	−0.02	0.14	1.83	319
202	8.5	0.320×10^{-2}	0.026	0.664	0.664	1.03	1.33	0.82	1.87	0.17	−0.22	0.27	1.91	319
203	8.5	0.500×10^{-2}	0.017	0.635	0.635	0.76	1.25	0.80	1.67	0.25	0.03	0.37	1.73	319
204	8.5	0.200×10^{-1}	0.004	0.458	0.458	0.82	1.85	1.58	2.57	0.14	0.42	0.44	2.64	319

Table 8: Continuation of table 6.

Bin #	Q^2 GeV^2	x	y	$\sigma_r^{+\,\mathrm{ave}}$	F_2^{ave}	$\delta_{\mathrm{ave,stat}}$ %	$\delta_{\mathrm{ave,uncor}}$ %	$\delta_{\mathrm{ave,cor}}$ %	$\delta_{\mathrm{ave,exp\ tot}}$ %	$\delta_{\mathrm{ave,rel}}$ %	$\delta_{\mathrm{ave,gp}}$ %	$\delta_{\mathrm{ave,had}}$ %	$\delta_{\mathrm{ave,tot}}$ %	$\sqrt{s}$ GeV
205	10.	0.130×10^{-3}	0.853	1.141	—	4.39	1.41	3.68	5.90	1.21	4.94	0.71	7.83	301
206	10.	0.200×10^{-3}	0.554	1.248	1.306	2.10	1.33	1.34	2.83	0.57	1.54	0.23	3.28	301
207	10.	0.320×10^{-3}	0.309	1.153	1.169	1.90	1.12	0.84	2.36	0.37	0.28	−0.03	2.41	319
208	10.	0.500×10^{-3}	0.198	1.069	1.074	1.77	1.19	0.76	2.26	0.17	−0.06	−0.22	2.28	319
209	10.	0.800×10^{-3}	0.124	0.983	0.985	1.83	1.31	0.73	2.37	0.20	−0.11	−0.09	2.38	319
210	10.	0.130×10^{-2}	0.076	0.898	0.899	2.11	1.21	0.93	2.61	−0.01	0.01	−0.03	2.61	319
211	10.	0.200×10^{-2}	0.049	0.809	0.809	2.03	1.77	0.80	2.81	0.23	0.04	0.39	2.85	319
212	10.	0.500×10^{-2}	0.020	0.633	0.633	1.11	0.77	0.82	1.58	0.19	0.02	0.47	1.66	319
213	10.	0.200×10^{-1}	0.005	0.516	0.516	1.05	1.27	1.28	2.09	0.33	−0.01	0.51	2.17	319
214	12.	0.161×10^{-3}	0.826	1.238	—	4.10	3.78	0.93	5.65	0.34	0.21	0.04	5.67	301
215	12.	0.200×10^{-3}	0.665	1.293	—	1.19	1.34	1.86	2.59	0.80	2.58	0.35	3.75	301
216	12.	0.200×10^{-3}	0.593	1.314	1.414	1.21	0.71	2.41	2.79	0.28	2.59	0.12	3.82	319
217	12.	0.320×10^{-3}	0.416	1.233	1.262	0.78	1.51	0.85	1.90	0.39	0.63	0.27	2.06	301
218	12.	0.320×10^{-3}	0.371	1.233	1.262	0.81	0.59	0.74	1.25	0.27	0.55	0.13	1.40	319
219	12.	0.500×10^{-3}	0.237	1.153	1.163	0.54	0.66	0.65	1.07	0.27	0.13	0.09	1.12	319
220	12.	0.800×10^{-3}	0.148	1.056	1.059	0.68	0.56	0.64	1.08	0.25	−0.01	0.13	1.12	319
221	12.	0.130×10^{-2}	0.091	0.941	0.942	1.02	0.83	0.65	1.47	0.21	−0.08	0.18	1.50	319
222	12.	0.200×10^{-2}	0.059	0.856	0.857	1.03	0.94	0.65	1.54	0.10	−0.02	0.15	1.55	319
223	12.	0.320×10^{-2}	0.037	0.757	0.758	1.12	1.36	0.75	1.91	0.17	−0.13	0.27	1.94	319
224	12.	0.500×10^{-2}	0.024	0.682	0.682	0.85	1.26	0.80	1.72	0.22	0.08	0.13	1.74	319
225	12.	0.200×10^{-1}	0.006	0.492	0.492	0.90	1.85	1.27	2.41	0.17	0.35	0.46	2.49	319
226	15.	0.200×10^{-3}	0.831	1.270	—	3.19	3.61	0.93	4.91	0.34	0.21	0.04	4.92	301
227	15.	0.246×10^{-3}	0.676	1.370	—	1.17	1.52	1.39	2.37	0.51	1.94	0.38	3.13	301
228	15.	0.320×10^{-3}	0.520	1.300	1.355	0.94	1.36	0.92	1.90	0.47	1.07	0.11	2.23	301
229	15.	0.320×10^{-3}	0.463	1.324	1.380	0.84	0.70	1.35	1.74	0.26	1.32	0.12	2.20	319
230	15.	0.500×10^{-3}	0.296	1.217	1.235	0.47	0.65	0.66	1.04	0.29	0.21	0.11	1.10	319
231	15.	0.800×10^{-3}	0.185	1.115	1.121	0.47	0.63	0.65	1.02	0.27	0.09	0.05	1.06	319
232	15.	0.130×10^{-2}	0.114	0.988	0.990	0.51	0.65	0.69	1.08	0.27	0.04	0.11	1.12	319
233	15.	0.200×10^{-2}	0.074	0.875	0.876	0.53	0.66	0.72	1.11	0.26	0.04	0.24	1.17	319
234	15.	0.320×10^{-2}	0.046	0.789	0.789	0.56	0.78	0.70	1.18	0.26	0.05	0.22	1.23	319
235	15.	0.500×10^{-2}	0.030	0.718	0.718	0.59	0.62	0.65	1.08	0.24	0.04	0.29	1.14	319
236	15.	0.800×10^{-2}	0.019	0.636	0.636	0.50	0.73	0.67	1.11	0.25	0.04	0.22	1.16	319
237	15.	0.200×10^{-1}	0.007	0.532	0.532	0.69	0.93	1.10	1.59	0.26	0.03	0.25	1.63	319
238	18.	0.268×10^{-3}	0.745	1.332	—	3.24	3.67	0.92	4.98	0.34	0.21	0.04	4.99	301
239	18.	0.328×10^{-3}	0.608	1.375	—	1.25	1.67	1.03	2.32	0.45	1.07	0.31	2.62	301
240	18.	0.500×10^{-3}	0.399	1.276	1.305	0.93	1.00	0.86	1.62	0.51	0.90	0.19	1.93	301
241	18.	0.500×10^{-3}	0.356	1.277	1.306	0.73	0.70	0.79	1.29	0.26	0.53	0.14	1.42	319
242	18.	0.800×10^{-3}	0.222	1.168	1.177	0.46	0.59	0.65	0.99	0.27	0.12	0.10	1.04	319
243	18.	0.130×10^{-2}	0.137	1.052	1.054	0.46	0.63	0.66	1.02	0.28	0.08	0.07	1.06	319
244	18.	0.200×10^{-2}	0.089	0.950	0.951	0.51	0.62	0.69	1.06	0.25	0.05	0.07	1.09	319
245	18.	0.320×10^{-2}	0.056	0.836	0.837	0.53	0.65	0.66	1.07	0.25	0.04	0.21	1.12	319
246	18.	0.500×10^{-2}	0.036	0.750	0.750	0.56	0.60	0.65	1.05	0.24	0.03	0.24	1.10	319
247	18.	0.800×10^{-2}	0.022	0.668	0.668	0.45	0.66	0.70	1.06	0.25	0.04	0.24	1.12	319
248	18.	0.200×10^{-1}	0.009	0.539	0.539	0.55	1.76	1.11	2.15	0.28	0.04	0.32	2.19	319
249	22.	0.500×10^{-3}	0.488	1.342	1.392	2.56	1.22	1.13	3.05	1.10	1.33	0.46	3.54	301
250	22.	0.800×10^{-3}	0.272	1.269	1.284	2.19	0.65	0.80	2.42	0.25	0.31	0.04	2.46	319
251	22.	0.130×10^{-2}	0.167	1.071	1.075	2.25	1.40	0.86	2.79	0.23	−0.07	−0.24	2.81	319
252	22.	0.200×10^{-2}	0.109	1.019	1.021	2.71	0.77	0.85	2.94	0.61	−0.01	0.30	3.02	319
253	22.	0.320×10^{-2}	0.068	0.906	0.906	2.55	1.18	0.74	2.90	0.01	0.06	−0.20	2.91	319
254	22.	0.500×10^{-2}	0.043	0.774	0.774	2.36	0.89	0.71	2.63	0.24	0.00	0.39	2.67	319
255	22.	0.800×10^{-2}	0.027	0.660	0.660	2.42	0.93	0.76	2.70	0.42	0.04	0.57	2.79	319
256	22.	0.130×10^{-1}	0.017	0.591	0.591	1.93	1.83	1.07	2.87	0.14	0.00	0.14	2.88	319
257	22.	0.320×10^{-1}	0.007	0.523	0.523	1.80	1.61	1.39	2.79	0.41	−0.04	0.89	2.96	319
258	27.	0.335×10^{-3}	0.894	1.402	—	4.09	3.92	0.91	5.74	0.34	0.21	0.05	5.75	301
259	27.	0.410×10^{-3}	0.730	1.417	—	1.15	2.10	1.08	2.63	0.43	1.06	0.16	2.87	301
260	27.	0.500×10^{-3}	0.599	1.418	1.508	1.15	1.46	0.83	2.03	0.57	0.81	0.28	2.28	301
261	27.	0.500×10^{-3}	0.534	1.420	1.510	0.94	0.75	1.08	1.61	0.26	0.98	0.15	1.91	319
262	27.	0.800×10^{-3}	0.374	1.296	1.322	2.45	0.83	0.77	2.70	0.51	0.48	0.30	2.80	301
263	27.	0.800×10^{-3}	0.333	1.298	1.324	0.47	0.72	0.65	1.08	0.27	0.15	0.13	1.13	319
264	27.	0.130×10^{-2}	0.205	1.164	1.172	0.47	0.65	0.66	1.04	0.28	0.09	0.09	1.08	319
265	27.	0.200×10^{-2}	0.133	1.054	1.056	0.52	0.64	0.67	1.06	0.25	0.05	0.08	1.09	319
266	27.	0.320×10^{-2}	0.083	0.920	0.921	0.53	0.66	0.68	1.08	0.25	0.04	0.21	1.13	319
267	27.	0.500×10^{-2}	0.053	0.806	0.806	0.54	0.65	0.67	1.08	0.28	0.04	0.21	1.14	319
268	27.	0.800×10^{-2}	0.033	0.712	0.712	0.57	0.66	0.67	1.10	0.25	0.04	0.23	1.16	319
269	27.	0.130×10^{-1}	0.021	0.639	0.639	0.55	0.67	0.71	1.12	0.25	0.03	0.26	1.17	319
270	27.	0.200×10^{-1}	0.013	0.581	0.581	0.84	0.77	0.85	1.42	0.26	0.04	0.27	1.47	319
271	27.	0.320×10^{-1}	0.008	0.529	0.529	0.62	1.78	1.34	2.31	0.30	0.05	0.30	2.35	319
272	35.	0.574×10^{-3}	0.676	1.521	—	1.36	2.01	0.92	2.60	0.40	0.71	0.11	2.72	301
273	35.	0.800×10^{-3}	0.485	1.407	1.460	0.95	0.81	0.83	1.50	0.79	0.72	0.21	1.85	301
274	35.	0.800×10^{-3}	0.432	1.395	1.447	0.83	0.74	0.78	1.36	0.25	0.38	0.14	1.44	319
275	35.	0.130×10^{-2}	0.266	1.234	1.248	0.54	0.51	0.64	0.98	0.31	0.11	0.04	1.04	319
276	35.	0.200×10^{-2}	0.173	1.108	1.113	0.55	0.57	0.64	1.02	0.30	0.08	0.05	1.07	319
277	35.	0.320×10^{-2}	0.108	0.976	0.978	0.58	0.59	0.69	1.08	0.20	0.02	0.08	1.10	319
278	35.	0.500×10^{-2}	0.069	0.857	0.858	0.60	0.54	0.67	1.05	0.27	0.04	0.23	1.11	319
279	35.	0.800×10^{-2}	0.043	0.751	0.751	0.60	0.58	0.67	1.07	0.28	0.04	0.27	1.14	319
280	35.	0.130×10^{-1}	0.027	0.666	0.666	0.65	0.62	0.68	1.13	0.25	0.03	0.28	1.19	319
281	35.	0.200×10^{-1}	0.017	0.595	0.595	0.64	0.63	0.78	1.19	0.30	0.03	0.20	1.25	319
282	35.	0.320×10^{-1}	0.011	0.519	0.519	0.80	0.93	1.22	1.73	0.58	0.04	0.41	1.87	319
283	35.	0.800×10^{-1}	0.004	0.450	0.450	1.79	3.54	2.39	4.63	0.37	0.06	0.07	4.64	319

Table 9: Continuation of table 6.

Bin #	Q^2 GeV^2	x	y	$\sigma_r^{+\,\mathrm{ave}}$	F_2^{ave}	$\delta_{\mathrm{ave,stat}}$ %	$\delta_{\mathrm{ave,uncor}}$ %	$\delta_{\mathrm{ave,cor}}$ %	$\delta_{\mathrm{ave,exp\ tot}}$ %	$\delta_{\mathrm{ave,rel}}$ %	$\delta_{\mathrm{ave,gp}}$ %	$\delta_{\mathrm{ave,had}}$ %	$\delta_{\mathrm{ave,tot}}$ %	$\sqrt{s}$ GeV
284	45.	0.800×10^{-3}	0.624	1.493	—	1.80	1.45	1.41	2.71	0.70	1.23	0.72	3.14	301
285	45.	0.800×10^{-3}	0.556	1.468	1.571	1.38	0.89	0.80	1.82	0.25	0.51	0.17	1.91	319
286	45.	0.130×10^{-2}	0.384	1.317	1.344	0.95	0.61	0.78	1.37	0.56	0.12	−0.10	1.49	301
287	45.	0.130×10^{-2}	0.342	1.316	1.343	0.87	0.76	0.65	1.32	0.25	0.14	0.14	1.36	319
288	45.	0.200×10^{-2}	0.222	1.163	1.172	0.61	0.57	0.63	1.05	0.28	0.07	0.08	1.09	319
289	45.	0.320×10^{-2}	0.139	1.017	1.019	0.62	0.55	0.65	1.05	0.27	0.05	0.10	1.09	319
290	45.	0.500×10^{-2}	0.089	0.903	0.904	0.65	0.52	0.64	1.05	0.22	0.02	0.18	1.09	319
291	45.	0.800×10^{-2}	0.056	0.785	0.786	0.67	0.53	0.65	1.07	0.24	0.05	0.07	1.10	319
292	45.	0.130×10^{-1}	0.034	0.683	0.683	0.70	0.60	0.65	1.13	0.30	0.03	0.28	1.21	319
293	45.	0.200×10^{-1}	0.022	0.604	0.604	0.72	0.56	0.73	1.17	0.24	0.02	0.25	1.22	319
294	45.	0.320×10^{-1}	0.014	0.536	0.536	1.09	0.85	0.77	1.58	0.25	0.04	0.25	1.62	319
295	45.	0.500×10^{-1}	0.009	0.488	0.488	0.91	1.82	1.44	2.50	0.31	0.04	0.22	2.53	319
296	60.	0.130×10^{-2}	0.512	1.407	1.465	1.30	0.55	0.84	1.64	0.80	0.43	0.21	1.89	301
297	60.	0.130×10^{-2}	0.456	1.394	1.451	1.30	0.89	0.69	1.72	0.24	0.16	0.16	1.75	319
298	60.	0.200×10^{-2}	0.296	1.255	1.273	0.67	0.56	0.63	1.08	0.30	0.10	0.01	1.12	319
299	60.	0.320×10^{-2}	0.185	1.088	1.093	0.68	0.53	0.63	1.07	0.21	0.05	0.04	1.09	319
300	60.	0.500×10^{-2}	0.119	0.947	0.948	0.71	0.52	0.65	1.09	0.19	0.05	0.09	1.11	319
301	60.	0.800×10^{-2}	0.074	0.824	0.824	0.73	0.56	0.65	1.13	0.29	0.05	0.26	1.19	319
302	60.	0.130×10^{-1}	0.046	0.711	0.711	0.78	0.62	0.69	1.21	0.30	0.05	0.31	1.29	319
303	60.	0.200×10^{-1}	0.030	0.635	0.635	0.82	0.67	0.71	1.27	0.30	0.03	0.25	1.33	319
304	60.	0.320×10^{-1}	0.019	0.555	0.555	0.89	0.70	0.74	1.36	0.27	0.05	0.26	1.41	319
305	60.	0.500×10^{-1}	0.012	0.511	0.511	0.95	1.46	1.17	2.10	0.38	0.04	0.35	2.16	319
306	60.	0.130	0.005	0.396	0.396	2.95	3.88	2.05	5.28	0.32	0.00	0.20	5.30	301
307	70.	0.130×10^{-2}	0.597	1.453	1.541	1.76	0.60	0.98	2.10	0.91	0.33	0.46	2.36	301
308	70.	0.200×10^{-2}	0.388	1.274	1.300	1.72	0.33	0.84	1.94	0.31	0.27	−0.06	1.98	301
309	70.	0.320×10^{-2}	0.216	1.103	1.110	1.66	0.46	0.70	1.86	0.33	0.03	−0.11	1.89	319
310	70.	0.500×10^{-2}	0.138	0.999	1.001	1.54	0.43	0.68	1.74	0.29	0.00	0.15	1.77	319
311	70.	0.800×10^{-2}	0.086	0.824	0.825	1.61	0.48	0.66	1.81	0.24	0.00	0.23	1.84	319
312	70.	0.130×10^{-1}	0.053	0.720	0.720	1.88	0.51	0.77	2.10	0.38	0.03	0.67	2.23	319
313	70.	0.200×10^{-1}	0.035	0.640	0.640	1.77	0.67	0.70	2.02	0.32	0.05	0.54	2.11	319
314	70.	0.320×10^{-1}	0.022	0.564	0.564	2.10	0.92	0.76	2.41	0.00	0.01	−0.23	2.42	319
315	70.	0.500×10^{-1}	0.014	0.513	0.513	1.61	0.90	1.16	2.18	0.28	0.11	0.29	2.22	319
316	90.	0.130×10^{-2}	0.684	1.446	—	1.60	3.50	1.42	4.10	0.11	0.02	0.13	4.11	319
317	90.	0.200×10^{-2}	0.499	1.261	1.308	1.97	0.35	0.93	2.21	0.90	0.27	0.07	2.40	301
318	90.	0.200×10^{-2}	0.445	1.321	1.371	1.20	1.05	0.72	1.74	0.37	0.02	−0.05	1.78	319
319	90.	0.320×10^{-2}	0.278	1.176	1.189	0.84	0.61	0.66	1.23	0.26	0.06	0.09	1.26	319
320	90.	0.500×10^{-2}	0.178	1.035	1.039	0.79	0.59	0.64	1.17	0.34	0.05	0.08	1.22	319
321	90.	0.800×10^{-2}	0.111	0.891	0.892	0.86	0.56	0.69	1.24	0.28	0.02	0.01	1.27	319
322	90.	0.130×10^{-1}	0.068	0.759	0.759	0.90	0.69	0.70	1.33	0.24	0.04	0.23	1.37	319
323	90.	0.200×10^{-1}	0.044	0.654	0.654	0.94	0.62	0.71	1.33	0.27	0.04	0.42	1.42	319
324	90.	0.320×10^{-1}	0.028	0.561	0.561	1.00	0.73	0.73	1.44	0.24	0.03	0.25	1.48	319
325	90.	0.500×10^{-1}	0.018	0.491	0.490	1.27	0.71	0.93	1.73	0.07	0.06	0.06	1.73	319
326	90.	0.800×10^{-1}	0.011	0.439	0.438	1.23	0.92	0.95	1.81	0.31	0.06	0.37	1.88	319
327	90.	0.180	0.005	0.344	0.344	3.05	3.04	1.92	4.72	1.47	−0.23	1.28	5.11	319
328	120.	0.160×10^{-2}	0.741	1.401	—	1.80	2.70	1.22	3.47	−0.07	0.03	0.07	3.47	319
329	120.	0.200×10^{-2}	0.665	1.336	—	2.22	0.77	1.19	2.64	1.19	0.09	0.49	2.93	301
330	120.	0.200×10^{-2}	0.593	1.313	1.412	1.51	2.00	1.27	2.81	0.34	−0.02	−0.15	2.84	319
331	120.	0.320×10^{-2}	0.416	1.186	1.213	1.92	0.73	0.80	2.20	0.76	0.03	−0.03	2.33	301
332	120.	0.320×10^{-2}	0.371	1.212	1.239	1.30	1.80	1.03	2.45	0.24	0.01	−0.08	2.46	319
333	120.	0.500×10^{-2}	0.237	1.046	1.053	1.17	0.59	0.77	1.52	0.22	0.05	0.00	1.54	319
334	120.	0.800×10^{-2}	0.148	0.910	0.912	1.07	0.59	0.67	1.39	0.25	0.06	0.11	1.42	319
335	120.	0.130×10^{-1}	0.091	0.780	0.780	1.12	0.65	0.71	1.48	0.36	0.01	0.15	1.53	319
336	120.	0.200×10^{-1}	0.059	0.671	0.671	1.10	0.66	0.75	1.49	0.24	0.01	0.51	1.59	319
337	120.	0.320×10^{-1}	0.037	0.577	0.577	1.25	0.74	0.75	1.63	0.23	0.04	0.34	1.68	319
338	120.	0.500×10^{-1}	0.024	0.489	0.488	1.25	0.69	0.87	1.67	0.12	0.05	0.04	1.68	319
339	120.	0.800×10^{-1}	0.015	0.443	0.442	1.35	0.63	1.18	1.90	0.34	0.05	0.25	1.95	319
340	120.	0.180	0.007	0.333	0.333	2.37	2.69	1.51	3.89	0.90	−0.14	−0.26	4.01	301
341	150.	0.200×10^{-2}	0.741	1.389	—	2.00	2.70	1.28	3.60	−0.18	0.03	0.02	3.60	319
342	150.	0.320×10^{-2}	0.520	1.204	1.250	1.82	0.89	0.99	2.25	0.87	0.10	0.32	2.44	301
343	150.	0.320×10^{-2}	0.463	1.201	1.247	1.21	2.10	1.04	2.64	0.32	0.01	−0.20	2.66	319
344	150.	0.500×10^{-2}	0.296	1.058	1.071	1.08	0.87	0.69	1.54	0.26	−0.01	0.05	1.57	319
345	150.	0.800×10^{-2}	0.185	0.915	0.919	1.33	0.89	0.71	1.76	0.25	0.03	0.33	1.81	319
346	150.	0.130×10^{-1}	0.114	0.807	0.807	1.98	0.51	1.03	2.29	0.45	−0.03	0.30	2.35	319
347	150.	0.200×10^{-1}	0.074	0.693	0.693	1.67	0.68	0.88	2.01	0.30	0.03	0.54	2.11	319
348	150.	0.320×10^{-1}	0.046	0.588	0.588	1.87	0.80	0.96	2.25	0.10	−0.05	0.53	2.31	319
349	150.	0.500×10^{-1}	0.030	0.512	0.512	1.78	1.08	0.88	2.26	0.14	0.04	0.10	2.27	319
350	150.	0.800×10^{-1}	0.019	0.446	0.446	1.72	0.88	1.09	2.22	0.19	0.06	0.35	2.26	319
351	150.	0.180	0.008	0.325	0.325	2.56	2.19	1.61	3.73	0.93	−0.12	−0.30	3.86	319
352	200.	0.260×10^{-2}	0.760	1.286	—	2.20	2.60	1.08	3.57	0.18	0.03	0.09	3.58	319
353	200.	0.320×10^{-2}	0.693	1.171	—	3.80	2.00	1.30	4.48	1.40	0.17	0.56	4.73	301
354	200.	0.320×10^{-2}	0.618	1.221	—	1.92	2.20	1.21	3.16	0.30	−0.02	0.08	3.18	319
355	200.	0.500×10^{-2}	0.443	1.074	1.100	1.89	0.88	0.85	2.25	0.68	0.03	−0.04	2.35	301
356	200.	0.500×10^{-2}	0.395	1.103	1.129	1.14	0.69	0.93	1.62	0.34	0.02	0.00	1.66	319
357	200.	0.800×10^{-2}	0.247	0.934	0.940	0.92	0.58	0.73	1.31	0.17	0.04	0.06	1.33	319
358	200.	0.130×10^{-1}	0.152	0.806	0.807	0.94	0.46	0.69	1.25	0.27	0.03	0.22	1.30	319
359	200.	0.200×10^{-1}	0.099	0.698	0.698	1.13	0.64	0.71	1.48	0.11	0.02	0.25	1.51	319
360	200.	0.320×10^{-1}	0.062	0.586	0.586	1.20	0.82	0.71	1.62	0.15	0.04	0.40	1.67	319
361	200.	0.500×10^{-1}	0.040	0.521	0.521	1.25	0.73	0.73	1.62	0.04	0.02	0.12	1.63	319
362	200.	0.800×10^{-1}	0.025	0.431	0.431	1.16	0.47	0.99	1.59	−0.07	0.08	0.34	1.63	319
363	200.	0.130	0.015	0.355	0.355	2.56	3.20	1.78	4.47	0.38	0.00	0.23	4.49	319
364	200.	0.180	0.011	0.331	0.331	1.75	1.20	1.82	2.80	1.06	−0.06	−0.24	3.00	319
365	200.	0.250	0.008	0.273	0.273	3.60	4.20	2.67	6.14	1.36	−0.03	0.30	6.30	319
366	200.	0.400	0.005	0.139	0.139	4.61	4.30	5.09	8.10	2.35	−0.08	−0.93	8.49	319

Table 10: Continuation of table 6.

Bin #	Q^2 GeV^2	x	y	$\sigma_r^{+\,\mathrm{ave}}$	F_2^{ave}	$\delta_{\mathrm{ave,stat}}$ %	$\delta_{\mathrm{ave,uncor}}$ %	$\delta_{\mathrm{ave,cor}}$ %	$\delta_{\mathrm{ave,exp\ tot}}$ %	$\delta_{\mathrm{ave,rel}}$ %	$\delta_{\mathrm{ave,gp}}$ %	$\delta_{\mathrm{ave,had}}$ %	$\delta_{\mathrm{ave,tot}}$ %	$\sqrt{s}$ GeV
367	250.	0.330×10^{-2}	0.749	1.247	—	2.50	2.70	1.23	3.88	0.08	0.03	−0.12	3.89	319
368	250.	0.500×10^{-2}	0.554	1.079	1.123	2.29	1.61	0.97	2.97	1.02	0.06	0.18	3.14	301
369	250.	0.500×10^{-2}	0.494	1.102	1.148	1.61	2.10	0.90	2.80	0.07	0.02	−0.12	2.80	319
370	250.	0.800×10^{-2}	0.309	0.953	0.964	1.04	0.69	0.72	1.44	0.32	0.03	0.03	1.48	319
371	250.	0.130×10^{-1}	0.190	0.825	0.828	1.07	0.64	0.71	1.44	0.11	0.04	0.21	1.46	319
372	250.	0.200×10^{-1}	0.124	0.701	0.701	1.18	0.79	0.70	1.59	0.20	0.03	0.10	1.60	319
373	250.	0.320×10^{-1}	0.077	0.592	0.591	1.25	0.85	0.74	1.68	0.35	0.03	0.31	1.74	319
374	250.	0.500×10^{-1}	0.049	0.521	0.521	1.22	0.80	0.74	1.64	0.10	0.03	0.26	1.66	319
375	250.	0.800×10^{-1}	0.031	0.432	0.432	1.18	0.64	0.97	1.66	0.14	0.05	0.17	1.67	319
376	250.	0.130	0.019	0.342	0.341	1.77	2.68	0.93	3.34	0.54	0.01	0.35	3.40	319
377	250.	0.180	0.014	0.325	0.325	1.70	0.78	1.29	2.27	0.79	0.01	0.46	2.45	319
378	250.	0.250	0.010	0.263	0.263	2.13	3.68	2.21	4.79	2.16	−0.03	0.00	5.26	319
379	250.	0.400	0.006	0.140	0.139	3.13	3.97	4.32	6.65	3.26	−0.08	−0.70	7.44	319
380	300.	0.390×10^{-2}	0.760	1.185	—	2.71	2.70	1.05	3.96	0.06	0.03	−0.12	3.97	319
381	300.	0.500×10^{-2}	0.665	1.127	—	2.94	2.64	0.93	4.06	0.46	0.14	0.32	4.10	301
382	300.	0.500×10^{-2}	0.593	1.124	1.197	2.51	2.60	1.08	3.77	−0.04	0.00	0.16	3.77	319
383	300.	0.800×10^{-2}	0.416	0.982	1.000	2.29	1.12	0.88	2.70	0.58	0.07	0.07	2.76	301
384	300.	0.800×10^{-2}	0.371	0.971	0.989	1.46	0.94	0.93	1.96	0.24	0.03	−0.02	1.98	319
385	300.	0.130×10^{-1}	0.228	0.818	0.822	1.15	0.71	0.71	1.53	0.26	0.02	0.04	1.55	319
386	300.	0.200×10^{-1}	0.148	0.699	0.700	1.28	0.90	0.72	1.72	0.36	0.03	0.10	1.76	319
387	300.	0.320×10^{-1}	0.093	0.613	0.613	1.32	0.90	0.75	1.76	0.15	0.03	0.32	1.80	319
388	300.	0.500×10^{-1}	0.059	0.503	0.503	1.35	0.81	0.74	1.74	0.30	0.02	0.12	1.77	319
389	300.	0.800×10^{-1}	0.037	0.434	0.433	1.29	0.64	0.77	1.63	0.15	0.04	0.14	1.65	319
390	300.	0.130	0.023	0.353	0.352	1.85	3.03	1.01	3.69	0.81	0.01	0.22	3.79	319
391	300.	0.180	0.016	0.318	0.318	1.82	0.93	0.88	2.23	0.32	0.06	0.36	2.28	319
392	300.	0.250	0.012	0.263	0.262	2.13	4.45	2.35	5.47	2.12	−0.03	0.04	5.86	319
393	300.	0.400	0.007	0.155	0.155	3.25	5.38	3.69	7.28	3.46	−0.07	−0.60	8.09	319
394	400.	0.530×10^{-2}	0.746	1.158	—	2.90	2.90	1.04	4.23	0.16	0.03	−0.05	4.24	319
395	400.	0.800×10^{-2}	0.554	0.961	0.996	2.63	1.77	0.78	3.27	0.40	0.13	0.02	3.29	301
396	400.	0.800×10^{-2}	0.494	1.023	1.060	1.70	0.91	1.09	2.22	0.41	0.02	−0.03	2.25	319
397	400.	0.130×10^{-1}	0.341	0.859	0.867	2.95	0.57	0.74	3.10	0.48	0.04	0.15	3.14	301
398	400.	0.130×10^{-1}	0.304	0.846	0.854	1.50	1.09	0.76	2.00	0.25	0.03	0.02	2.02	319
399	400.	0.200×10^{-1}	0.198	0.711	0.713	1.46	0.93	0.72	1.88	0.12	0.05	0.12	1.88	319
400	400.	0.320×10^{-1}	0.124	0.607	0.607	1.47	0.94	0.72	1.89	0.34	0.02	0.15	1.93	319
401	400.	0.500×10^{-1}	0.079	0.509	0.509	1.47	0.83	0.73	1.84	0.24	0.03	0.32	1.88	319
402	400.	0.800×10^{-1}	0.049	0.444	0.444	1.48	0.78	0.77	1.85	−0.01	0.04	0.17	1.85	319
403	400.	0.130	0.030	0.363	0.362	1.60	0.86	0.77	1.97	0.31	0.05	0.24	2.01	319
404	400.	0.250	0.016	0.257	0.256	1.86	1.38	1.19	2.60	1.22	−0.03	0.07	2.87	319
405	400.	0.400	0.010	0.160	0.160	3.65	3.70	3.66	6.36	2.67	−0.07	−0.48	6.91	319
406	500.	0.660×10^{-2}	0.749	1.016	—	3.31	2.90	0.92	4.49	0.19	0.03	−0.09	4.50	319
407	500.	0.800×10^{-2}	0.693	1.011	—	4.23	5.00	1.05	6.63	0.02	0.00	0.28	6.64	301
408	500.	0.800×10^{-2}	0.618	1.029	—	3.51	3.00	1.06	4.73	0.00	0.01	0.10	4.74	319
409	500.	0.130×10^{-1}	0.426	0.883	0.898	3.34	5.00	0.98	6.09	0.15	0.03	−0.04	6.10	301
410	500.	0.130×10^{-1}	0.380	0.884	0.900	2.42	2.70	1.01	3.76	0.53	0.02	−0.22	3.81	319
411	500.	0.200×10^{-1}	0.247	0.737	0.741	2.00	2.07	0.80	2.99	0.12	0.03	0.06	2.99	319
412	500.	0.320×10^{-1}	0.154	0.623	0.623	2.01	2.05	0.76	2.97	0.17	0.03	0.03	2.98	319
413	500.	0.500×10^{-1}	0.099	0.517	0.516	2.11	2.25	1.01	3.25	0.54	0.03	−0.05	3.29	319
414	500.	0.800×10^{-1}	0.062	0.438	0.437	2.22	2.18	0.85	3.23	0.13	0.03	0.28	3.24	319
415	500.	0.130	0.038	0.347	0.346	2.64	2.24	1.16	3.65	0.00	0.04	0.47	3.68	319
416	500.	0.180	0.027	0.291	0.290	2.96	2.95	1.16	4.34	0.74	0.01	0.33	4.41	319
417	500.	0.250	0.020	0.254	0.253	3.59	3.47	2.32	5.51	2.83	−0.03	−0.25	6.20	319
418	500.	0.400	0.012	0.166	0.165	5.10	5.86	4.50	8.98	4.31	−0.10	−0.21	9.96	319
419	650.	0.850×10^{-2}	0.848	0.922	—	4.63	1.82	1.33	5.15	1.41	0.09	0.48	5.36	301
420	650.	0.850×10^{-2}	0.756	0.986	—	3.81	3.70	0.91	5.38	−0.09	0.03	−0.05	5.39	319
421	650.	0.130×10^{-1}	0.554	0.846	0.874	2.65	1.13	0.76	2.98	0.34	0.04	−0.09	3.00	301
422	650.	0.130×10^{-1}	0.494	0.851	0.880	1.94	0.88	0.92	2.32	0.22	0.03	0.04	2.33	319
423	650.	0.200×10^{-1}	0.360	0.702	0.709	4.15	3.70	0.96	5.64	0.20	0.03	0.05	5.64	301
424	650.	0.200×10^{-1}	0.321	0.745	0.753	1.92	0.83	0.70	2.20	0.25	0.04	0.05	2.22	319
425	650.	0.320×10^{-1}	0.201	0.615	0.617	1.82	0.95	0.72	2.18	0.30	0.04	0.09	2.20	319
426	650.	0.500×10^{-1}	0.128	0.512	0.512	1.85	0.92	0.72	2.18	0.26	0.02	0.28	2.22	319
427	650.	0.800×10^{-1}	0.080	0.446	0.446	1.86	0.92	0.70	2.19	0.26	0.04	0.15	2.21	319
428	650.	0.130	0.049	0.364	0.363	2.05	0.96	0.77	2.39	0.41	0.05	0.28	2.44	319
429	650.	0.180	0.036	0.303	0.302	3.34	3.45	1.30	4.98	1.10	0.01	0.30	5.10	319
430	650.	0.250	0.026	0.252	0.251	2.45	1.42	0.95	2.99	0.86	0.02	0.08	3.11	319
431	650.	0.400	0.016	0.144	0.144	5.40	3.20	3.08	6.99	3.36	−0.20	−0.95	7.82	319
432	650.	0.650	0.010	0.022	0.022	13.82	7.79	5.57	16.8	3.81	−0.11	−1.37	17.30	319
433	800.	0.105×10^{-1}	0.753	0.947	—	4.50	4.20	0.94	6.23	0.48	0.02	−0.01	6.25	319
434	800.	0.130×10^{-1}	0.682	0.890	—	3.45	1.49	0.86	3.85	1.10	−0.01	0.12	4.01	301
435	800.	0.130×10^{-1}	0.608	0.850	—	2.43	1.05	1.05	2.85	0.48	0.02	0.06	2.89	319
436	800.	0.200×10^{-1}	0.443	0.737	0.751	4.12	2.30	0.84	4.79	0.35	0.04	−0.15	4.81	301
437	800.	0.200×10^{-1}	0.395	0.752	0.766	2.55	1.32	0.92	3.02	0.02	0.04	0.09	3.02	319
438	800.	0.320×10^{-1}	0.247	0.642	0.645	2.06	1.01	0.69	2.39	0.45	0.03	0.09	2.44	319
439	800.	0.500×10^{-1}	0.158	0.516	0.516	2.05	0.99	0.73	2.39	0.31	0.03	0.26	2.43	319
440	800.	0.800×10^{-1}	0.099	0.448	0.447	2.17	1.04	0.78	2.53	0.25	0.03	0.32	2.56	319
441	800.	0.130	0.061	0.362	0.361	2.40	0.99	0.77	2.71	0.27	0.03	0.17	2.73	319
442	800.	0.180	0.044	0.325	0.324	3.76	3.09	0.97	4.97	0.51	0.02	0.27	5.00	319
443	800.	0.250	0.032	0.256	0.255	2.89	1.12	1.01	3.26	0.99	0.05	0.27	3.42	319
444	800.	0.400	0.020	0.130	0.129	5.98	3.41	2.48	7.31	2.54	−0.13	−0.50	7.76	319
445	800.	0.650	0.012	0.020	0.020	12.11	7.21	5.31	15.1	4.05	−0.12	−0.72	15.61	319

Table 11: Continuation of table 6.

Bin #	Q^2 GeV^2	x	y	$\sigma_r^{+\ \mathrm{ave}}$	F_2^{ave}	$\delta_{\mathrm{ave,stat}}$ %	$\delta_{\mathrm{ave,uncor}}$ %	$\delta_{\mathrm{ave,cor}}$ %	$\delta_{\mathrm{ave,exp\ tot}}$ %	$\delta_{\mathrm{ave,rel}}$ %	$\delta_{\mathrm{ave,gp}}$ %	$\delta_{\mathrm{ave,had}}$ %	$\delta_{\mathrm{ave,tot}}$ %	$\sqrt{s}$ GeV
446	1000.	0.130×10^{-1}	0.760	0.871	—	5.04	3.70	1.31	6.39	0.41	−0.02	−0.06	6.40	319
447	1000.	0.200×10^{-1}	0.554	0.738	0.762	5.46	3.70	1.00	6.67	0.11	0.01	−0.07	6.67	301
448	1000.	0.200×10^{-1}	0.494	0.732	0.756	3.93	3.00	0.97	5.04	0.28	0.02	−0.29	5.06	319
449	1000.	0.320×10^{-1}	0.309	0.637	0.644	3.29	2.46	1.00	4.23	0.43	0.03	−0.09	4.25	319
450	1000.	0.500×10^{-1}	0.198	0.556	0.557	3.21	2.35	0.78	4.05	0.27	0.03	−0.03	4.06	319
451	1000.	0.800×10^{-1}	0.124	0.444	0.444	3.35	2.28	0.81	4.13	0.16	0.03	0.26	4.15	319
452	1000.	0.130	0.076	0.394	0.393	3.99	2.65	0.95	4.88	0.45	0.03	0.04	4.90	319
453	1000.	0.180	0.055	0.327	0.326	4.35	2.68	0.79	5.17	0.45	0.02	0.24	5.19	319
454	1000.	0.250	0.040	0.256	0.255	4.90	3.36	1.33	6.09	1.03	0.00	0.33	6.18	319
455	1000.	0.400	0.025	0.125	0.124	7.64	5.71	2.88	9.96	3.01	−0.05	−0.17	10.41	319
456	1000.	0.650	0.015	0.019	0.019	13.98	7.73	5.35	16.8	6.73	−0.12	−0.07	18.14	319
457	1200.	0.140×10^{-1}	0.950	0.875	—	5.50	1.05	1.30	5.75	1.40	0.11	0.43	5.93	301
458	1200.	0.140×10^{-1}	0.847	0.838	—	3.53	0.90	2.47	4.40	0.19	0.06	0.06	4.40	319
459	1200.	0.200×10^{-1}	0.665	0.705	—	4.18	1.13	0.71	4.39	0.37	0.09	−0.03	4.41	301
460	1200.	0.200×10^{-1}	0.593	0.786	0.826	2.87	1.04	0.98	3.20	0.29	0.03	0.00	3.22	319
461	1200.	0.320×10^{-1}	0.416	0.591	0.601	3.95	1.51	0.70	4.29	−0.03	0.08	0.09	4.29	301
462	1200.	0.320×10^{-1}	0.371	0.649	0.660	2.80	1.11	0.88	3.14	0.32	0.03	−0.01	3.15	319
463	1200.	0.500×10^{-1}	0.237	0.516	0.519	2.17	0.69	0.70	2.38	0.31	0.02	0.22	2.41	319
464	1200.	0.800×10^{-1}	0.148	0.453	0.453	2.22	0.68	0.70	2.43	0.29	0.03	0.21	2.46	319
465	1200.	0.130	0.091	0.368	0.366	2.45	0.62	0.82	2.66	0.43	0.04	0.21	2.70	319
466	1200.	0.180	0.066	0.328	0.326	4.93	2.53	0.92	5.62	0.31	0.03	0.42	5.64	319
467	1200.	0.250	0.047	0.248	0.247	2.75	0.78	0.81	2.97	0.58	0.04	0.14	3.03	319
468	1200.	0.400	0.030	0.137	0.136	4.30	2.24	1.71	5.14	1.87	−0.04	−0.19	5.48	319
469	1200.	0.650	0.018	0.021	0.021	13.76	7.84	4.47	16.5	5.89	−0.20	−0.51	17.49	319
470	1500.	0.200×10^{-1}	0.831	0.731	—	6.00	3.87	0.89	7.20	0.28	0.02	0.19	7.21	301
471	1500.	0.200×10^{-1}	0.741	0.689	—	3.89	1.31	1.51	4.37	0.52	0.01	0.04	4.40	319
472	1500.	0.320×10^{-1}	0.520	0.557	0.575	6.44	2.29	0.78	6.88	0.11	0.06	−0.05	6.88	301
473	1500.	0.320×10^{-1}	0.463	0.620	0.639	3.54	1.27	0.81	3.85	0.17	0.03	0.00	3.85	319
474	1500.	0.500×10^{-1}	0.296	0.553	0.560	2.58	0.87	0.73	2.82	0.22	0.02	0.07	2.83	319
475	1500.	0.800×10^{-1}	0.185	0.446	0.448	2.63	0.96	0.73	2.89	0.37	0.02	0.21	2.93	319
476	1500.	0.130	0.114	0.341	0.340	3.41	1.11	0.79	3.68	0.17	0.04	0.17	3.68	319
477	1500.	0.180	0.082	0.318	0.316	3.32	0.92	0.79	3.53	0.50	0.03	0.11	3.57	319
478	1500.	0.250	0.059	0.255	0.253	3.82	1.53	0.86	4.20	0.81	0.03	0.16	4.28	319
479	1500.	0.400	0.037	0.124	0.123	5.66	2.31	1.47	6.29	1.91	−0.04	0.23	6.58	319
480	1500.	0.650	0.023	0.013	0.013	18.46	6.82	3.77	20.0	5.50	−0.01	−1.43	20.82	319
481	2000.	0.320×10^{-1}	0.693	0.595	—	6.11	2.45	0.75	6.63	0.12	−0.02	−0.04	6.63	301
482	2000.	0.320×10^{-1}	0.618	0.624	—	4.13	1.47	1.49	4.63	0.18	0.03	0.02	4.64	319
483	2000.	0.500×10^{-1}	0.443	0.496	0.510	5.68	1.70	0.71	5.97	0.32	0.02	0.04	5.98	301
484	2000.	0.500×10^{-1}	0.395	0.503	0.516	4.16	1.34	0.80	4.45	0.29	0.03	0.06	4.46	319
485	2000.	0.800×10^{-1}	0.247	0.433	0.437	3.16	0.90	0.72	3.37	0.15	0.03	0.22	3.38	319
486	2000.	0.130	0.152	0.370	0.370	3.61	1.18	0.73	3.87	0.42	0.02	0.17	3.90	319
487	2000.	0.180	0.110	0.316	0.314	3.90	1.10	0.75	4.13	0.31	0.03	0.08	4.14	319
488	2000.	0.250	0.079	0.239	0.236	4.47	1.47	0.81	4.78	0.56	0.04	0.08	4.81	319
489	2000.	0.400	0.049	0.128	0.126	6.19	2.60	1.61	6.91	2.31	−0.03	−0.01	7.28	319
490	2000.	0.650	0.030	0.021	0.021	19.26	9.70	4.66	22.1	12.3	−0.10	0.19	25.29	319
491	3000.	0.500×10^{-1}	0.665	0.522	—	5.63	2.20	0.79	6.10	0.05	0.03	−0.19	6.10	301
492	3000.	0.500×10^{-1}	0.593	0.540	0.582	4.20	1.84	0.85	4.66	0.28	0.03	−0.07	4.67	319
493	3000.	0.800×10^{-1}	0.416	0.445	0.461	5.78	1.98	0.71	6.15	0.03	0.01	0.00	6.15	301
494	3000.	0.800×10^{-1}	0.371	0.417	0.432	4.38	1.53	0.84	4.72	0.48	0.02	−0.04	4.74	319
495	3000.	0.130	0.228	0.343	0.347	4.16	1.57	0.80	4.52	0.26	0.03	0.22	4.53	319
496	3000.	0.180	0.165	0.303	0.303	4.23	1.66	0.82	4.62	0.53	0.02	0.09	4.65	319
497	3000.	0.250	0.119	0.218	0.215	5.14	1.64	0.92	5.47	0.84	0.02	0.11	5.54	319
498	3000.	0.400	0.074	0.121	0.118	6.41	2.58	1.33	7.04	1.39	0.02	0.22	7.18	319
499	3000.	0.650	0.046	0.016	0.016	12.48	4.23	2.37	13.4	3.24	0.01	−0.36	13.78	319
500	5000.	0.800×10^{-1}	0.693	0.362	—	6.86	2.22	0.77	7.25	0.30	0.17	−0.10	7.26	301
501	5000.	0.800×10^{-1}	0.618	0.419	—	4.46	1.62	0.97	4.84	0.41	0.03	−0.01	4.86	319
502	5000.	0.130	0.426	0.332	0.353	7.83	2.14	0.87	8.16	0.63	0.03	0.22	8.19	301
503	5000.	0.130	0.380	0.350	0.372	5.48	1.72	0.81	5.80	0.24	0.03	0.03	5.81	319
504	5000.	0.180	0.274	0.264	0.271	4.91	1.47	0.71	5.18	0.31	0.03	0.14	5.19	319
505	5000.	0.250	0.198	0.235	0.235	5.51	2.09	0.82	5.95	1.62	0.02	0.23	6.17	319
506	5000.	0.400	0.124	0.120	0.117	7.14	2.08	0.86	7.48	0.67	0.04	0.05	7.51	319
507	5000.	0.650	0.076	0.010	0.010	27.08	12.77	3.65	30.2	4.19	−0.05	1.06	30.47	319
508	8000.	0.130	0.682	0.256	—	10.94	3.07	0.70	11.4	0.35	0.04	−0.01	11.39	301
509	8000.	0.130	0.608	0.321	—	7.20	2.09	1.07	7.57	0.32	0.03	0.04	7.58	319
510	8000.	0.180	0.493	0.277	0.311	10.95	3.44	0.92	11.5	0.41	0.03	0.24	11.52	301
511	8000.	0.180	0.439	0.299	0.336	7.44	2.33	0.86	7.84	1.17	0.03	−0.03	7.93	319
512	8000.	0.250	0.355	0.231	0.243	11.80	3.15	1.39	12.3	1.08	−0.01	0.11	12.34	301
513	8000.	0.250	0.316	0.208	0.219	8.93	2.82	1.22	9.44	0.64	0.03	0.04	9.46	319
514	8000.	0.400	0.198	0.101	0.100	9.99	3.55	0.94	10.6	0.84	0.03	−0.10	10.67	319
515	8000.	0.650	0.122	0.017	0.016	17.17	6.60	2.00	18.5	7.35	−0.01	0.11	19.91	319
516	12000.	0.180	0.739	0.208	—	17.37	2.43	0.88	17.6	0.87	0.03	0.25	17.59	301
517	12000.	0.180	0.659	0.291	—	10.20	2.87	1.72	10.7	0.77	0.02	0.15	10.76	319
518	12000.	0.250	0.532	0.150	0.179	20.21	3.46	0.73	20.5	0.31	0.02	0.03	20.51	301
519	12000.	0.250	0.474	0.154	0.183	15.27	4.11	1.01	15.8	1.10	0.01	−0.13	15.88	319
520	12000.	0.400	0.296	0.073	0.076	15.58	4.59	1.05	16.3	2.73	0.02	−0.05	16.50	319
521	12000.	0.650	0.182	0.017	0.016	33.62	18.57	3.59	38.6	2.17	−0.01	0.69	38.65	319

Table 12: Continuation of table 6.

Bin #	Q^2 GeV^2	x	y	$\sigma_r^{+\,\mathrm{ave}}$	F_2^{ave}	$\delta_{\mathrm{ave,stat}}$ %	$\delta_{\mathrm{ave,uncor}}$ %	$\delta_{\mathrm{ave,cor}}$ %	$\delta_{\mathrm{ave,exp\ tot}}$ %	$\delta_{\mathrm{ave,rel}}$ %	$\delta_{\mathrm{ave,gp}}$ %	$\delta_{\mathrm{ave,had}}$ %	$\delta_{\mathrm{ave,tot}}$ %	$\sqrt{s}$ GeV
522	20000.	0.250	0.887	0.135	—	30.72	3.58	0.96	30.9	0.85	0.02	0.36	30.96	301
523	20000.	0.250	0.791	0.096	—	22.47	2.01	2.50	22.7	0.63	0.05	0.14	22.71	319
524	20000.	0.400	0.554	0.116	0.146	31.65	7.66	1.29	32.6	1.60	−0.01	−0.51	32.63	301
525	20000.	0.400	0.494	0.047	0.059	35.20	7.96	2.49	36.2	0.21	0.01	−0.03	36.17	319
526	20000.	0.650	0.304	0.014	0.014	50.08	28.03	4.07	57.5	7.64	−0.01	−0.23	58.04	319
527	30000.	0.400	0.831	0.110	—	66.01	5.29	1.46	66.2	0.54	0.00	0.25	66.24	301
528	30000.	0.400	0.741	0.086	—	35.54	4.75	13.06	38.2	5.53	−0.07	0.09	38.56	319

Table 13: Continuation of table 6.

Bin #	Q^2 GeV^2	x	y	$\sigma_r^{-\text{ ave}}$	F_2^{ave}	$\delta_{\text{ave,stat}}$ %	$\delta_{\text{ave,uncor}}$ %	$\delta_{\text{ave,cor}}$ %	$\delta_{\text{ave,exp tot}}$ %	$\delta_{\text{ave,rel}}$ %	$\delta_{\text{ave,gp}}$ %	$\delta_{\text{ave,had}}$ %	$\delta_{\text{ave,tot}}$ %	$\sqrt{s}$ GeV
1	90.	0.130×10^{-2}	0.684	1.372	—	4.00	5.50	1.72	7.01	−0.26	0.01	−0.10	7.02	319
2	90.	0.200×10^{-2}	0.445	1.257	1.292	3.43	3.30	1.87	5.11	0.57	−0.04	−0.26	5.15	319
3	120.	0.160×10^{-2}	0.741	1.343	—	4.20	4.80	1.69	6.60	−0.07	0.01	−0.16	6.60	319
4	120.	0.200×10^{-2}	0.593	1.317	1.390	3.31	3.20	1.95	5.00	0.23	−0.05	0.26	5.01	319
5	120.	0.320×10^{-2}	0.371	1.192	1.211	3.01	3.20	1.59	4.67	0.39	−0.01	−0.15	4.69	319
6	150.	0.200×10^{-2}	0.741	1.331	—	4.41	4.80	1.54	6.70	0.24	0.00	−0.20	6.71	319
7	150.	0.320×10^{-2}	0.463	1.204	1.238	2.72	3.00	1.78	4.42	0.43	−0.02	−0.49	4.47	319
8	150.	0.500×10^{-2}	0.296	1.137	1.147	2.82	3.00	1.64	4.43	−0.05	0.00	−0.15	4.43	319
9	150.	0.800×10^{-2}	0.185	0.949	0.951	4.14	5.40	3.51	7.65	−1.25	0.00	0.30	7.76	319
10	200.	0.260×10^{-2}	0.760	1.186	—	4.80	4.80	1.68	6.99	0.17	0.01	−0.19	7.00	319
11	200.	0.320×10^{-2}	0.618	1.273	—	4.10	3.50	2.06	5.77	0.05	−0.03	−0.01	5.77	319
12	200.	0.500×10^{-2}	0.395	1.129	1.147	2.09	1.27	1.47	2.86	0.05	0.00	−0.24	2.87	319
13	200.	0.800×10^{-2}	0.247	0.940	0.943	2.10	1.15	1.35	2.76	0.14	0.00	−0.11	2.76	319
14	200.	0.130×10^{-1}	0.152	0.826	0.826	2.17	1.20	1.39	2.84	−0.04	0.00	0.05	2.84	319
15	200.	0.200×10^{-1}	0.099	0.707	0.706	2.66	1.54	1.35	3.35	−0.10	0.00	0.04	3.36	319
16	200.	0.320×10^{-1}	0.062	0.581	0.580	2.92	1.65	1.37	3.62	−0.09	0.00	0.10	3.63	319
17	200.	0.500×10^{-1}	0.040	0.500	0.499	2.90	1.26	1.49	3.49	0.13	0.00	0.03	3.50	319
18	200.	0.800×10^{-1}	0.025	0.419	0.418	2.66	1.18	1.68	3.36	0.22	0.00	0.05	3.37	319
19	200.	0.180	0.011	0.319	0.319	3.86	2.00	1.51	4.60	0.28	0.00	0.00	4.61	319
20	250.	0.330×10^{-2}	0.749	1.125	—	5.70	4.90	1.78	7.73	0.40	0.00	−0.19	7.74	319
21	250.	0.500×10^{-2}	0.494	1.117	1.148	2.79	1.79	1.53	3.65	0.25	−0.01	−0.27	3.67	319
22	250.	0.800×10^{-2}	0.309	0.994	1.001	2.39	1.50	1.43	3.17	0.04	0.00	−0.13	3.17	319
23	250.	0.130×10^{-1}	0.190	0.844	0.844	2.48	1.38	1.47	3.19	0.16	0.00	−0.08	3.20	319
24	250.	0.200×10^{-1}	0.124	0.697	0.696	2.72	1.58	1.35	3.42	0.17	0.00	0.05	3.42	319
25	250.	0.320×10^{-1}	0.077	0.598	0.596	2.87	1.57	1.45	3.58	0.44	0.00	0.15	3.61	319
26	250.	0.500×10^{-1}	0.049	0.511	0.509	2.87	1.42	1.40	3.50	0.15	0.01	0.14	3.50	319
27	250.	0.800×10^{-1}	0.031	0.428	0.427	2.74	1.62	1.53	3.54	0.18	0.01	0.03	3.54	319
28	250.	0.130	0.019	0.317	0.316	5.25	5.20	1.64	7.57	0.67	−0.01	0.42	7.61	319
29	250.	0.180	0.014	0.299	0.299	4.05	4.45	1.45	6.19	0.23	0.00	0.00	6.20	319
30	250.	0.250	0.010	0.231	0.231	7.40	8.60	1.95	11.5	1.18	−0.03	0.44	11.58	319
31	250.	0.400	0.006	0.140	0.140	9.22	6.80	1.62	11.6	0.50	−0.02	−0.05	11.58	319
32	300.	0.390×10^{-2}	0.760	1.071	—	6.09	4.90	1.64	7.99	−0.15	0.01	−0.02	7.99	319
33	300.	0.500×10^{-2}	0.593	1.153	1.203	5.60	3.90	1.76	7.05	0.41	−0.02	0.00	7.06	319
34	300.	0.800×10^{-2}	0.371	1.001	1.011	2.92	1.72	1.31	3.63	0.00	0.00	−0.21	3.64	319
35	300.	0.130×10^{-1}	0.228	0.856	0.857	2.75	1.43	1.44	3.41	0.01	0.00	−0.12	3.42	319
36	300.	0.200×10^{-1}	0.148	0.725	0.723	3.05	1.60	1.41	3.72	0.24	0.00	−0.01	3.73	319
37	300.	0.320×10^{-1}	0.093	0.592	0.590	3.16	1.71	1.33	3.83	0.19	0.00	0.03	3.83	319
38	300.	0.500×10^{-1}	0.059	0.521	0.519	3.20	1.63	1.38	3.85	0.14	0.00	0.00	3.85	319
39	300.	0.800×10^{-1}	0.037	0.426	0.425	3.09	1.26	1.39	3.62	0.42	0.00	0.05	3.64	319
40	300.	0.130	0.023	0.336	0.335	5.37	6.70	1.58	8.73	0.44	0.00	0.26	8.74	319
41	300.	0.180	0.016	0.310	0.309	4.16	2.25	1.51	4.97	0.22	0.00	−0.02	4.97	319
42	300.	0.250	0.012	0.287	0.286	6.78	9.40	2.35	11.8	1.60	−0.03	0.51	11.94	319
43	300.	0.400	0.007	0.146	0.145	10.21	8.90	2.07	13.7	1.34	−0.02	0.07	13.77	319
44	400.	0.530×10^{-2}	0.746	1.106	—	6.39	5.10	1.65	8.34	−0.19	0.01	−0.01	8.34	319
45	400.	0.800×10^{-2}	0.494	1.043	1.064	3.27	1.59	1.52	3.94	0.28	0.00	−0.23	3.96	319
46	400.	0.130×10^{-1}	0.304	0.868	0.870	3.55	2.33	1.44	4.49	0.19	0.00	−0.22	4.50	319
47	400.	0.200×10^{-1}	0.198	0.719	0.716	3.67	1.95	1.32	4.36	0.04	0.00	0.16	4.36	319
48	400.	0.320×10^{-1}	0.124	0.591	0.589	3.64	1.93	1.30	4.32	0.35	0.00	−0.12	4.34	319
49	400.	0.500×10^{-1}	0.079	0.511	0.508	3.54	1.52	1.39	4.09	0.12	0.00	0.15	4.10	319
50	400.	0.800×10^{-1}	0.049	0.435	0.433	3.74	1.71	1.36	4.33	0.26	0.00	0.05	4.34	319
51	400.	0.130	0.030	0.376	0.375	3.88	1.80	1.36	4.49	0.43	0.00	0.10	4.51	319
52	400.	0.250	0.016	0.268	0.267	4.66	3.28	1.41	5.87	0.79	−0.01	0.11	5.92	319
53	400.	0.400	0.010	0.147	0.147	10.64	7.30	1.96	13.1	1.19	−0.03	0.19	13.11	319
54	500.	0.660×10^{-2}	0.749	1.097	—	6.91	5.20	1.42	8.76	−0.15	0.01	−0.13	8.76	319
55	500.	0.800×10^{-2}	0.618	1.042	—	7.81	4.60	1.71	9.22	0.04	−0.02	−0.30	9.23	319
56	500.	0.130×10^{-1}	0.380	1.000	1.003	5.11	3.90	1.73	6.65	0.38	0.00	−0.39	6.68	319
57	500.	0.200×10^{-1}	0.247	0.763	0.760	5.11	4.20	1.66	6.82	0.42	0.00	−0.33	6.84	319
58	500.	0.320×10^{-1}	0.154	0.604	0.600	5.30	3.80	1.69	6.74	0.44	0.01	−0.04	6.75	319
59	500.	0.500×10^{-1}	0.099	0.518	0.515	5.59	3.80	1.46	6.92	0.06	0.01	0.17	6.92	319
60	500.	0.800×10^{-1}	0.062	0.396	0.394	6.37	5.80	1.78	8.79	0.75	0.00	0.27	8.83	319
61	500.	0.130	0.038	0.363	0.361	7.20	4.10	1.82	8.48	−0.23	0.02	0.51	8.50	319
62	500.	0.180	0.027	0.289	0.287	8.12	6.60	2.16	10.7	1.44	−0.02	0.39	10.79	319
63	500.	0.250	0.020	0.259	0.258	10.40	8.40	2.18	13.5	1.32	−0.02	0.46	13.61	319
64	500.	0.400	0.012	0.144	0.143	15.14	12.00	3.56	19.6	3.24	−0.05	0.19	19.91	319
65	500.	0.650	0.008	0.027	0.027	19.26	10.50	2.10	22.0	−0.36	−0.01	0.96	22.06	319

Table 14: HERA combined reduced cross section $\sigma_r^{-\text{ ave}}$ for NC e^-p scattering. F_2^{ave} represents the structure function F_2 calculated from σ_r^{ave} by using the HERAPDF1.0 parametrisation of $\tilde{F}_L, x\tilde{F}_3, F_2^{\gamma Z}$ for $y < 0.6$. $\delta_{\text{ave,stat}}$, $\delta_{\text{ave,uncor}}$, $\delta_{\text{ave,cor}}$ and $\delta_{\text{ave,exp tot}}$ represent the statistical, uncorrelated systematic, correlated systematic and total experimental uncertainty, respectively. $\delta_{\text{ave,rel}}$, $\delta_{\text{ave,gp}}$ and $\delta_{\text{ave,had}}$ are the three correlated sources of uncertainties arising from the combination procedure, see section 3.2.3. $\delta_{\text{ave,tot}}$ is the total uncertainty calculated by adding $\delta_{\text{ave,exp tot}}$ and the procedural errors in quadrature. The uncertainties are quoted in percent relative to $\sigma_r^{-\text{ ave}}$. The overall normalisation uncertainty of 0.5% is not included.

Bin #	Q^2 GeV^2	x	y	$\sigma_r^{-\,\mathrm{ave}}$	F_2^{ave}	$\delta_{\mathrm{ave,stat}}$ %	$\delta_{\mathrm{ave,uncor}}$ %	$\delta_{\mathrm{ave,cor}}$ %	$\delta_{\mathrm{ave,exp\ tot}}$ %	$\delta_{\mathrm{ave,rel}}$ %	$\delta_{\mathrm{ave,gp}}$ %	$\delta_{\mathrm{ave,had}}$ %	$\delta_{\mathrm{ave,tot}}$ %	$\sqrt{s}$ GeV
66	650.	0.850×10^{-2}	0.756	0.972	—	4.91	2.20	1.70	5.64	0.03	0.00	0.01	5.64	319
67	650.	0.130×10^{-1}	0.494	0.950	0.959	3.64	1.48	1.56	4.23	0.07	0.00	−0.17	4.23	319
68	650.	0.200×10^{-1}	0.321	0.794	0.790	4.59	1.98	1.35	5.18	0.27	0.00	−0.23	5.19	319
69	650.	0.320×10^{-1}	0.201	0.645	0.638	5.01	2.32	1.32	5.68	0.29	0.00	−0.13	5.69	319
70	650.	0.500×10^{-1}	0.128	0.525	0.520	5.14	2.66	1.41	5.96	0.38	0.00	−0.04	5.97	319
71	650.	0.800×10^{-1}	0.080	0.419	0.415	5.48	2.58	1.39	6.21	0.50	0.00	0.19	6.23	319
72	650.	0.130	0.049	0.344	0.341	5.96	2.59	1.41	6.65	0.33	0.00	−0.14	6.66	319
73	650.	0.180	0.036	0.336	0.333	9.02	6.80	1.86	11.4	0.71	−0.01	0.64	11.49	319
74	650.	0.250	0.026	0.259	0.257	6.68	4.02	1.49	7.94	0.68	−0.01	0.12	7.97	319
75	650.	0.400	0.016	0.088	0.087	23.18	9.30	1.90	25.1	0.63	0.00	−0.64	25.07	319
76	800.	0.105×10^{-1}	0.753	0.942	—	9.18	5.90	1.46	11.0	−0.19	0.00	−0.05	11.01	319
77	800.	0.130×10^{-1}	0.608	0.885	—	4.80	1.63	1.53	5.30	0.20	0.00	0.06	5.30	319
78	800.	0.200×10^{-1}	0.395	0.808	0.803	4.98	2.07	1.39	5.57	0.31	−0.01	−0.13	5.58	319
79	800.	0.320×10^{-1}	0.247	0.662	0.653	5.13	1.94	1.49	5.68	0.55	0.00	−0.17	5.71	319
80	800.	0.500×10^{-1}	0.158	0.590	0.581	5.05	1.86	1.32	5.54	0.05	0.00	0.14	5.54	319
81	800.	0.800×10^{-1}	0.099	0.501	0.494	5.58	2.26	1.43	6.19	0.09	0.00	0.12	6.19	319
82	800.	0.130	0.061	0.368	0.363	6.89	2.48	1.92	7.57	0.77	0.01	0.09	7.61	319
83	800.	0.180	0.044	0.303	0.300	11.58	6.20	1.76	13.3	0.43	0.01	0.44	13.27	319
84	800.	0.250	0.032	0.241	0.239	8.86	3.38	1.66	9.63	0.62	−0.01	0.00	9.65	319
85	800.	0.400	0.020	0.120	0.119	20.64	11.60	2.31	23.8	1.50	−0.02	0.60	23.84	319
86	800.	0.650	0.012	0.015	0.015	21.50	12.50	3.31	25.1	2.87	−0.04	0.04	25.25	319
87	1000.	0.130×10^{-1}	0.760	0.777	—	11.47	6.50	2.18	13.4	0.07	−0.06	0.80	13.39	319
88	1000.	0.200×10^{-1}	0.494	0.776	0.770	7.96	4.30	1.60	9.18	0.52	−0.01	−0.59	9.22	319
89	1000.	0.320×10^{-1}	0.309	0.567	0.556	9.04	4.20	1.45	10.1	0.19	0.00	−0.36	10.08	319
90	1000.	0.500×10^{-1}	0.198	0.575	0.563	8.41	4.30	1.42	9.56	−0.03	0.01	−0.12	9.56	319
91	1000.	0.800×10^{-1}	0.124	0.453	0.444	9.27	4.90	1.70	10.6	0.75	−0.01	0.31	10.65	319
92	1000.	0.130	0.076	0.494	0.486	10.27	5.00	1.65	11.5	−0.44	0.01	0.00	11.55	319
93	1000.	0.180	0.055	0.250	0.246	13.48	5.40	1.43	14.6	0.43	0.00	0.05	14.59	319
94	1000.	0.250	0.040	0.315	0.311	12.92	8.20	2.31	15.5	0.64	0.01	0.94	15.51	319
95	1000.	0.400	0.025	0.124	0.123	22.73	13.30	2.13	26.4	1.19	−0.04	0.29	26.45	319
96	1200.	0.140×10^{-1}	0.847	0.902	—	6.56	1.95	3.31	7.61	0.03	0.00	−0.20	7.61	319
97	1200.	0.200×10^{-1}	0.593	0.741	0.735	5.63	1.47	1.36	5.98	0.29	−0.01	−0.16	5.98	319
98	1200.	0.320×10^{-1}	0.371	0.625	0.609	5.60	1.52	1.38	5.97	0.36	0.00	−0.16	5.98	319
99	1200.	0.500×10^{-1}	0.237	0.552	0.536	5.20	1.34	1.48	5.57	0.23	0.00	−0.03	5.57	319
100	1200.	0.800×10^{-1}	0.148	0.424	0.413	5.54	1.28	1.40	5.86	0.19	0.00	−0.03	5.86	319
101	1200.	0.130	0.091	0.363	0.355	6.00	1.62	1.42	6.38	0.20	0.00	−0.02	6.38	319
102	1200.	0.180	0.066	0.341	0.334	13.60	4.70	1.67	14.5	0.41	0.00	0.40	14.49	319
103	1200.	0.250	0.047	0.266	0.261	6.82	1.50	1.41	7.13	0.29	0.00	0.03	7.13	319
104	1200.	0.400	0.030	0.104	0.103	12.36	7.66	1.89	14.7	0.79	−0.01	0.32	14.69	319
105	1500.	0.200×10^{-1}	0.741	0.838	—	7.20	2.18	1.89	7.76	0.00	−0.01	0.04	7.76	319
106	1500.	0.320×10^{-1}	0.463	0.732	0.707	6.45	1.65	1.53	6.83	0.08	0.00	−0.20	6.84	319
107	1500.	0.500×10^{-1}	0.296	0.578	0.555	6.29	1.26	1.35	6.56	0.27	0.00	−0.07	6.57	319
108	1500.	0.800×10^{-1}	0.185	0.469	0.452	6.53	1.45	1.43	6.84	0.23	0.00	−0.09	6.85	319
109	1500.	0.130	0.114	0.399	0.386	7.83	1.77	1.47	8.16	0.37	0.00	−0.06	8.17	319
110	1500.	0.180	0.082	0.310	0.302	8.69	1.57	1.39	8.94	0.12	0.00	−0.04	8.94	319
111	1500.	0.250	0.059	0.248	0.242	10.17	2.27	1.38	10.5	0.66	0.00	0.17	10.54	319
112	1500.	0.400	0.037	0.145	0.142	15.85	12.25	2.05	20.1	1.30	−0.02	0.48	20.19	319
113	1500.	0.650	0.023	0.014	0.014	35.02	14.50	2.93	38.0	2.31	−0.05	0.46	38.09	319
114	2000.	0.320×10^{-1}	0.618	0.751	—	7.31	1.99	1.83	7.80	0.26	−0.01	−0.21	7.80	319
115	2000.	0.500×10^{-1}	0.395	0.558	0.524	7.79	1.65	1.45	8.10	0.46	0.00	−0.14	8.11	319
116	2000.	0.800×10^{-1}	0.247	0.479	0.452	7.63	1.73	1.67	8.00	0.75	0.00	0.03	8.04	319
117	2000.	0.130	0.152	0.326	0.310	9.91	2.49	1.33	10.3	0.86	0.00	0.11	10.34	319
118	2000.	0.180	0.110	0.270	0.258	10.87	1.98	1.50	11.2	0.33	0.00	−0.12	11.15	319
119	2000.	0.250	0.079	0.258	0.248	11.64	2.39	1.51	12.0	0.75	0.00	−0.02	12.00	319
120	2000.	0.400	0.049	0.104	0.101	17.11	5.25	2.07	18.0	0.81	0.00	0.18	18.04	319
121	3000.	0.500×10^{-1}	0.593	0.626	0.558	7.79	2.90	1.94	8.54	0.62	−0.03	−0.44	8.57	319
122	3000.	0.800×10^{-1}	0.371	0.498	0.446	8.02	2.06	1.39	8.39	0.31	0.00	−0.09	8.40	319
123	3000.	0.130	0.228	0.425	0.387	9.18	3.08	1.32	9.77	−0.01	0.00	0.19	9.77	319
124	3000.	0.180	0.165	0.320	0.294	10.64	2.62	1.36	11.1	0.41	0.00	−0.09	11.05	319
125	3000.	0.250	0.119	0.267	0.249	12.06	3.13	1.61	12.6	0.19	−0.01	0.06	12.56	319
126	3000.	0.400	0.074	0.145	0.137	16.10	5.47	1.82	17.1	0.74	−0.02	0.39	17.12	319
127	3000.	0.650	0.046	0.020	0.019	43.21	5.95	2.27	43.7	0.17	0.00	0.06	43.67	319
128	5000.	0.800×10^{-1}	0.618	0.637	—	7.12	1.92	1.45	7.51	0.39	−0.01	−0.28	7.53	319
129	5000.	0.130	0.380	0.479	0.394	9.55	2.46	1.34	9.95	0.34	0.00	−0.20	9.96	319
130	5000.	0.180	0.274	0.425	0.359	9.68	2.48	1.38	10.1	0.08	0.00	−0.01	10.09	319
131	5000.	0.250	0.198	0.302	0.262	12.35	3.53	1.56	12.9	1.16	0.00	0.20	12.99	319
132	5000.	0.400	0.124	0.126	0.112	18.56	5.69	2.01	19.5	1.58	0.00	−0.31	19.58	319
133	5000.	0.650	0.076	0.010	0.009	40.99	17.70	3.14	44.8	1.73	−0.03	0.63	44.79	319
134	8000.	0.130	0.608	0.586	—	10.57	2.54	2.58	11.2	0.71	0.00	−0.25	11.20	319
135	8000.	0.180	0.439	0.386	0.285	13.69	2.83	1.50	14.1	0.04	0.00	−0.18	14.06	319
136	8000.	0.250	0.316	0.301	0.233	15.36	3.59	1.55	15.8	0.38	−0.01	0.05	15.86	319
137	8000.	0.400	0.198	0.161	0.131	21.81	7.34	2.02	23.1	0.99	0.00	−0.30	23.13	319
138	8000.	0.650	0.122	0.020	0.017	64.03	3.95	1.56	64.2	−0.06	−0.01	−0.02	64.17	319

Table 15: Continuation of table 14

Bin #	Q^2 GeV^2	x	y	$\sigma_r^{-\text{ ave}}$	F_2^{ave}	$\delta_{\text{ave,stat}}$ %	$\delta_{\text{ave,uncor}}$ %	$\delta_{\text{ave,cor}}$ %	$\delta_{\text{ave,exp tot}}$ %	$\delta_{\text{ave,rel}}$ %	$\delta_{\text{ave,gp}}$ %	$\delta_{\text{ave,had}}$ %	$\delta_{\text{ave,tot}}$ %	$\sqrt{s}$ GeV
139	12000.	0.180	0.659	0.453	—	16.43	2.69	3.02	16.9	0.50	0.00	0.10	16.92	319
140	12000.	0.250	0.474	0.282	0.189	21.74	4.83	1.55	22.3	0.05	0.00	−0.50	22.33	319
141	12000.	0.400	0.296	0.093	0.068	35.72	10.68	2.55	37.4	0.84	−0.02	−0.11	37.38	319
142	20000.	0.250	0.791	0.406	—	26.54	3.29	2.47	26.9	0.38	−0.01	−0.07	26.86	319
143	20000.	0.400	0.494	0.194	0.118	33.37	7.52	1.55	34.2	0.51	0.00	−0.25	34.25	319
144	20000.	0.650	0.304	0.013	0.009	73.47	34.51	7.37	81.5	3.18	−0.04	−0.40	81.56	319
145	30000.	0.400	0.741	0.247	—	47.25	6.75	5.97	48.1	−0.63	0.00	0.52	48.11	319

Table 16: Continuation of table 14

Bin #	Q^2 GeV^2	x	y	$\mathrm{d}^2\sigma_{CC}^{e^+p\text{ ave}}/\mathrm{d}x\mathrm{d}Q^2$ pb/GeV^2	$\sigma_{r,\mathrm{CC}}^{+\text{ ave}}$ %	$\delta_{\text{ave,stat}}$ %	$\delta_{\text{ave,uncor}}$ %	$\delta_{\text{ave,cor}}$ %	$\delta_{\text{ave,exp tot}}$ %	$\delta_{\text{ave,rel}}$ %	$\delta_{\text{ave,gp}}$ %	$\delta_{\text{ave,had}}$ %	$\delta_{\text{ave,tot}}$ GeV	$\sqrt{s}$
1	300.	0.800×10^{-2}	0.371	0.136	1.417	19.12	2.80	3.97	19.7	−1.25	0.01	0.09	19.77	319
2	300.	0.130×10^{-1}	0.228	0.695	1.173	8.83	2.54	3.59	9.86	0.40	−0.05	−0.32	9.87	319
3	300.	0.320×10^{-1}	0.093	0.210	0.875	8.09	1.86	2.00	8.54	1.20	0.00	0.15	8.62	319
4	300.	0.800×10^{-1}	0.037	0.466×10^{-1}	0.484	10.74	3.11	1.68	11.3	0.64	−0.01	0.36	11.33	319
5	500.	0.130×10^{-1}	0.380	0.505	0.904	8.09	2.67	2.65	8.92	0.75	−0.02	−0.16	8.95	319
6	500.	0.320×10^{-1}	0.154	0.168	0.740	6.93	1.84	1.24	7.28	0.59	0.00	0.14	7.30	319
7	500.	0.800×10^{-1}	0.062	0.509×10^{-1}	0.561	7.36	1.74	1.15	7.65	−0.41	0.03	−0.04	7.66	319
8	500.	0.130	0.038	0.242×10^{-1}	0.433	11.87	2.63	2.13	12.3	0.16	0.02	0.22	12.35	319
9	1000.	0.130×10^{-1}	0.760	0.323	0.664	10.67	2.99	2.93	11.5	−0.80	−0.03	0.24	11.49	319
10	1000.	0.320×10^{-1}	0.309	0.139	0.701	5.11	1.38	1.16	5.42	0.02	−0.01	0.04	5.42	319
11	1000.	0.800×10^{-1}	0.124	0.434×10^{-1}	0.549	5.73	1.43	0.77	5.95	0.12	0.02	0.20	5.96	319
12	1000.	0.130	0.076	0.213×10^{-1}	0.437	8.25	2.19	0.96	8.59	0.29	0.01	0.08	8.59	319
13	1000.	0.250	0.040	0.702×10^{-2}	0.278	13.28	4.01	1.80	14.0	1.01	−0.01	−0.38	14.03	319
14	1500.	0.320×10^{-1}	0.463	0.961×10^{-1}	0.553	7.91	1.19	1.27	8.10	0.11	0.02	0.16	8.10	319
15	1500.	0.800×10^{-1}	0.185	0.312×10^{-1}	0.449	7.82	0.57	0.82	7.89	−0.18	0.00	0.07	7.89	319
16	1500.	0.130	0.114	0.156×10^{-1}	0.365	10.45	0.74	1.13	10.5	−0.28	0.02	0.09	10.54	319
17	1500.	0.250	0.059	0.555×10^{-2}	0.250	12.65	1.40	1.24	12.8	−0.16	−0.02	0.57	12.81	319
18	2000.	0.320×10^{-1}	0.618	0.806×10^{-1}	0.524	7.67	3.18	1.84	8.50	0.53	0.03	0.24	8.52	319
19	2000.	0.800×10^{-1}	0.247	0.251×10^{-1}	0.408	7.60	2.88	0.94	8.18	0.28	0.03	0.30	8.19	319
20	2000.	0.130	0.152	0.146×10^{-1}	0.386	9.52	3.79	1.01	10.3	1.11	0.03	0.61	10.37	319
21	2000.	0.250	0.079	0.418×10^{-2}	0.212	13.93	5.18	1.13	14.9	1.58	0.01	0.38	14.99	319
22	3000.	0.800×10^{-1}	0.371	0.192×10^{-1}	0.390	5.20	1.61	1.13	5.56	0.29	0.03	−0.26	5.58	319
23	3000.	0.130	0.228	0.939×10^{-2}	0.310	6.65	1.54	1.08	6.91	0.38	0.01	0.08	6.92	319
24	3000.	0.250	0.119	0.284×10^{-2}	0.181	8.98	2.25	1.18	9.33	0.42	0.00	0.02	9.34	319
25	3000.	0.400	0.074	0.731×10^{-3}	0.074	20.21	5.06	2.06	20.9	1.08	−0.06	0.35	20.96	319
26	5000.	0.800×10^{-1}	0.618	0.826×10^{-2}	0.246	8.94	2.30	1.73	9.40	0.66	0.04	−0.08	9.42	319
27	5000.	0.130	0.380	0.482×10^{-2}	0.234	7.32	1.83	1.18	7.64	0.61	0.02	0.00	7.66	319
28	5000.	0.250	0.198	0.175×10^{-2}	0.163	8.63	1.98	1.48	8.98	0.93	0.00	0.51	9.04	319
29	5000.	0.400	0.124	0.462×10^{-3}	0.069	16.59	3.98	2.24	17.2	2.48	−0.03	0.47	17.40	319
30	8000.	0.130	0.608	0.175×10^{-2}	0.135	11.30	3.60	3.06	12.2	0.90	0.05	−0.13	12.29	319
31	8000.	0.250	0.316	0.808×10^{-3}	0.120	10.68	3.25	2.12	11.4	1.51	0.01	−0.01	11.46	319
32	8000.	0.400	0.198	0.222×10^{-3}	0.053	19.92	6.77	3.35	21.3	1.86	−0.05	0.42	21.39	319
33	15000.	0.250	0.593	0.120×10^{-3}	0.039	21.82	5.09	3.75	22.7	1.75	0.06	−0.17	22.79	319
34	15000.	0.400	0.371	0.113×10^{-3}	0.059	17.93	7.02	3.41	19.6	2.16	−0.03	0.42	19.68	319

Table 17: HERA combined double differential $\mathrm{d}^2\sigma_{CC}^{e^+p\text{ ave}}/\mathrm{d}x\mathrm{d}Q^2$ and reduced $\sigma_{r,\mathrm{CC}}^{+\text{ ave}}$ cross section for CC e^+p scattering. $\delta_{\text{ave,stat}}$, $\delta_{\text{ave,uncor}}$, $\delta_{\text{ave,cor}}$ and $\delta_{\text{ave,exp tot}}$ represent the statistical, uncorrelated systematic, correlated systematic and total experimental uncertainty, respectively. $\delta_{\text{ave,rel}}$, $\delta_{\text{ave,gp}}$ and $\delta_{\text{ave,had}}$ are the three correlated sources of uncertainties arising from the combination procedure, see section 3.2.3. $\delta_{\text{ave,tot}}$ is the total uncertainty calculated by adding $\delta_{\text{ave,exp tot}}$ and the procedural errors in quadrature. The uncertainties are quoted in percent relative to $\mathrm{d}^2\sigma_{CC}^{e^+p\text{ ave}}/\mathrm{d}x\mathrm{d}Q^2$. The overall normalisation uncertainty of 0.5% is not included.

Bin #	Q^2 GeV^2	x	y	$\mathrm{d}^2\sigma^{e^-p\ \mathrm{ave}}_{CC}/\mathrm{d}x\mathrm{d}Q^2$ pb/GeV^2	$\sigma^{-\ \mathrm{ave}}_{r,\mathrm{CC}}$ %	$\delta_{\mathrm{ave,stat}}$ %	$\delta_{\mathrm{ave,uncor}}$ %	$\delta_{\mathrm{ave,cor}}$ %	$\delta_{\mathrm{ave,exp\ tot}}$ %	$\delta_{\mathrm{ave,rel}}$ %	$\delta_{\mathrm{ave,gp}}$ %	$\delta_{\mathrm{ave,had}}$ %	$\delta_{\mathrm{ave,tot}}$ GeV	$\sqrt{s}$
1	300.	0.130×10^{-1}	0.228	0.393	0.663	60.18	7.49	11.91	61.8	7.73	−0.24	0.43	62.29	319
2	300.	0.320×10^{-1}	0.093	0.286	1.188	22.51	6.15	6.22	24.1	6.87	−0.06	0.45	25.11	319
3	300.	0.800×10^{-1}	0.037	0.632×10^{-1}	0.657	42.56	8.72	6.47	43.9	3.32	−0.20	0.86	44.05	319
4	500.	0.130×10^{-1}	0.380	0.477	0.854	27.75	7.42	6.96	29.6	1.64	−0.03	0.18	29.60	319
5	500.	0.320×10^{-1}	0.154	0.249	1.097	17.39	4.45	3.94	18.4	2.27	−0.12	0.51	18.52	319
6	500.	0.800×10^{-1}	0.062	0.764×10^{-1}	0.841	19.54	4.50	2.36	20.2	−0.28	0.00	0.58	20.20	319
7	500.	0.130	0.038	0.545×10^{-1}	0.976	29.14	6.50	1.99	29.9	−0.40	−0.01	0.89	29.94	319
8	1000.	0.130×10^{-1}	0.760	0.708	1.456	25.99	16.51	5.59	31.3	−1.81	0.00	0.07	31.35	319
9	1000.	0.320×10^{-1}	0.309	0.169	0.855	14.43	4.05	2.32	15.2	0.28	−0.01	0.35	15.17	319
10	1000.	0.800×10^{-1}	0.124	0.628×10^{-1}	0.794	13.16	4.18	2.13	14.0	−0.15	0.00	0.31	13.97	319
11	1000.	0.130	0.076	0.344×10^{-1}	0.708	17.24	3.71	2.66	17.8	−0.30	0.02	0.47	17.84	319
12	1000.	0.250	0.040	0.140×10^{-1}	0.554	37.44	10.50	1.47	38.9	0.16	−0.01	−0.06	38.91	319
13	1500.	0.320×10^{-1}	0.463	0.155	0.895	18.04	8.80	2.66	20.2	0.21	−0.01	0.00	20.24	319
14	1500.	0.800×10^{-1}	0.185	0.549×10^{-1}	0.791	14.02	3.60	1.86	14.6	−0.01	−0.01	−0.03	14.60	319
15	1500.	0.130	0.114	0.321×10^{-1}	0.752	18.04	3.10	2.24	18.4	−0.15	−0.01	−0.13	18.44	319
16	1500.	0.250	0.059	0.102×10^{-1}	0.458	24.02	2.05	2.56	24.2	−0.37	0.00	−0.11	24.24	319
17	2000.	0.320×10^{-1}	0.618	0.131	0.854	15.55	4.30	2.30	16.3	0.35	0.00	0.47	16.30	319
18	2000.	0.800×10^{-1}	0.247	0.567×10^{-1}	0.923	13.04	3.80	1.51	13.7	−0.11	0.00	0.31	13.67	319
19	2000.	0.130	0.152	0.197×10^{-1}	0.521	21.20	4.40	1.48	21.7	−0.24	0.00	0.47	21.71	319
20	2000.	0.250	0.079	0.861×10^{-2}	0.438	25.51	6.50	1.41	26.4	−0.11	0.00	0.30	26.36	319
21	3000.	0.800×10^{-1}	0.371	0.333×10^{-1}	0.677	9.91	2.60	1.75	10.4	−0.10	0.00	0.28	10.40	319
22	3000.	0.130	0.228	0.211×10^{-1}	0.698	10.88	3.49	1.45	11.5	0.84	0.01	−0.01	11.55	319
23	3000.	0.250	0.119	0.746×10^{-2}	0.474	13.44	3.33	1.36	13.9	−0.08	0.00	0.21	13.91	319
24	3000.	0.400	0.074	0.246×10^{-2}	0.250	26.82	10.03	2.99	28.8	1.59	−0.05	−1.08	28.86	319
25	5000.	0.800×10^{-1}	0.618	0.195×10^{-1}	0.581	12.66	4.23	3.05	13.7	0.88	0.02	0.07	13.72	319
26	5000.	0.130	0.380	0.129×10^{-1}	0.626	11.18	3.42	1.33	11.8	0.37	0.00	−0.12	11.77	319
27	5000.	0.250	0.198	0.429×10^{-2}	0.400	13.35	2.74	1.41	13.7	0.59	0.00	0.10	13.71	319
28	5000.	0.400	0.124	0.189×10^{-2}	0.283	18.80	5.71	2.53	19.8	2.41	−0.02	−0.96	19.97	319
29	8000.	0.130	0.608	0.802×10^{-2}	0.619	12.72	4.37	2.16	13.6	0.44	0.01	−0.43	13.64	319
30	8000.	0.250	0.316	0.380×10^{-2}	0.565	11.44	3.23	1.59	12.0	0.54	0.00	−0.34	12.01	319
31	8000.	0.400	0.198	0.105×10^{-2}	0.250	19.41	4.61	2.91	20.2	0.99	0.00	−0.92	20.20	319
32	15000.	0.250	0.593	0.133×10^{-2}	0.434	16.39	6.52	3.49	18.0	0.27	0.01	−0.83	18.00	319
33	15000.	0.400	0.371	0.372×10^{-3}	0.195	23.55	5.91	3.33	24.5	1.54	0.01	−1.36	24.59	319
34	30000.	0.400	0.741	0.106×10^{-3}	0.160	54.99	3.60	9.58	55.9	1.38	0.03	−0.20	55.95	319

Table 18: HERA combined double differential $\mathrm{d}^2\sigma^{e^-p\ \mathrm{ave}}_{CC}/\mathrm{d}x\mathrm{d}Q^2$ and reduced $\sigma^{-\ \mathrm{ave}}_{r,\mathrm{CC}}$ cross section for CC e^-p scattering. $\delta_{\mathrm{ave,stat}}$, $\delta_{\mathrm{ave,uncor}}$, $\delta_{\mathrm{ave,cor}}$ and $\delta_{\mathrm{ave,exp\ tot}}$ represent the statistical, uncorrelated systematic, correlated systematic and total experimental uncertainty, respectively. $\delta_{\mathrm{ave,rel}}$, $\delta_{\mathrm{ave,gp}}$ and $\delta_{\mathrm{ave,had}}$ are the three correlated sources of uncertainties arising from the combination procedure, see section 3.2.3. $\delta_{\mathrm{ave,tot}}$ is the total uncertainty calculated by adding $\delta_{\mathrm{ave,exp\ tot}}$ and the procedural errors in quadrature. The uncertainties are quoted in percent relative to $\mathrm{d}^2\sigma^{e^-p\ \mathrm{ave}}_{CC}/\mathrm{d}x\mathrm{d}Q^2$. The overall normalisation uncertainty of 0.5% is not included.

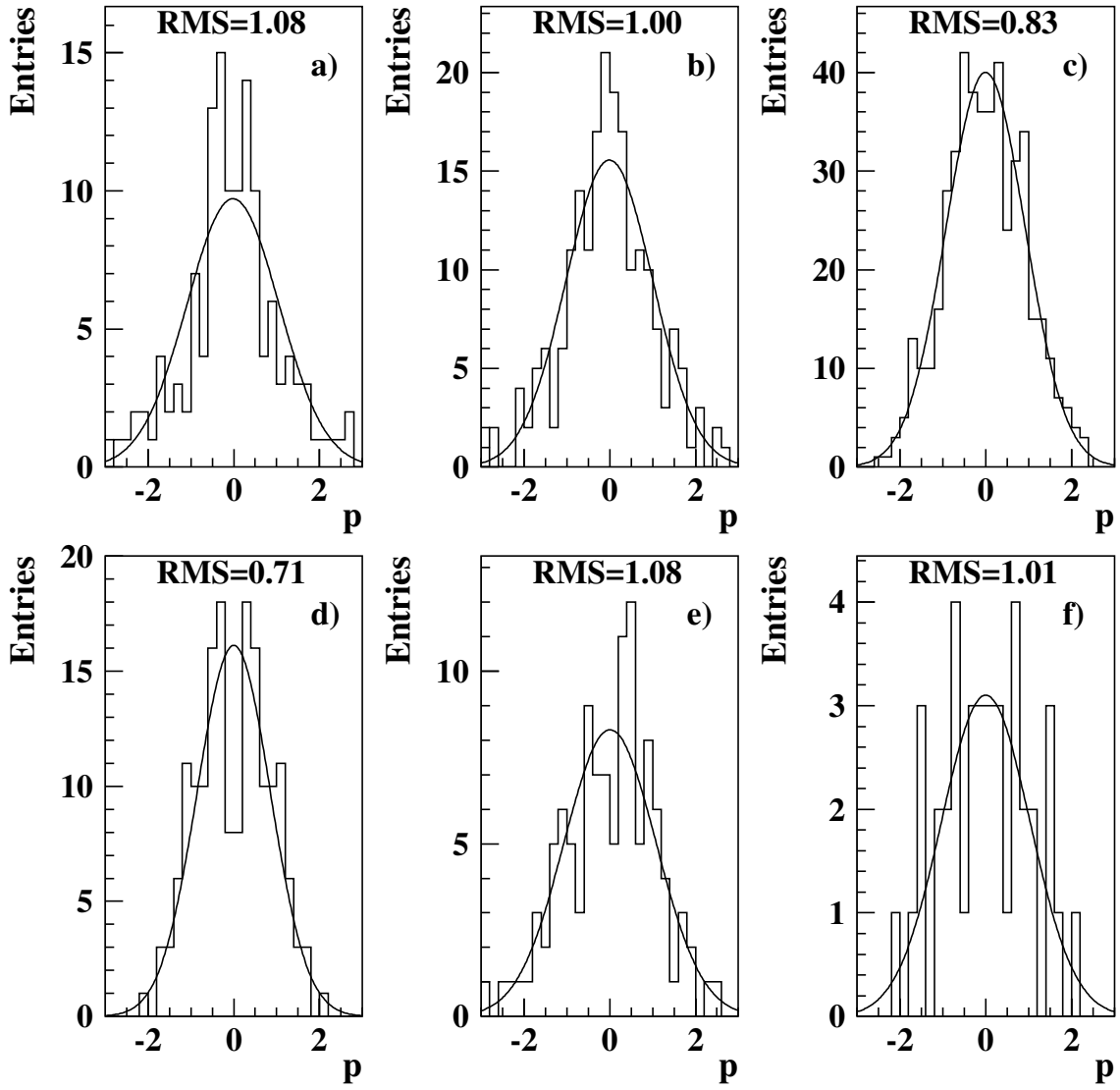

Figure 1: Distribution of pulls p for the following samples: a) NC e^+p for $Q^2 < 3.5$ GeV^2; b) NC e^+p for $3.5 \leq Q^2 < 100$ GeV^2; c) NC e^+p for $Q^2 \geq 100$ GeV^2; d) NC e^-p; e) CC e^+p and f) CC e^-p. There are no entries outside the histogram ranges. RMS gives the root mean square of each distribution calculated as $\overline{p^2}$. The curves show the results of binned log-likelihood Gaussian fits to the distributions.

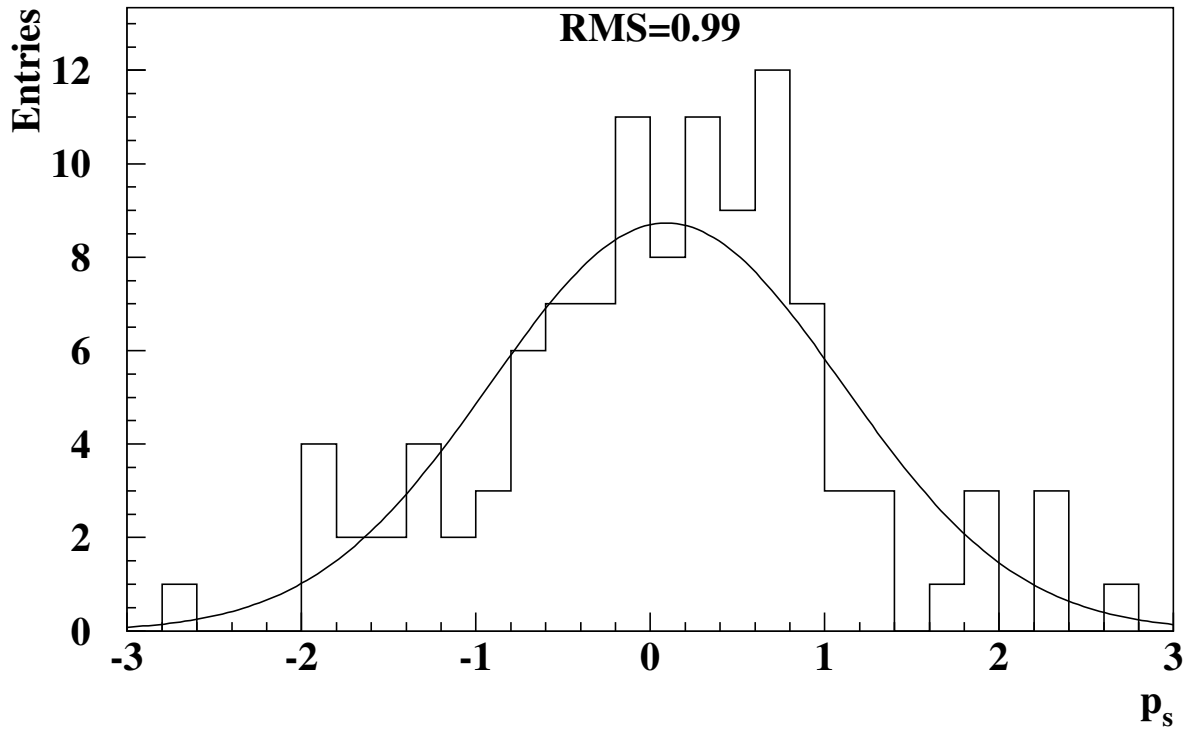

Figure 2: Distribution of pulls p_s for correlated systematic uncertainties including global normalisations. There are no entries outside the histogram range. RMS gives the root mean square of the distribution calculated as $\overline{p_s^2}$. The curve shows the result of a binned log-likelihood Gaussian fit to the distribution.

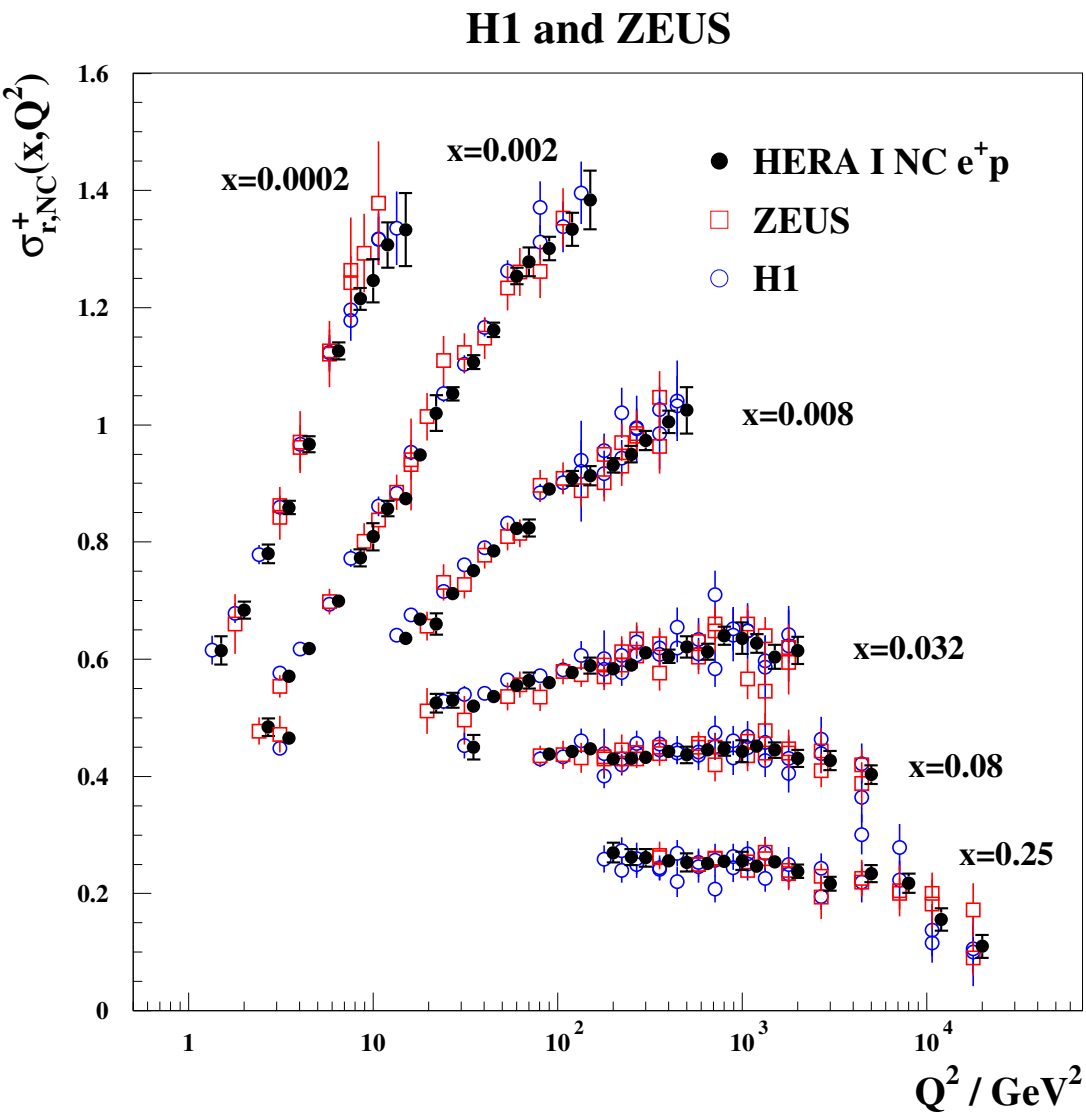

Figure 3: HERA combined NC e^+p reduced cross section as a function of Q^2 for six x-bins compared to the separate H1 and ZEUS data input to the averaging procedure. The error bars indicate the total experimental uncertainty. The individual measurements are displaced horizontally for better visibility.

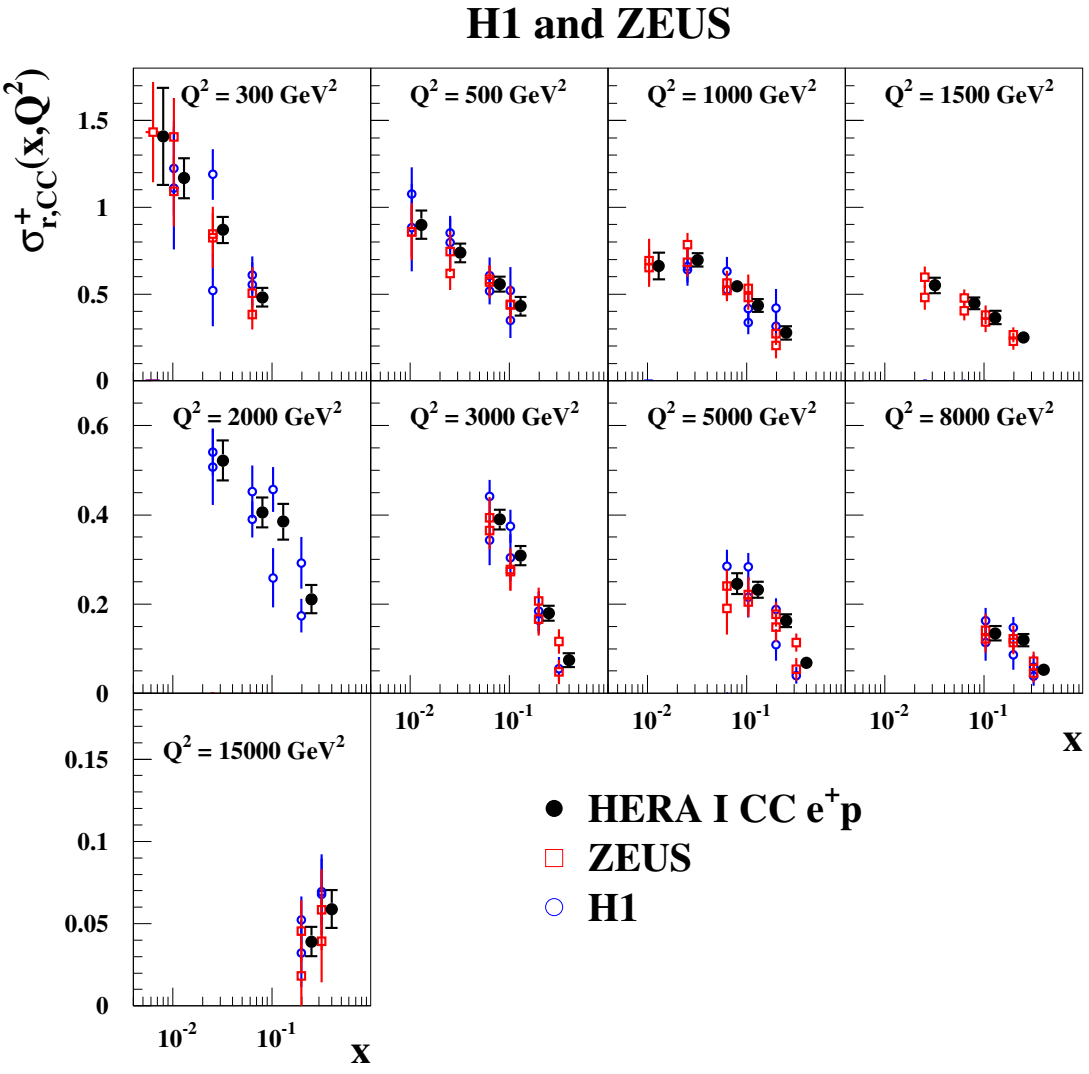

Figure 4: HERA combined CC e^+p reduced cross section compared to the separate H1 and ZEUS data input to the averaging procedure. The error bars indicate the total experimental uncertainty. The individual measurements are displaced horizontally for better visibility.

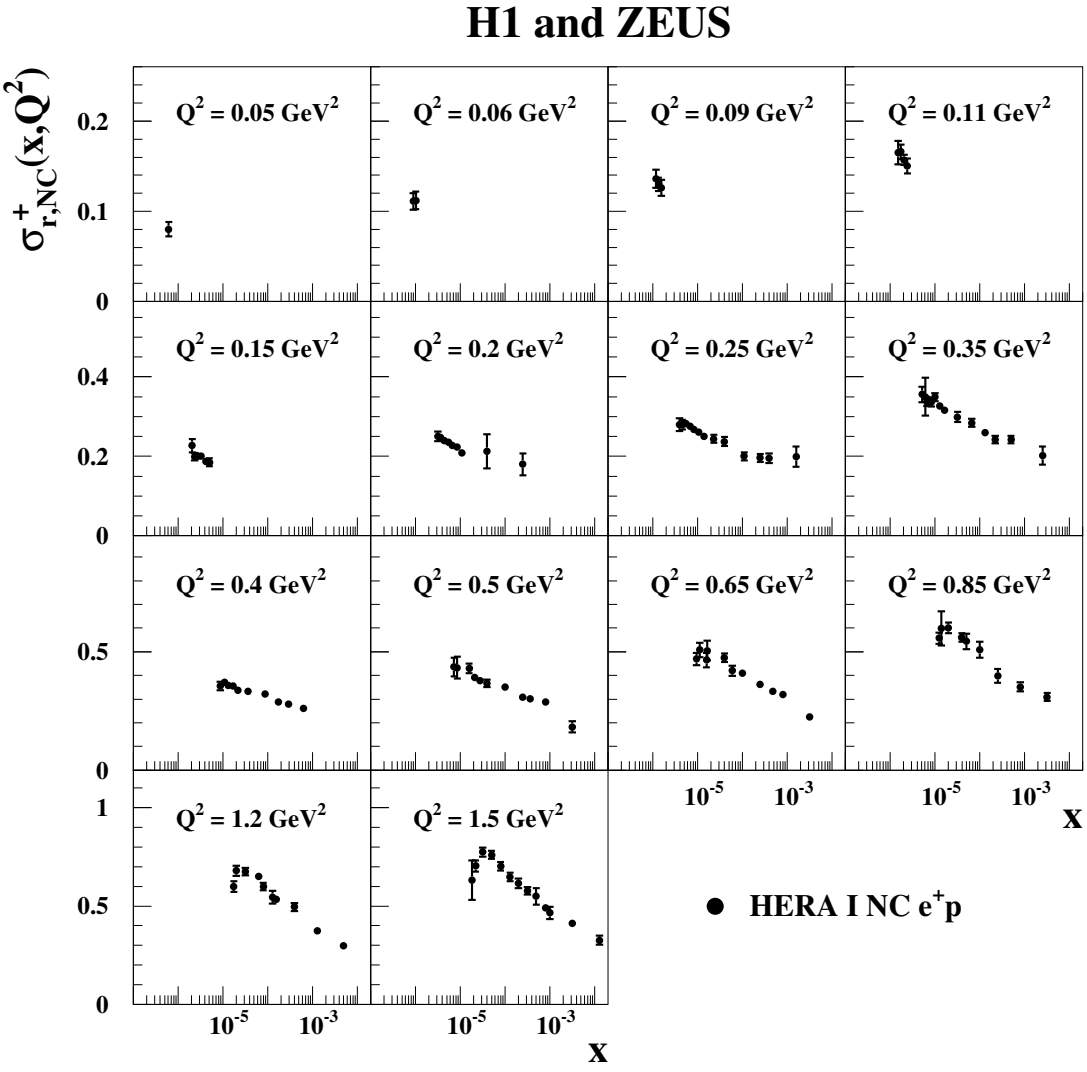

Figure 5: HERA combined NC e^+p reduced cross section at very low Q^2. The error bars indicate the total experimental uncertainty.

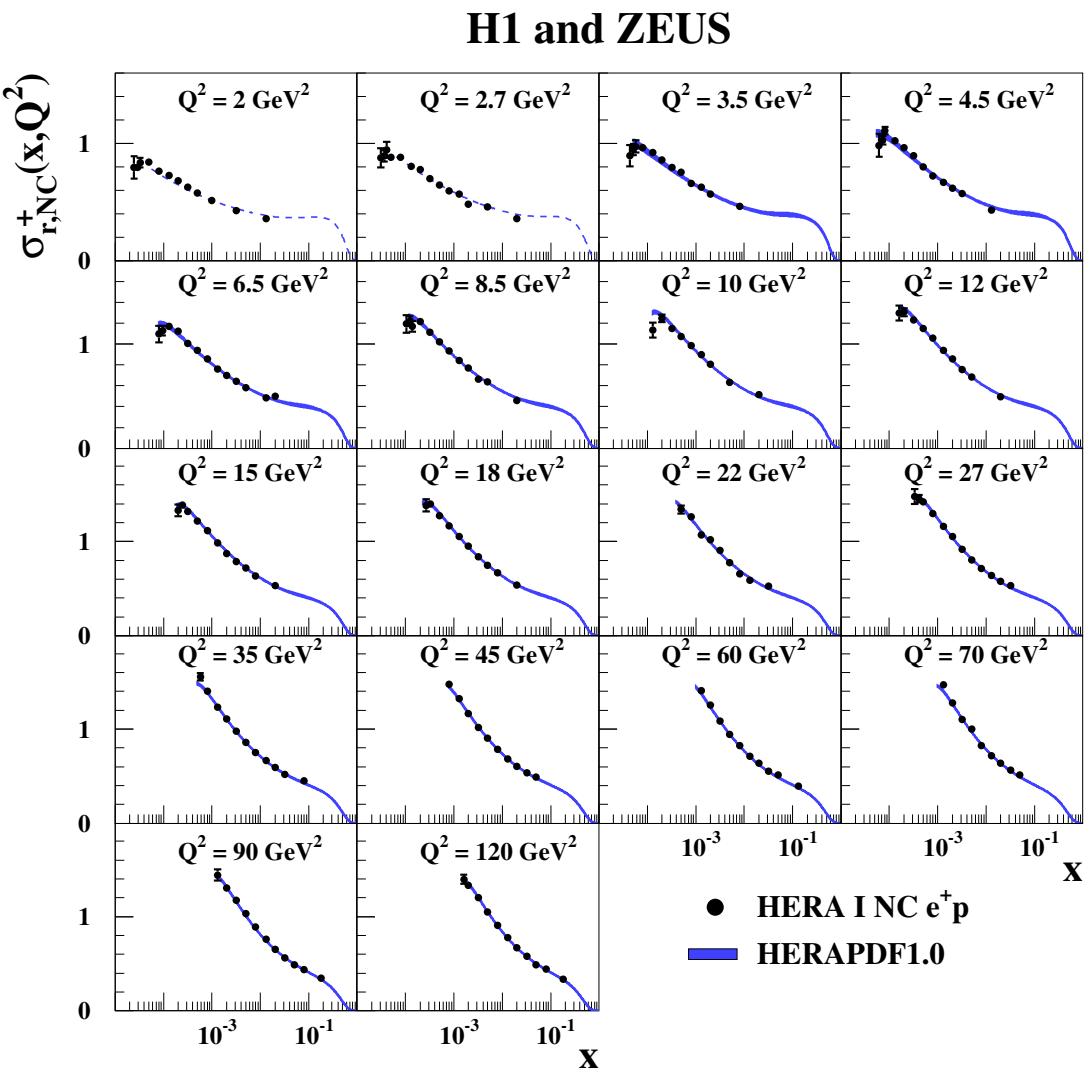

Figure 6: HERA combined NC e^+p reduced cross section at low Q^2. The error bars indicate the total experimental uncertainty. The HERAPDF1.0 fit is superimposed. The bands represent the total uncertainty of the fit. Dashed lines are shown for Q^2 bins not included in the QCD analysis.

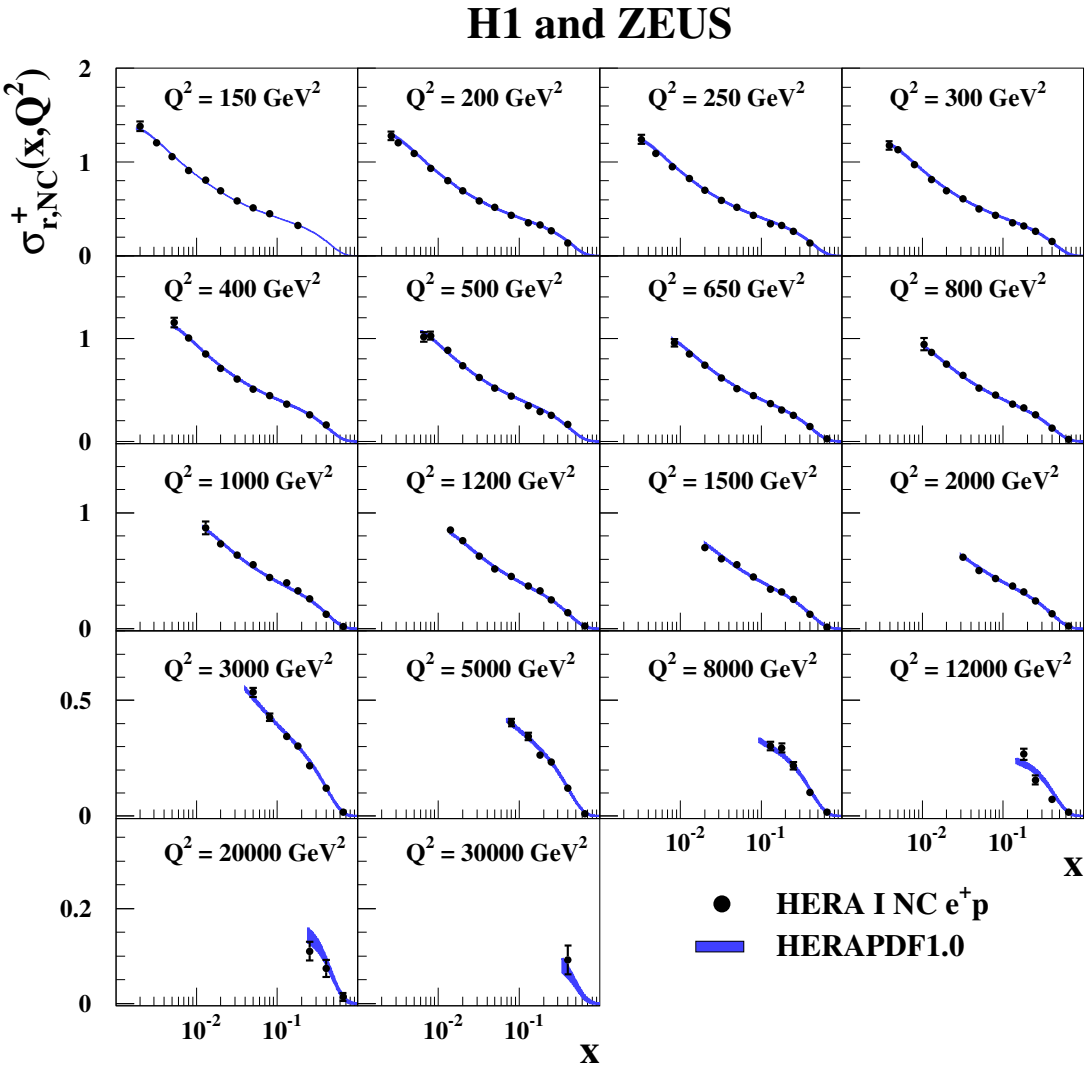

Figure 7: HERA combined NC e^+p reduced cross section for high Q^2. The error bars indicate the total experimental uncertainty. The predictions of the HERAPDF1.0 fit are superimposed. The bands represent the total uncertainty of the fit.

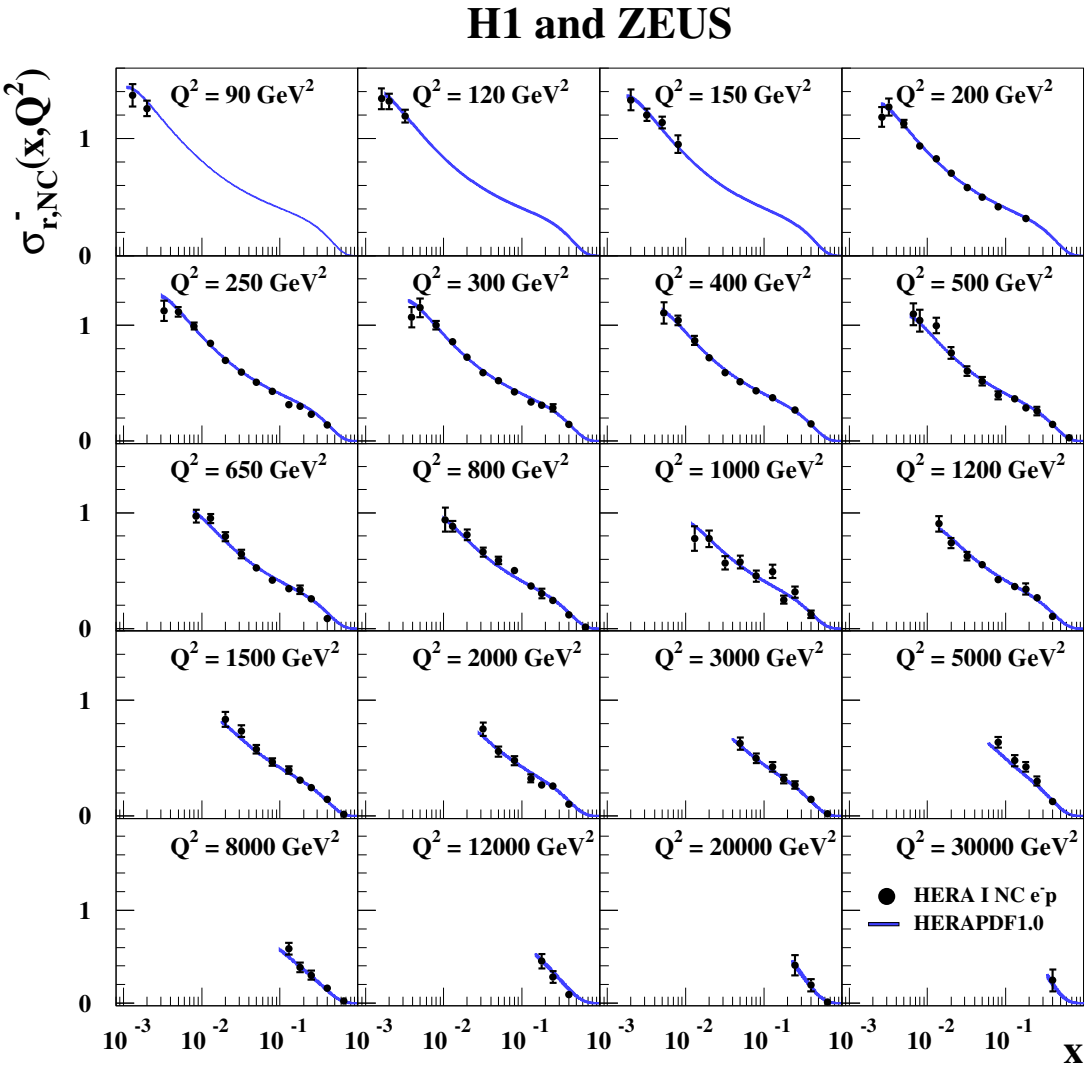

Figure 8: HERA combined NC e^-p reduced cross section. The error bars indicate the total experimental uncertainty. The HERAPDF1.0 fit is superimposed. The bands represent the total uncertainty of the fit.

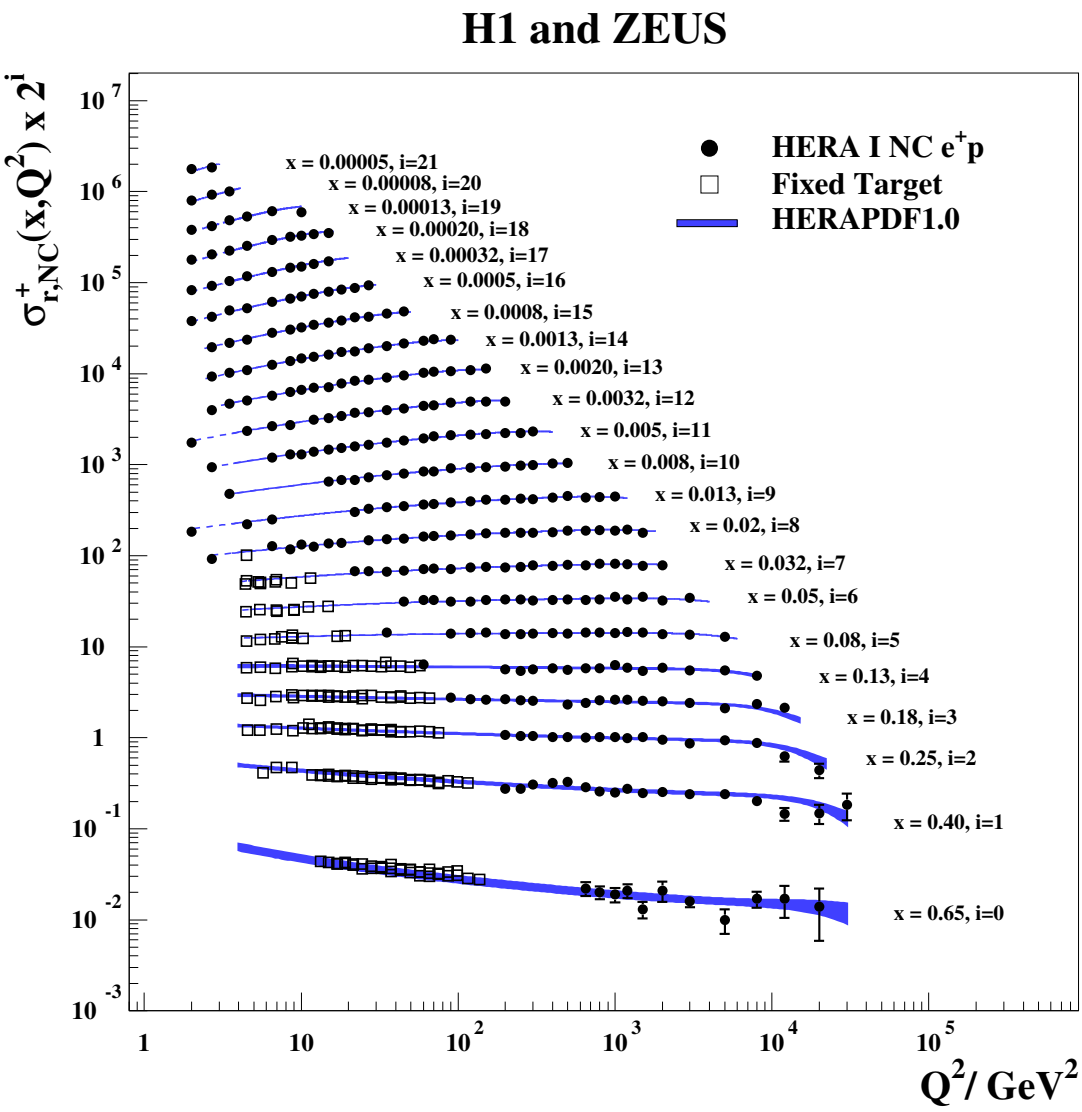

Figure 9: HERA combined NC e^+p reduced cross section and fixed-target data as a function of Q^2. The error bars indicate the total experimental uncertainty. The HERAPDF1.0 fit is superimposed. The bands represent the total uncertainty of the fit. Dashed lines are shown for Q^2 values not included in the QCD analysis.

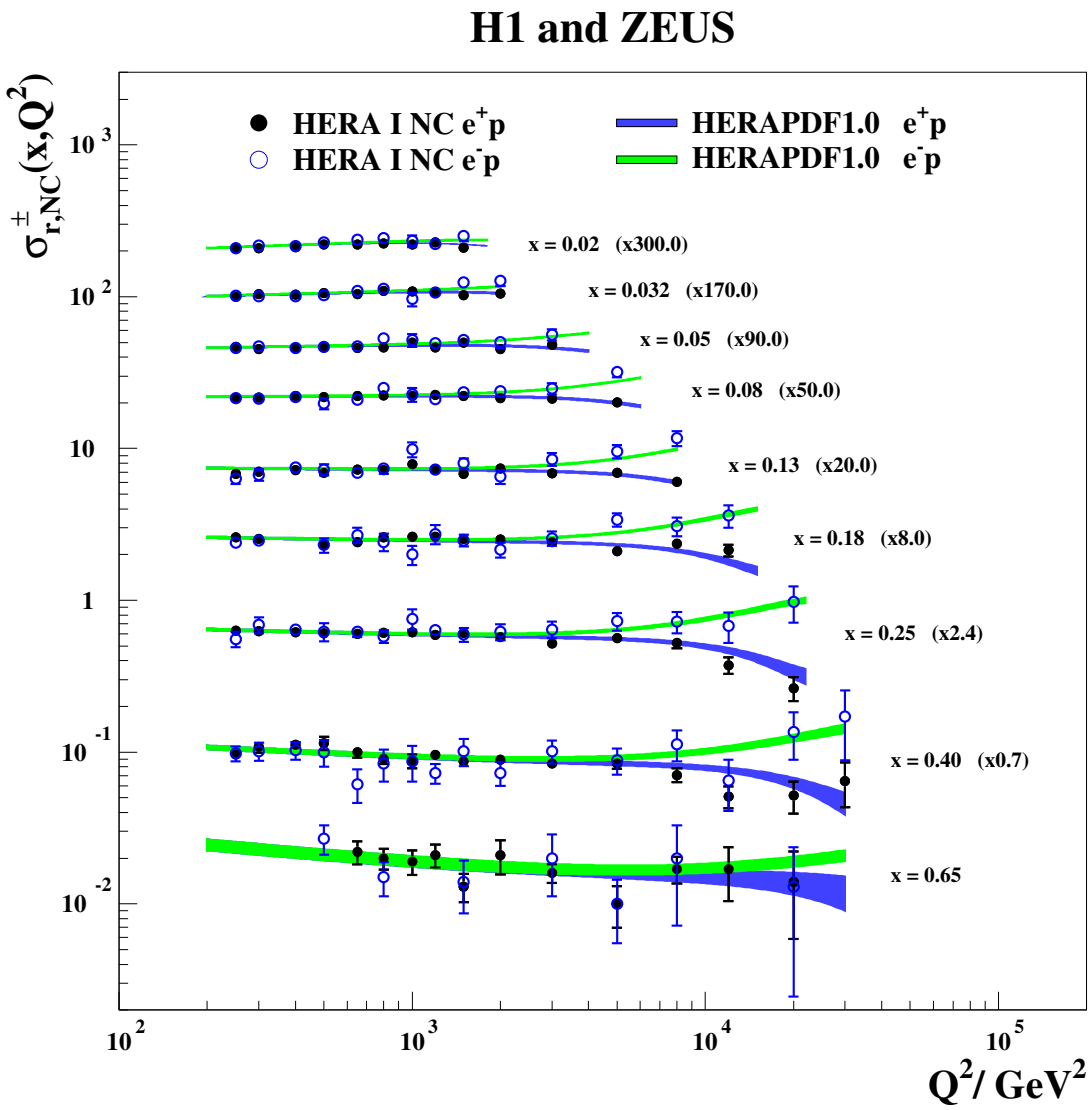

Figure 10: HERA combined NC $e^{\pm}p$ reduced cross sections at high Q^2. The error bars indicate the total experimental uncertainty. The HERAPDF1.0 fit is superimposed. The bands represent the total uncertainty of the fit.

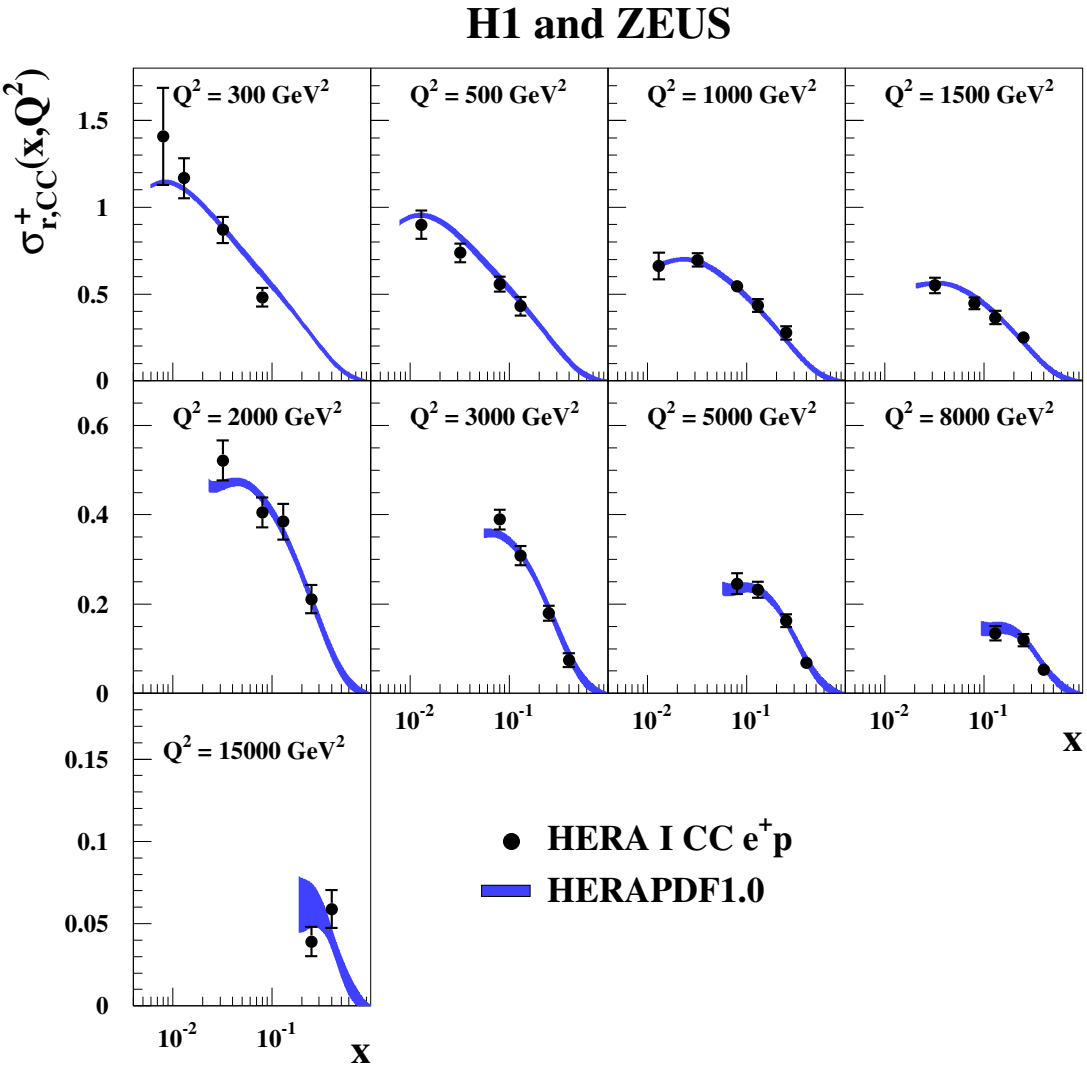

Figure 11: HERA combined CC e^+p reduced cross section. The error bars indicate the total experimental uncertainty. The HERAPDF1.0 fit is superimposed. The bands represent the total uncertainty of the fit.

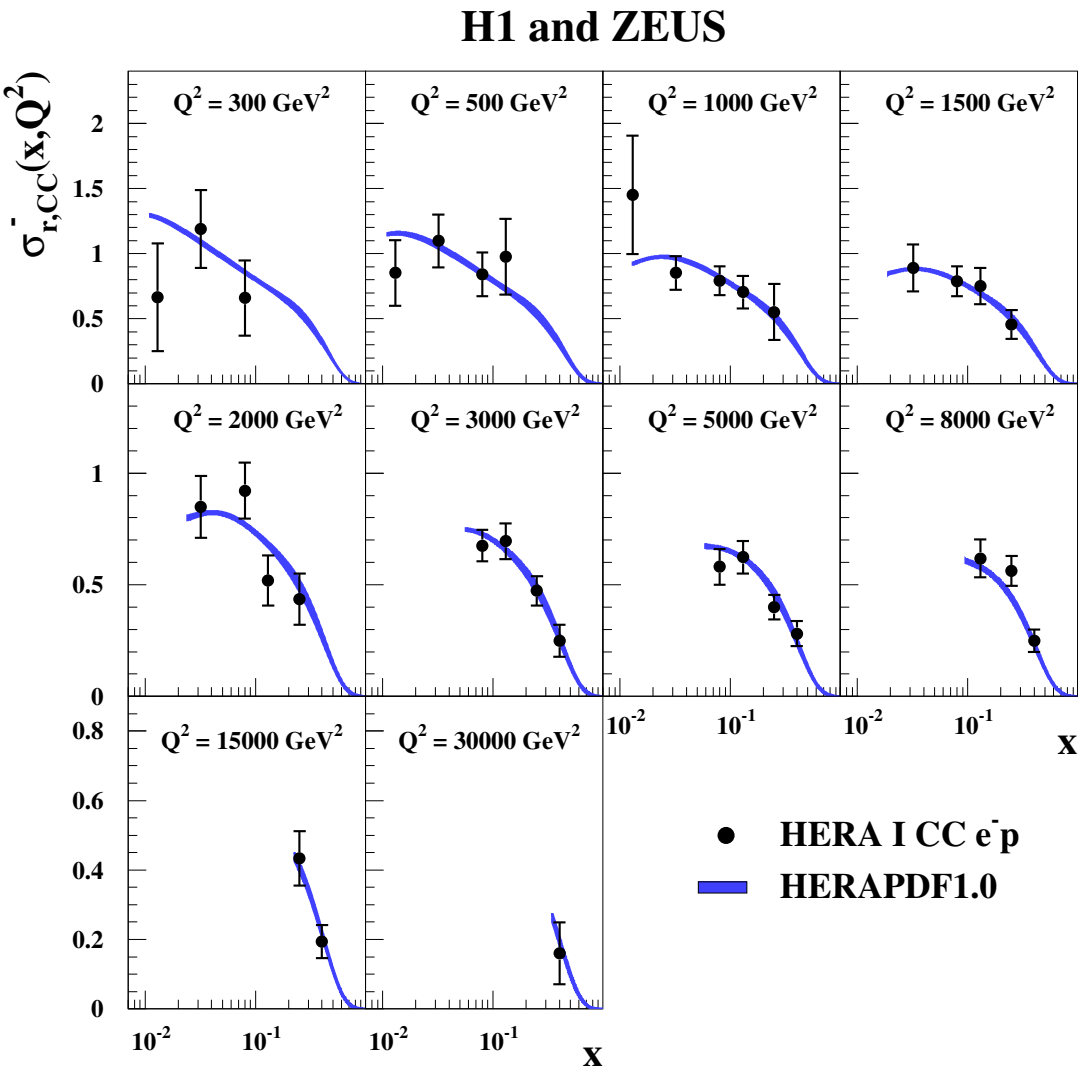

Figure 12: HERA combined CC $e^- p$ reduced cross section. The error bars indicate the total experimental uncertainty. The HERAPDF1.0 fit is superimposed. The bands represent the total uncertainty of the fit.

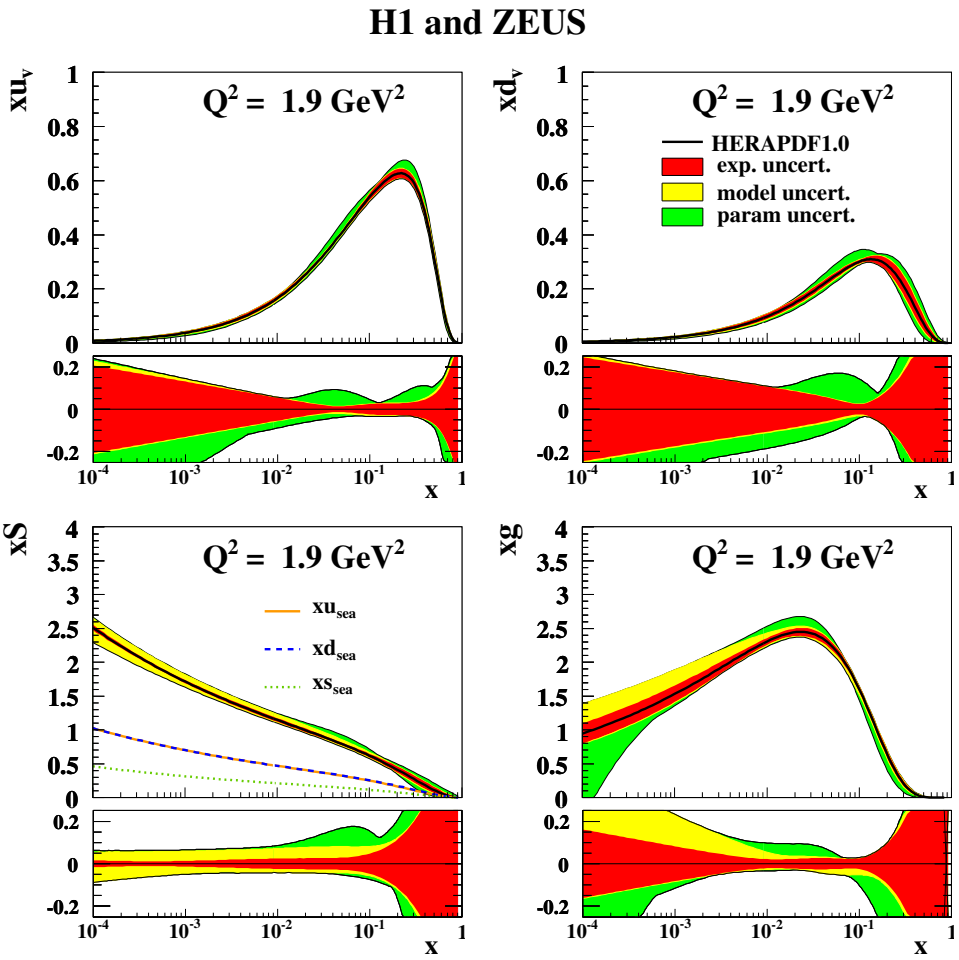

Figure 13: The parton distribution functions from HERAPDF1.0, xu_v, xd_v, $xS = 2x(\bar{U}+\bar{D})$, xg, at $Q^2 = 1.9$ GeV^2. The break-up of the Sea PDF, xS, into the flavours, $xu_{sea} = 2x\bar{u}$, $xd_{sea} = 2x\bar{d}$, $xs_{sea} = 2x\bar{s}$, is illustrated. Fractional uncertainty bands are shown below each PDF. The experimental, model and parametrisation uncertainties are shown separately.

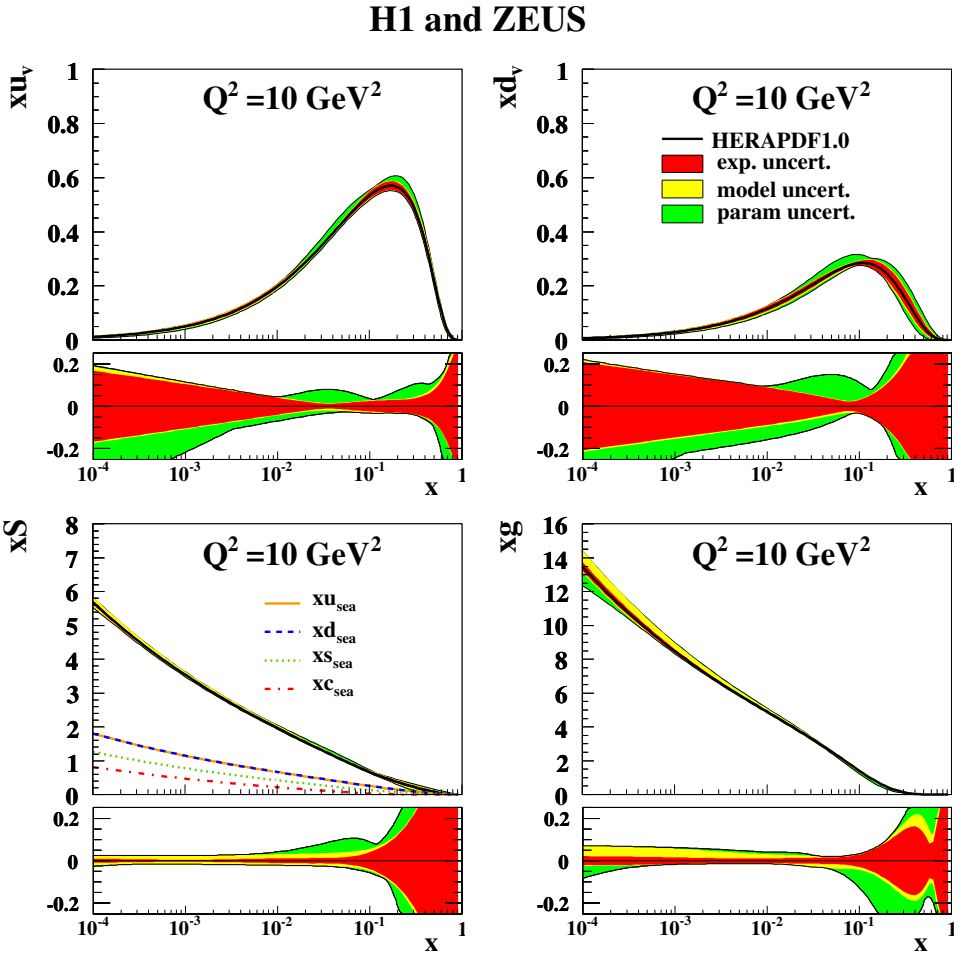

Figure 14: The parton distribution functions from HERAPDF1.0, xu_v, xd_v, $xS = 2x(\bar{U}+\bar{D})$, xg, at $Q^2 = 10$ GeV^2. The break-up of the Sea PDF, xS, into the flavours, $xu_{sea} = 2x\bar{u}$, $xd_{sea} = 2x\bar{d}$, $xs_{sea} = 2x\bar{s}$, $xc_{sea} = 2x\bar{c}$ is illustrated. Fractional uncertainty bands are shown below each PDF. The experimental, model and parametrisation uncertainties are shown separately.

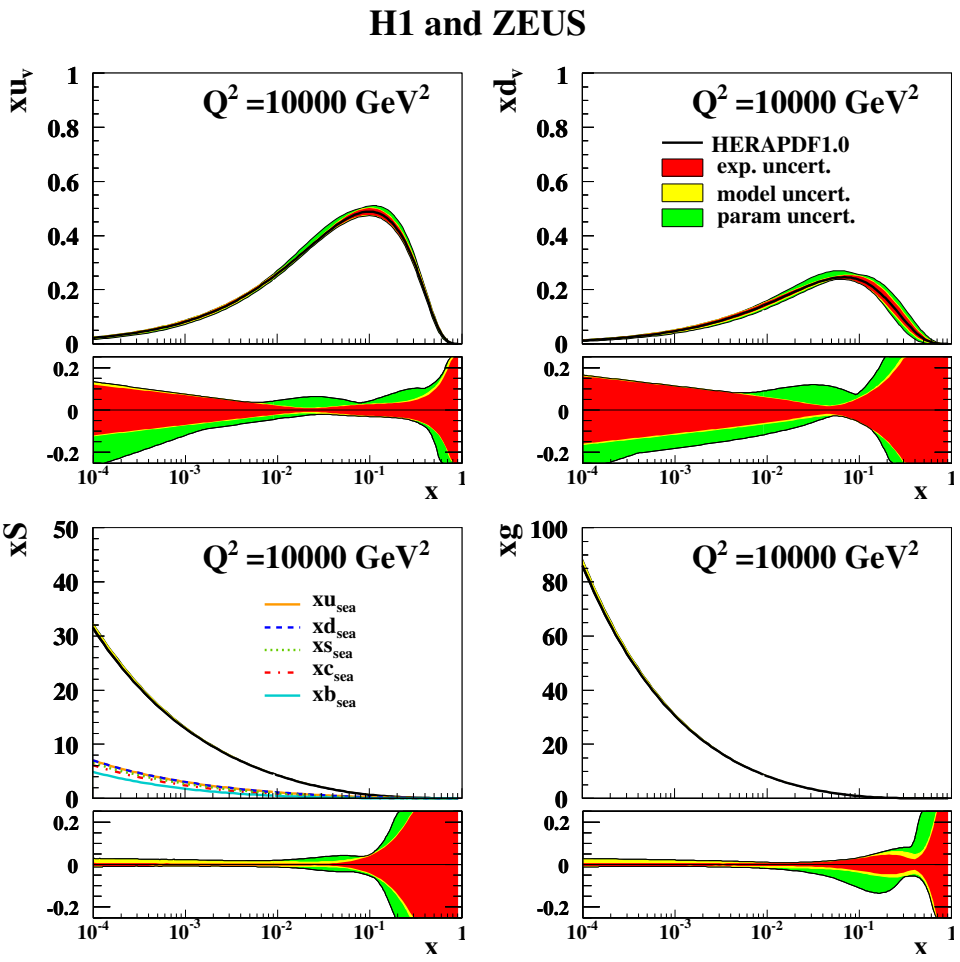

Figure 15: The parton distribution functions from HERAPDF1.0, xu_v, xd_v, $xS = 2x(\bar{U}+\bar{D})$, xg, at $Q^2 = 10{,}000$ GeV^2. The break-up of the Sea PDF, xS, into the flavours, $xu_{sea} = 2x\bar{u}$, $xd_{sea} = 2x\bar{d}$, $xs_{sea} = 2x\bar{s}$, $xc_{sea} = 2x\bar{c}$, $xb_{sea} = 2x\bar{b}$ is illustrated. Fractional uncertainty bands are shown below each PDF. The experimental, model and parametrisation uncertainties are shown separately.

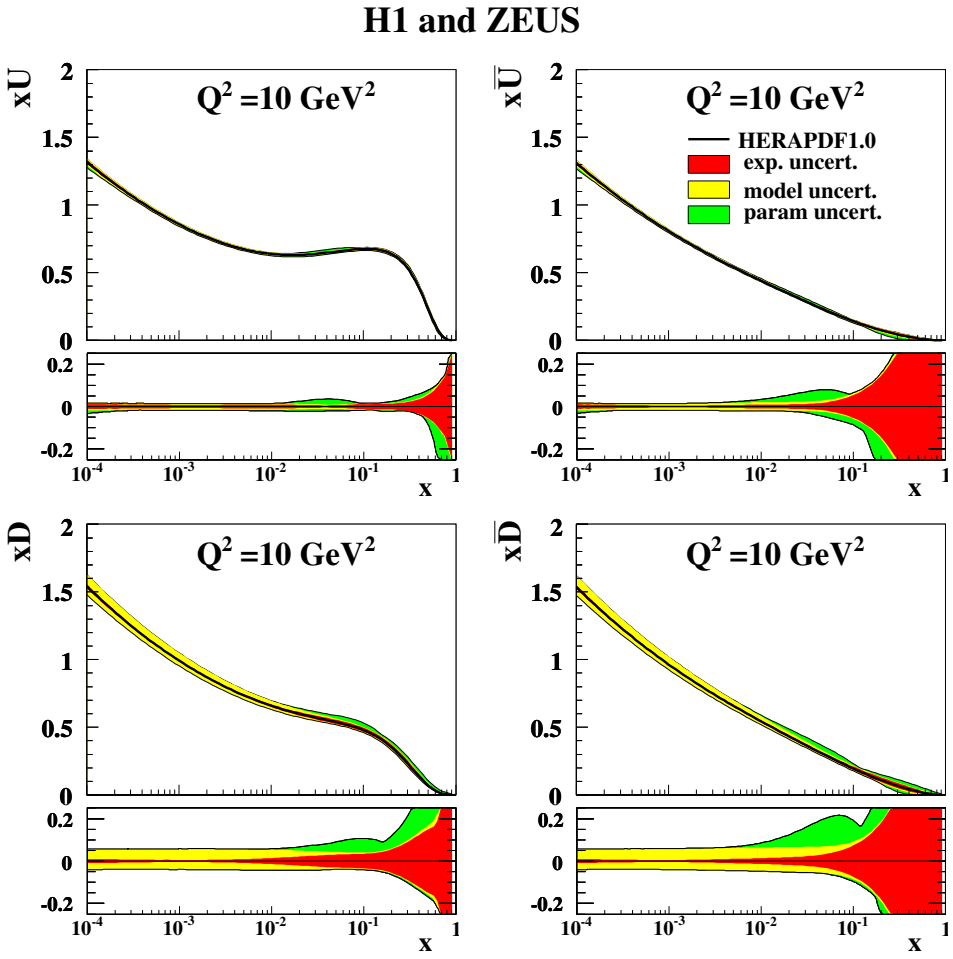

Figure 16: The parton distribution functions from HERAPDF1.0, $xU, xD, x\bar{U}, x\bar{D}$ at $Q^2 = 10$ GeV^2. Fractional uncertainty bands are shown below each PDF. The experimental, model and parametrisation uncertainties are shown separately.

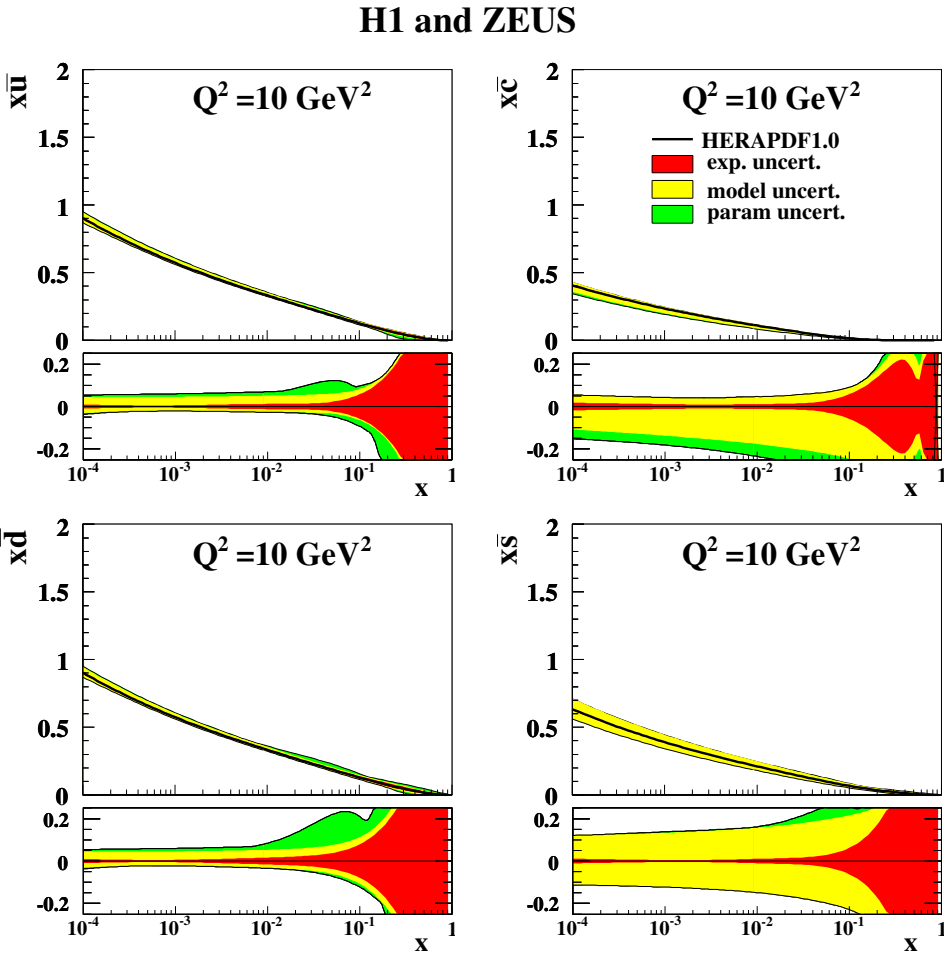

Figure 17: The parton distribution functions from HERAPDF1.0, $x\bar{u}, x\bar{d}, x\bar{c}, x\bar{s}$ at Q^2 = 10 GeV^2. Fractional uncertainty bands are shown below each PDF. The experimental, model and parametrisation uncertainties are shown separately.

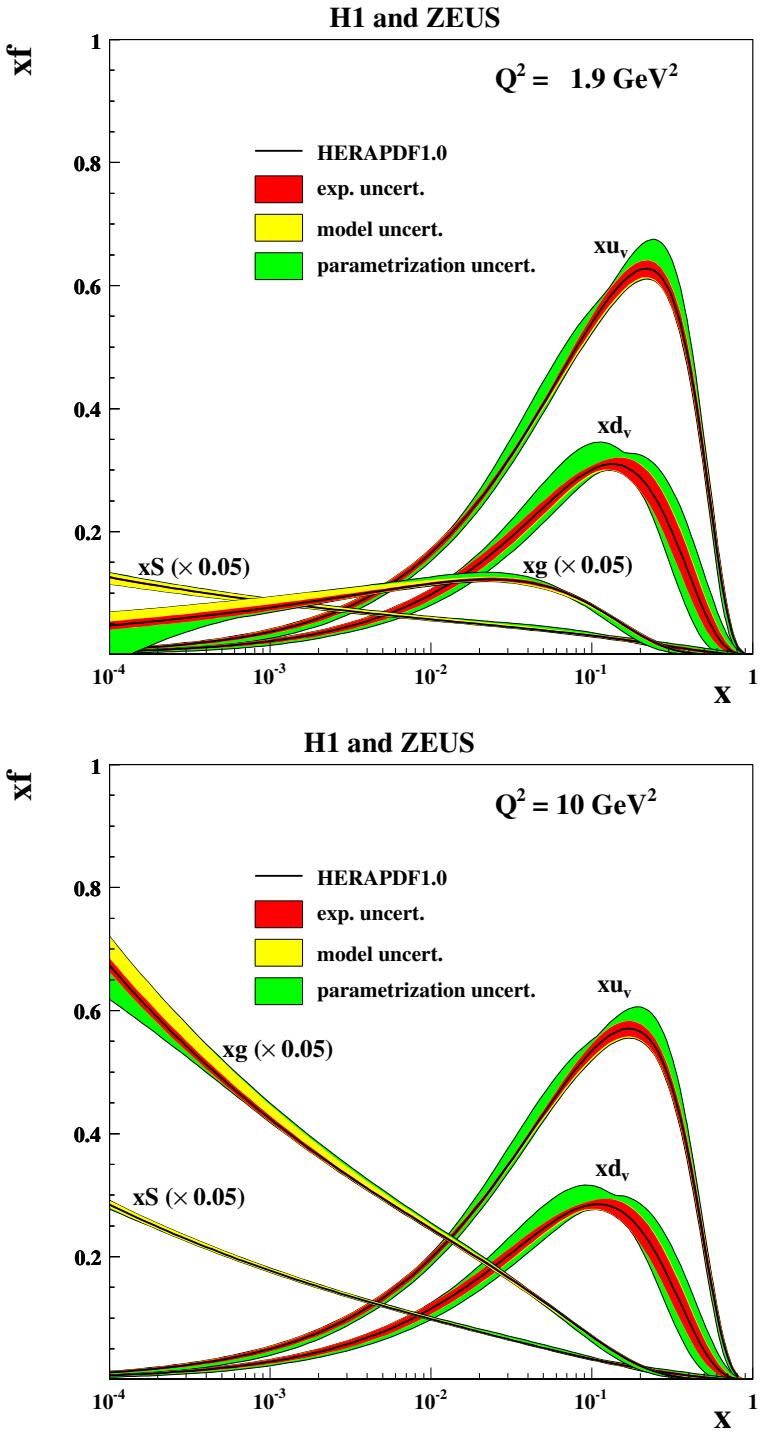

Figure 18: The parton distribution functions from HERAPDF1.0, xu_v, xd_v, $xS = 2x(\bar{U}+\bar{D})$, xg, at $Q^2 = 1.9$ GeV^2 (top) and $Q^2 = 10$ GeV^2 (bottom). The gluon and sea distributions are scaled down by a factor 20. The experimental, model and parametrisation uncertainties are shown separately.

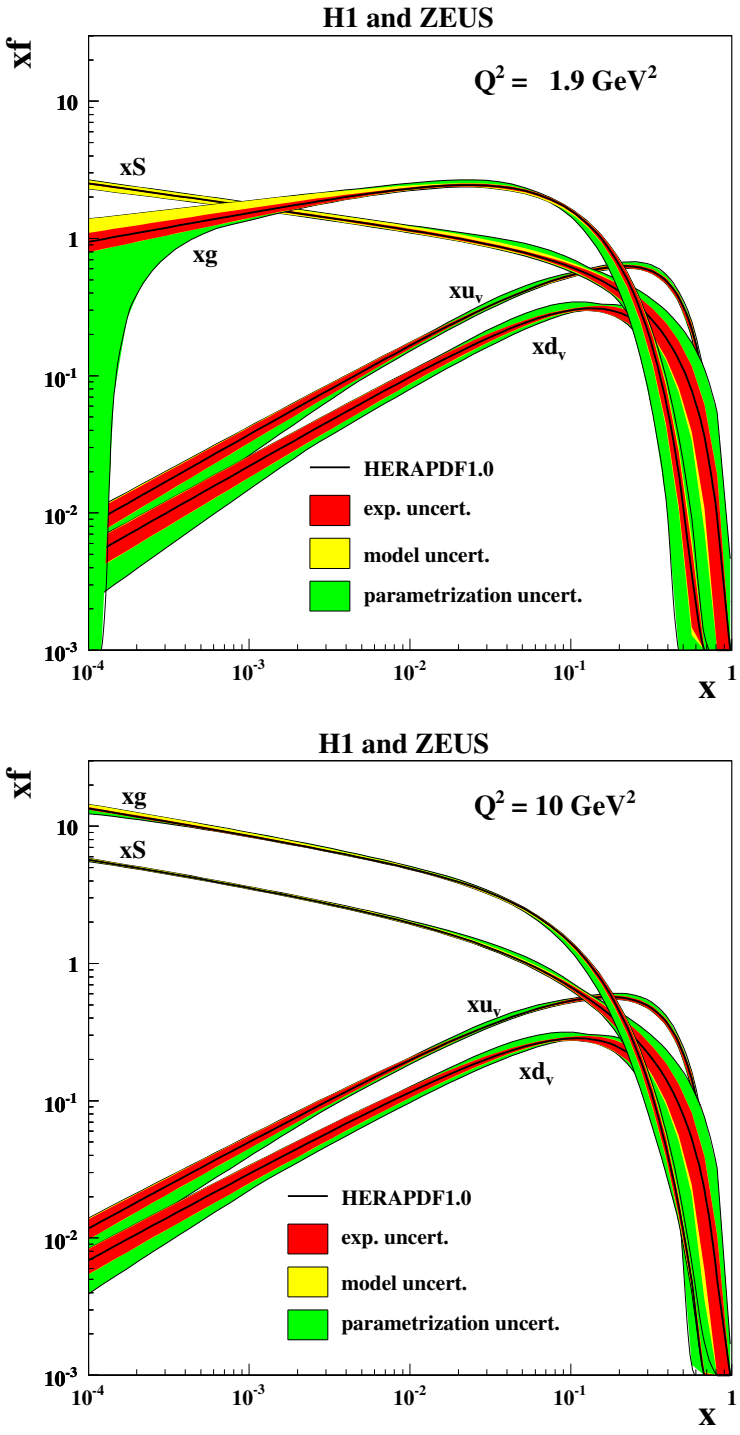

Figure 19: The parton distribution functions from HERAPDF1.0, xu_v, xd_v, $xS = 2x(\bar{U}+\bar{D})$, xg, at $Q^2 = 1.9$ GeV^2 (top) and $Q^2 = 10$ GeV^2 (bottom). The experimental, model and parametrisation uncertainties are shown separately.

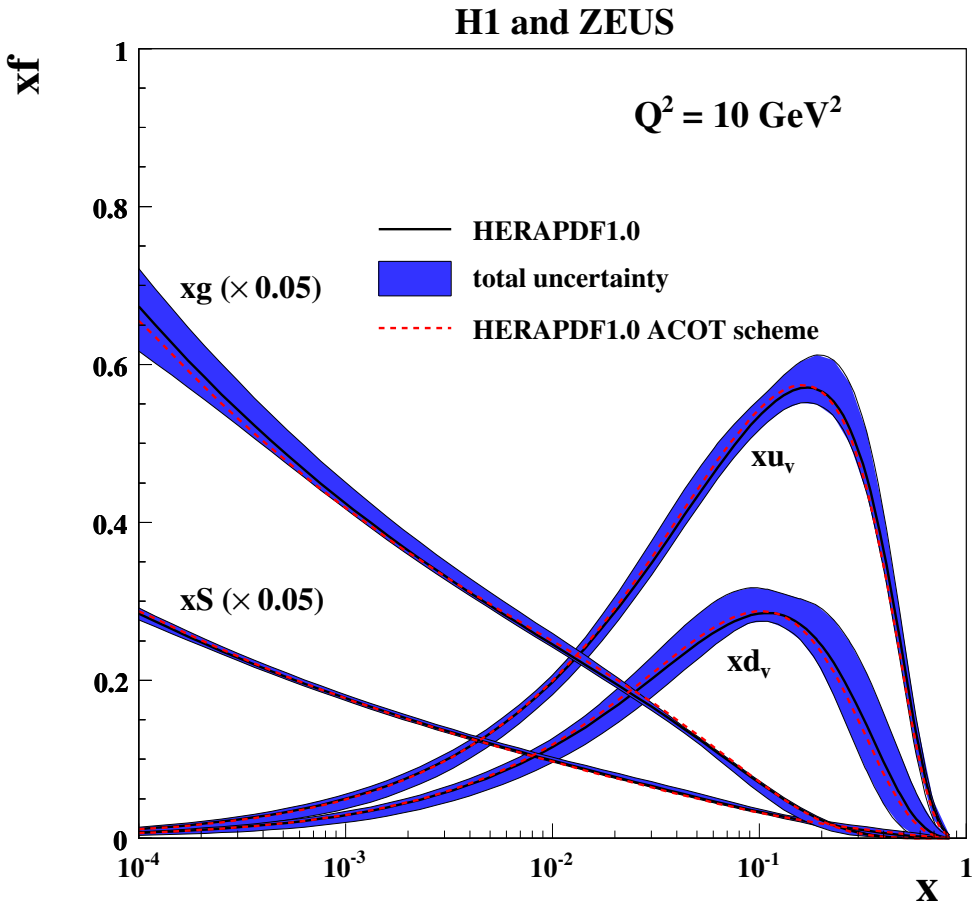

Figure 20: The parton distribution functions obtained using ACOT heavy-flavour scheme compared to HERAPDF1.0 for xu_v, xd_v, $xS = 2x(\bar{U} + \bar{D})$, xg, at $Q^2 = 10$ GeV^2. The bands show total uncertainties of the HERAPDF1.0 fit.

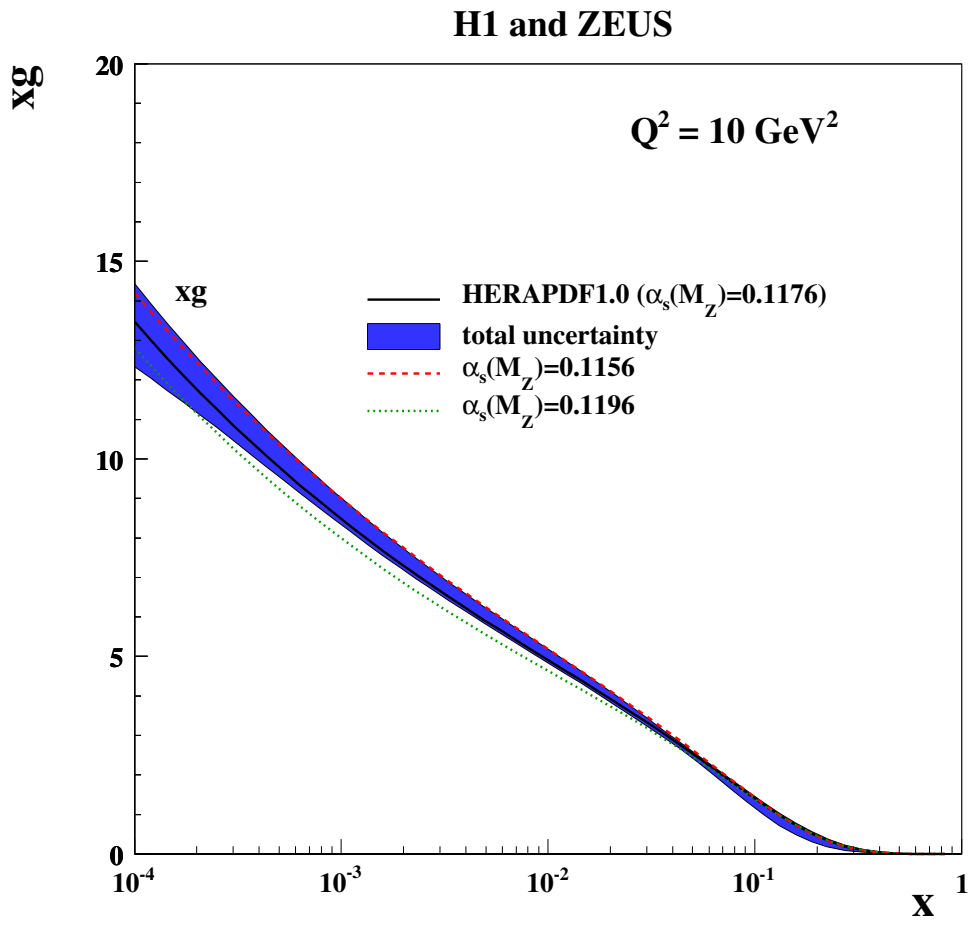

Figure 21: The gluon density xg from HERAPDF1.0 compared for different values of α_S. The band shows total uncertainties of the HERAPDF1.0 fit.